TENSILE TRUE STRESS - STRAIN CURVES AND ESSENTIAL WORK OF

FRACTURE ANALYSIS OF POLYETHYLENE BLOWN FILMS

A Dissertation

by

CHIN-FU LEE

Submitted to the Office of Graduate and Professional Studies of
Texas A&M University
in partial fulfillment of the requirements for the degree of

DOCTOR OF PHILOSOPHY

Chair of Committee,	Hung-Jue Sue
Committee Members,	David E Bergbreiter
	Jodie Lutkenhaus
	Terry Creasy
Head of Department,	Ibrahim Karaman

May 2015

Major Subject: Materials Science and Engineering

ABSTRACT

Characterization of mode-I fracture toughness of ductile polymeric thin films is nontrivial. In order to gain understanding about the fracture mechanics and the processing-structure-property relationships of metallocene linear low-density polyethylene (m-LLDPE) thin film, a custom-built double-edge notched tensile (DENT) test fixture was developed to perform the mode-I fracture test on m-LLDPE thin films, and the *essential work of fracture* (EWF) analysis, which employs an unique energy partitioning concept, was used to characterize the fracture toughness of the thin films. Effects of specimen geometry, strain rate, film orientation, processing parameters, and resin densities on the specific essential work of fracture, w_e, and the specific non-essential work of fracture, w_p, were investigated. The usefulness of the methodology incorporating the EWF analysis and the custom-built film fixture for characterizing LLDPE fracture toughness is evaluated and discussed, and the correlations between the EWF parameters and the films' Elmendorf tear properties were also made. The visual, full-field stress distributions of the EWF film specimens were measured *in-situ* during mode-I facture testing by the photoelastic method, and the deformation in the process zone of post-mortem specimen was also characterized. A new experimental approach has been developed to directly quantify and partition the total mode-I fracture energy of m-LLDPE blown films. Three distinctive deformation zones have been identified from the photoelastic observation of the m-LLDPE blown films during the mode-I facture testing. These three zones include the essential work zone due to necking and crack

propagation, the non-essential plastic deformation zone, and a newly proposed recoverable viscoelastic deformation zone. The tensile true stress-strain curves of m-LLDPE blown films and the full-field strain mapping of the mode-I DENT specimen were generated to allow for quantitative energy partitioning at each deformation zone *in-situ* as defined by the EWF approach. The current approach allows to perform directly quantification and partitioning of the total mode-I fracture energy for the exact physical interpretation of the EWF parameters and their correlation to material characteristics.

DEDICATION

To my parents

ACKNOWLEDGEMENTS

TABLE OF CONTENTS

LIST OF FIGURES

x

xi

LIST OF TABLES

CHAPTER I

INTRODUCTION

In 2012, the global packaging film market was estimated at $89 billion (*1*). The global market was expected to grow at a compound annual growth rate of 5 % from 2013 to 2019 (*1, 2*), and the plastic films & sheets market size by value is projected to reach $119 billion by 2019. The demand for plastic film in the USA is expected to grow 1.5 % annually through 2018 to 15.4 billion pounds, with a market value of $26.2 billion (*3*). Linear low density polyethylene (LLDPE) is the most widely used material for film, and it will see gains in diverse markets due to its superior ductility, strength, durability, relatively low cost and versatility. Several million tons of polyethylene films are produced in the USA every year, which amounts to half of annual polyethylene consumption (*4, 5*). Demand for LLDPE film is forecast to register strong advances through 2016, and it will represent almost 50 percent of film demand in 2016 (*1*). While 90% of LLDPE is used in film applications, 70% of commercial LLDPE films are produced through the blown film extrusion process (*4-6*). However, there have been only a handful of investigations focusing on both the fracture mechanics and the processing-structure-property relationships of ductile polymeric thin film (*6-9*).

1.1 Linear Low Density Polyethylene

LLDPEs are made by the copolymerization of ethylene and varying amounts of α-olefin comonomers, such as 1-butene, 1-hexene, and 1-octene, using Ziegler-Natta

(ZN) or metallocene (m) catalysts. The α-olefin comonomer introduces short chain branches, such as ethyl, butyl and hexyl branches, on the polyethylene linear backbone. The number and length of short chain branches correlate with the concentration and type of α-olefin, while the distribution of branches is dependent on the polymerization conditions (*7, 8*). Control of branch distribution can mainly be attributed to the catalyst used and reaction conditions during polymerization (Figure 1.1). LLDPE resins produced using Ziegler-Natta heterogeneous catalysts are characterized by the heterogeneous distribution in the incorporation of comonomers and are considered to be a mixture of fractions of polyethylene copolymers with a range of molecular weights and short chain branch content. With the single site metallocene catalysts, narrow molecular weight distribution LLDPEs with considerably more homogenous distribution of short chain branches can be produced. The single-site metallocene catalyst prevents the formation of high- and low-molecular-weight tails, which have significant effects on the processing characteristics and physical properties in the resulting copolymers; consequently, m-LLDPEs have more controlled structure. The level and distribution of short chain branching influence the crystallization and lamellae formation of the polyethylene molecule (*9*).
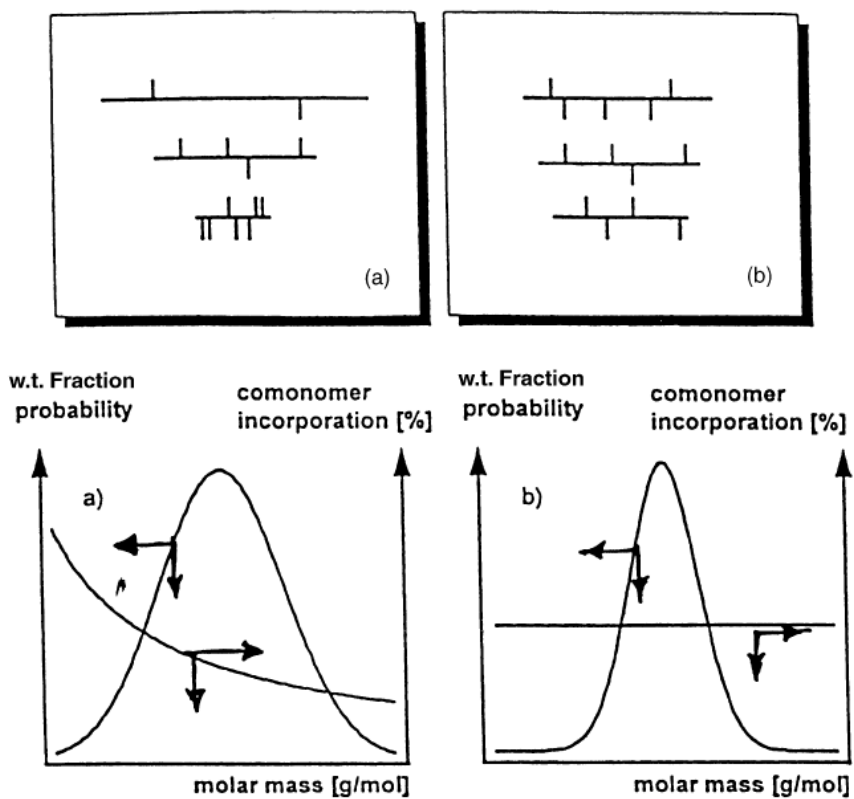
Figure 1.1. Schematic showing the primary differences for polyolefin copolymers in molecular weight distribution and short chain branching distribution between multi-site Ziegler–Natta (a) and single site metallocene catalysts (b) (*10*).

1.2 Blown Film Process

The blown film process (Figure 1.2) is the most common technology for the production of thin thermoplastic films (*11*). Molten polymer is extruded through an annular die, and air is fed through an inner concentric bubble tube at the bottom of the die to inflate the film bubble to several times its initial diameter and decrease the film thickness by applying a circumferential tension on the film bubble. Typically, the expansion ratio between the die diameter and the final blown tube of film is described as the blow-up ratio (BUR):

$$BUR = r_f/r_0 \tag{1.1}$$

where r_f is the radius of the film bubble at the frost line height (FLH) and r_0 is the radius of the film bubble at the die exit. The BUR usually ranges up to about 3. The concentric outer air ring cools the film bubble. The temperature of the melt decreases with increasing distance from the die, which increases the viscosity of the melt and leads to the film solidification. Simultaneously, the guide rolls above the die flatten the film, and the nip rolls apply tension to the film in the machine direction (MD). The draw down ratio (DDR) is an indicator of the elongation that occurs in the MD, and it is defined as the ratio of the film velocity at the tube puller to the average film velocity at the die outlet:

$$DDR = t/(t_d \times BUR) \tag{1.2}$$

where t is the final film thickness and t_d is the width of the die gap. As the bubble travels upward from the die face in the molten state, it is cooled and eventually reaches a temperature below the softening point where it solidifies and the diameter of the

4

extruded plastic bubble stabilizes. The FLH is the distance from the die face to where this solidification takes place. Although the chemistry and molecular structure of the polymeric resin are the major factors in establishing film properties, the many processing factors, including the melt temperature, speed of cooling, DDR, and BUR, also have significant effects on bubble geometry and film properties. Blown film generally has a better balance of mechanical properties than cast or extruded films because it is drawn in both the transverse and machine directions. Various aspects of the blown film extrusion process have been studied from both modeling and experimental perspectives (*12-15*). The film bubble is then collapsed and collected as double-layer flat film. A single die can be utilized to make films with many different thicknesses and sizes by carefully controlling the BUR and DDR of the blown film process. Thus, the blown film process offers a high level of flexibility for producing a wide variety of high performance films for demanding applications. The physical properties of LLDPE films are generally known to be influenced by the processing conditions and the molecular structural parameters, such as molecular weight, molecular weight distribution, and the type, amount, and distribution of short chain branches (*16-19*). The processing conditions and molecular structures of LLDPE copolymers can greatly affect the morphological features of LLDPE films, such as preferred molecular orientation, stacked lamellar crystalline morphology, the degree of crystallinity, surface roughness, and intercrystalline connectivity, which greatly influence the mechanical properties of LLDPE films (*16, 17, 19-21*).
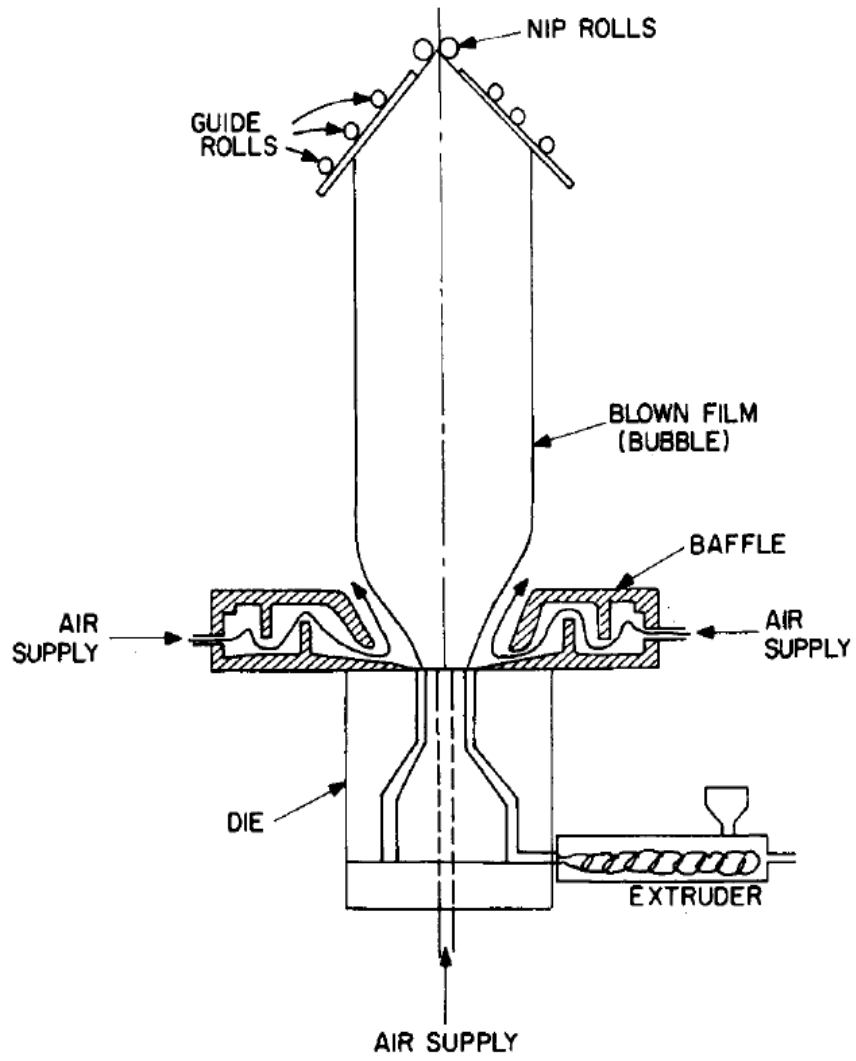
Figure 1.2. Schematic of the blown film process (*22*).

1.3 Linear Elastic Fracture Mechanics

In materials science, fracture toughness is a property which describes the ability of a material containing a crack to resist fracture, and is one of the most important properties of any material for many design applications. Fracture mechanics is the field of study in the mechanics related to the crack propagation of materials. The methods of analytical solid mechanics is applied to determine the driving force on a crack and to characterize the material's resistance to fracture. Prior to 1920, A.A. Griffith, who was the pioneer in fracture mechanics, began to study the fracture in soda-lime glasses (*23*). His work was motivated by Inglis's work in calculating the stress concentrations around elliptical holes and the findings that the observed fracture strength of glass was so much less than its theoretical strength which was estimated from the strength of atomic bonds, and the fracture stress of glass fiber increases as the fiber diameter decreases (*24*). However, the Inglis's thoery showed that the stress at the crack tip approached infinity and depended only on the geometrical shape of the crack and not its absolute size, which was contrary to the well known fact that larger cracks are propagated more easily than smaller ones. Griffith found that the low fracture strength observed in experiments, as well as the size-dependence of strength, was due to the presence of microscopic flaws in the bulk material, which caused localized stress concentrations. The highly stressed locations acted as the origins for the failures in glass. Rather than focusing on the crack-tip stresses directly, Griffith employed an energy-balance approach based on the first law of thermodynamics for the theoretical analysis of fracture (*25*). He proposed that the amount of strain energy released must be greater than or equal to the surface energy of

7

the two new crack faces, and the stress at the crack tip is a function of the stress concentration factor, which depends in the ratio of its radius of curvature to its length when the crack growth happens. The linear elastic fracture mechanics for fracture stress in an infinite elastic plate was developed by Griffith:

$$\sigma_f = \sqrt{\frac{2\gamma E}{\pi a}} \tag{1.3}$$

where E is the Young's Modulus, 2α is the initial flaw size of a non-edge flaw and γ is the surface energy of the material.

The Griffith's approach, which assumes that all mechanical energy put into a materials is used only to create new surface, are provide excellent approximation for brittle materials. When the material exhibits more ductility, consideration of the surface energy alone fails to provide an accurate model for fracture. This deficiency was later remedied by Irwin and Orowan independently (*26*). For ductile material (such as steel) which failed in a brittle manner, a plastic zone develops at the tip of the crack. The size of plastic zone increases until the crack grows, and the material behind the crack tip unloads. The energy dissipated in plastic zone has to be added to the energy balance relation devised by Griffith for brittle materials. Irwin's approach divided the energy into two parts: the stored elastic strain energy which is the thermodynamic driving force for fracture and released as a crack grows, and the dissipated energy which includes plastic dissipation and the surface energy which provides the thermodynamic resistance to fracture. The modified version of Griffith's energy criterion can then be written as:

$$\sigma_f = \sqrt{\frac{EG_c}{\pi a}} \tag{1.4}$$

where G_c is the critical strain energy release rate. Irwin and his colleagues also found a method of calculating the amount of energy available for fracture in terms of the asymptotic stress and displacement fields around a crack front in a linear elastic solid. The stress intensity factor, K, is used in fracture mechanics to represent the stress state near the tip of a crack caused by a remote load or residual stresses (*27*). Linear Elastic Fracture Mechanics (LEFM) has been used to characterize the fracture of brittle and semi-ductile polymers for decades. It is based on the assumption that a material will fracture when the intensity of the stress accumulated at a crack tip exceeds a critical value, K_{IC}, and plastic yielding is limited to a small area immediately in the vicinity of the crack tip (*28*).   In addition, Irwin also introduced three different loading modes, including mode-I, mode-II, and mode-III (Figure 1.3). However, the LEFM approach is not adequate to characterize the failure of ductile polymers, where a large plastic zone usually exists around the crack tip.
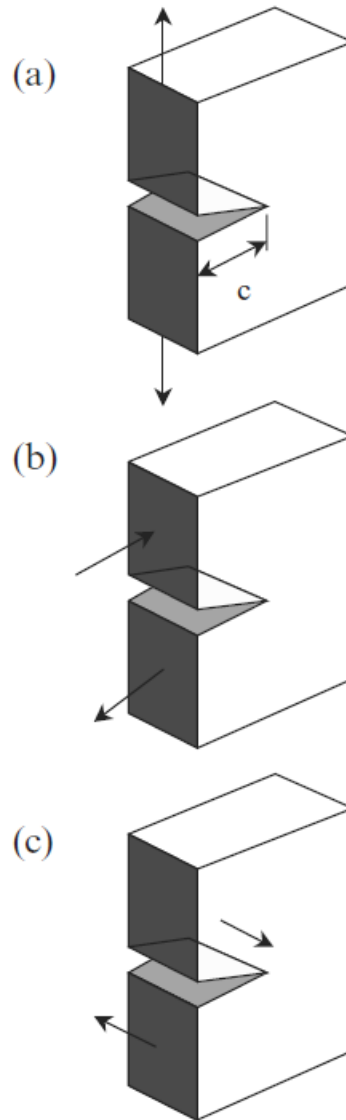
Figure 1.3. Three modes of fracture. (a) Mode I, (b) Mode II, and (c) Mode III (*24*).

1.4 J-Integral

The J-integral proposed by Rice in 1968 provided a major breakthrough to characterize the elastic-plastic fracture mechanics (*29*). The J-integral is a path independent contour integral around the crack tip, and it can be viewed as an average measurement of the crack tip elastic-plastic mechanical field. It provides the analysis of mechanical field near crack tips in both linear elastic and nonlinear elastic materials. The two-dimensional J-integral is defined as (Figure 1.4):

$$J = \int_\Gamma (w dy - T_i \frac{\partial u_i}{\partial x} ds) \tag{1.5}$$

where w is the strain energy density, T_i are components of the traction vector, u_i are the displacement vector components, and ds is a length increment along the contour Γ. J represents the rate of change of net potential energy with respect to crack advance for a non-linear elastic material, which can be considered as the energy flow into the crack tip. Thus, J is a measure of singularity strength at the crack tip for the case of elastic-plastic fracture response. The critical value, J_C, refers to crack initiation under plane strain conditions from essentially elastic to fully plastic behavior. Although the J-integral approach has been practiced for toughness characterization of ductile polymeric materials, the sample preparation procedure is quite tedious and extreme care is needed to ensure a valid critical J_C value (*30*). It is extremely difficult to meet the above requirements for thin films, and complex data collection and reduction procedures are required.

11
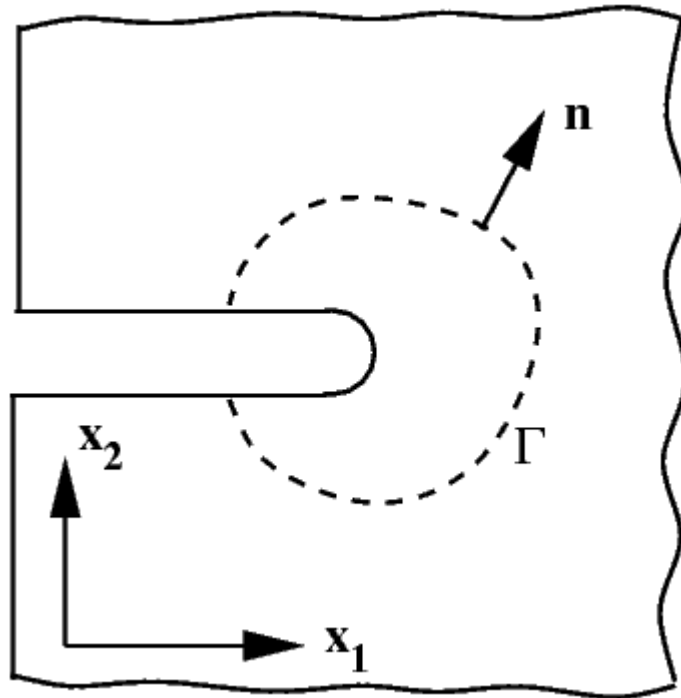
Figure 1.4. J-integral contour around a notch in two dimensions (*29*).

1.5 Essential Work of Fracture

Instead of J-integral method, essential work of fracture (EWF) approach has been implemented to quantify the fracture toughness of materials showing significant crack tip plasticity (*30-33*). The EWF approach is a much simpler technique that has gained a lot of attention and acceptance as an alternative method for determining the toughness of various ductile polymeric materials, especially for samples in the form of film or sheet geometry (*31-33*). It has earned popularity because of its simplicity in sample preparation, experimental testing, and data reduction procedure. The EWF method was originally suggested by Broberg (*34*) and then developed by Mai and Cotterell (*35-37*) to characterize the plane-stress fracture toughness of ductile materials. The fundamental concept of the EWF method is based on the energy partition, which separates the total

12

fracture energy (W_f) into two components: the essential work of fracture (W_e) and the

non-essential work of fracture (W_p):

$$W_f = W_e + W_p = w_e tL + \beta w_p tL^2 \tag{1.6}$$

$$w_f = \frac{W_f}{Lt} = w_e + \beta w_p L \tag{1.7}$$

where W_e represents the energy dissipated in the inner fracture process zone (IFPZ),

which is responsible for the creation of the fracture surface; W_p is the energy dissipated

in the outer plastic deformation zone (OPDZ); β is a shape factor associated with the

volume of the plastic deformation zone; L is the ligament length; t is the thickness of the

specimen (Figure 1.5). The specific total work of fracture (w_f) can be obtained by

normalizing W_f with the cross-sectional area of the ligament where w_e is the specific

essential work of fracture and w_p is the specific non-essential work of fracture. There is a

positive linear dependence between w_f and ligament length. The positive intercept (w_e)

indicates the crack resistance of the material, and the slope indicates the capability of the

material to dissipate energy plastically. The European Structure Integrity Society (ESIS)

has proposed a protocol specifying test conditions, including the following criterion for a

valid range of the ligament length, for the EWF test in 1997 (*38*):

$$(3t \sim 5t) \leq L \leq \min \left(\frac{W}{3}, 2R_p\right) \tag{1.8}$$

where W is the width of the specimen, and R_p is the radius of the plastic zone. The ESIS

criterion ensures that the specimen tested in the plane-stress conditions and the ligament

is fully yielded before crack propagation for the EWF analysis. Its upper limit also

allows the specimen to avoid the edge effects. The detailed description of the EWF

method can be found elsewhere (*34, 35*).

13
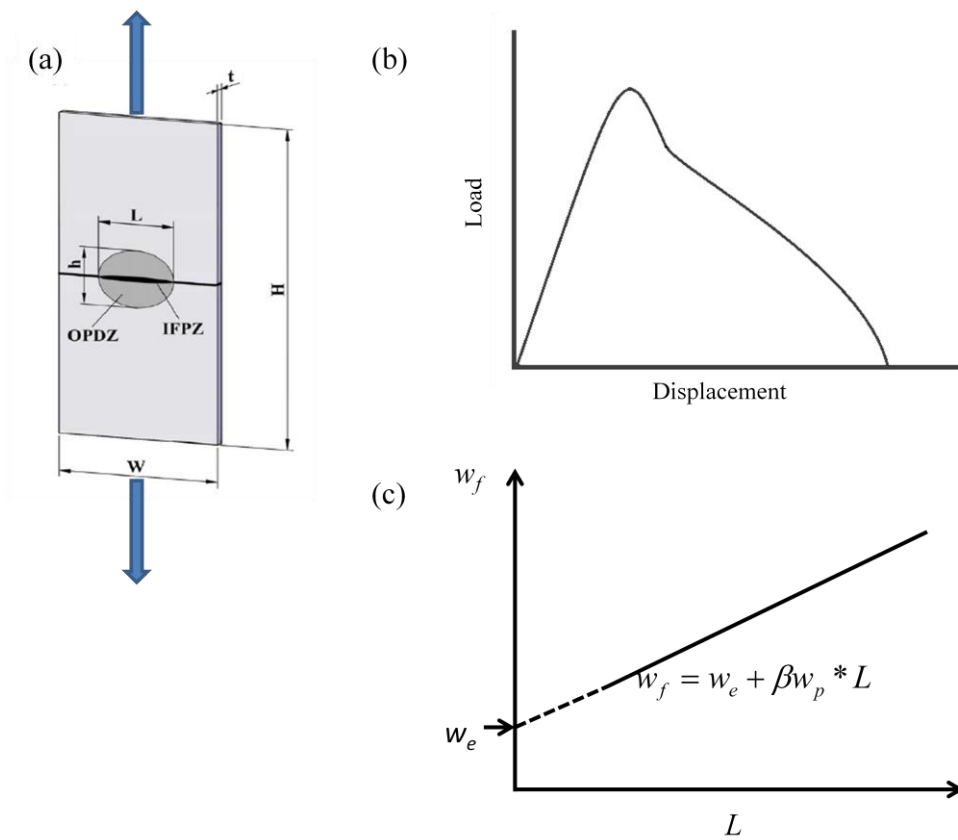
Figure 1.5. Schematic diagrams showing (a) double-edge-notch tensile specimen (*39*); (b) load-displacement curve; (c) the data reduction method of the EWF

1.6 Objectives and Overview of the Dissertation

The primary objective of this research is to gain understanding about the fracture mechanics and the processing-structure-property relationships of m-LLDPE thin film. To achieve the objective of this research, the project can be divided into three parts. The first part is to develop a new film fixture to provide sensitive, reproducible, and consistent measurements for characterizing the Mode-I DENT fracture toughness of m-LLDPE films and to validate the effectiveness and capability of the EWF method for investigating the fracture performance of ductile polymeric blown films. Second, based on the newly developed experimental setup and the EWF method, the effects of the film orientations, processing parameters, and density on the Mode-I fracture toughness of m-LLDPE films are investigated. Third, a new method is developed to partition and quantify the fracture energy dissipation in different deformation zones of the Mode-I DENT m-LLDPE film specimens to gain insights about the underlying physics and its correlation with EWF parameters.

The development of the new film fixture mainly focuses on eliminating the out-of-plane buckling without interfering with the fracture process to provide sensitive, reproducible, and consistent measurements with minimal data scattering for the EWF analysis on the Mode-I DENT m-LLDPE film specimens. The out-of-plane buckling is due to the limited geometric stability of m-LLDPE films under tensile loading when using the traditional fixture, and it probably alters the stress distribution within the ligament zone. The new film fixture is designed to reinforce the mechanical stability of m-LLDPE films to counteract the Poisson effect, which leads to the out-of-plane

buckling. The effects of testing conditions, including testing speed, gauge length, and specimen width on the EWF parameters, are examined to validate the effectiveness and capability of the EWF method for investigating the fracture performance of ductile polymeric blown films.

The experimental approach, which is based on the new film fixture and the EWF method, is further utilized to study the effects of the film orientations, DDR, BUR, FLH, haze-zone region, and density on the mode-I fracture toughness of m-LLDPE films. The morphological observation and Elmendorf test are also performed on m-LLDPE films with different processing conditions. The film geometric development during the EWF test, especially within the necked zone, is carefully analyzed. Correlation between EWF parameters and the tear resistance of m-LLDPE blown films is also investigated.

To understand the underlying physics and its correlation with EWF parameters, it is necessary to experimentally quantify the energy absorption by m-LLDPE films in the regions of crack propagation (W_e) and plastic deformation (W_p), and, possibly, a new viscoelastic deformation zone (W_v) under the Mode-I tensile loading. To partition the fracture energy dissipation in different deformation zones of the Mode-I m-LLDPE films, it is necessary to determine the size of each deformation zone and the corresponding true stress - true strain curves. The comparison between the experimental measurements and the EWF estimations in fracture energy dissipation in different deformation zones provides important insights into the physics behind the fracture energy dissipation and the EWF method.

This research provides a useful and reliable technique, which is based on the EWF method and the newly developed film fixture, to characterize the fracture performance of ductile polymeric thin films. It also provides insights toward the fracture mechanics and the processing-structure-property relationships of m-LLDPE thin film and the physics behind the EWF method.

CHAPTER II

REFINED FIXTURE DESIGN FOR EFFECTIVE ESSENTIAL WORK OF

FRACTURE TOUGHNESS CHARACTERIZATION OF M-LLDPE THIN FILMS*

Linear low-density polyethylenes (LLDPE) have been widely used in the packaging industry due to superior mechanical and thermal properties. The properties of LLDPE, that is composed of ethylene and a small amount of α-olefin comonomers, are strongly affected by the level and distribution of short chain branching. The number and length of short chain branches are correlated to the concentration and type of α-olefin while the distribution of branches is dependent on the polymerization conditions (*7, 8*). About 70% of commercial LLDPE resins have been used to produce thin blown films. There have been only a handful of investigations focusing on both the fracture mechanics and the processing-structure-property relationships of ductile polymeric thin film (*11, 40-42*).

Most commodity and specialty packaging films are made by blown film extrusion processes. The film blowing process consists of extruding a tube of molten thermoplastic and inflating it to several times its initial diameter to form a thin tubular polymeric film. Typically, the expansion ratio between the die diameter and the final blown tube of film ranges up to about 3. The melt's temperature decreases with

_____

increasing distance from the die, and it varies around the die exit that leads to localized differences in the morphology of polymeric film (Figure 2.1). These differences lead to haze bands and clear zones across the film. To characterize the fracture toughness of polymeric films, the above morphological variations have to be taken into account. The technique utilized for the measurement needs to be sensitive to the above morphological variation and highly reproducible, with minimal data scattering.
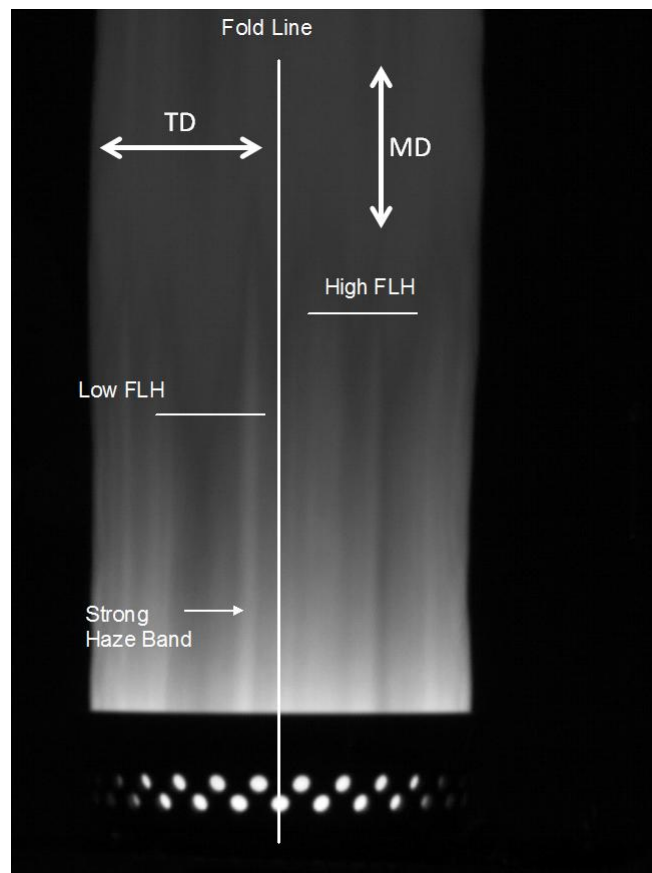
Figure 2.1. Infrared image of 0.030 mm, 2.5 BUR LLDPE blown film.

Linear Elastic Fracture Mechanics (LEFM) has been used to characterize the fracture of brittle and semi-ductile polymers for decades. It is based on the assumption that a material will fracture when the intensity of the stress accumulated at a crack tip exceeds a critical value, K_{IC}, and plastic yielding is limited to a small area immediately in the vicinity of the crack tip (*28*). The LEFM approach is not adequate to characterize the failure of ductile polymers, where a large plastic zone usually exists around the crack tip. Instead, J-integral and Essential Work of Fracture (EWF) approaches have been implemented to quantify the fracture toughness of materials showing significant crack tip plasticity (*30-33*). Although the J-integral approach has been practiced for toughness characterization of ductile polymeric materials, the sample preparation procedure is quite tedious and extreme care is needed to ensure valid critical J_C value (*28*). It is extremely difficult to meet the above requirements for thin films, and complex data collection and reduction procedures are required.

The EWF approach is a much simpler technique that has gained lots of attention and acceptance as an alternative method for determining the toughness of various ductile polymeric materials, especially for samples in the form of film or sheet geometry (*31-33*). It has earned popularity because of its simplicity in sample preparation, experimental testing, and data reduction procedure. The EWF method was originally suggested by Broberg (*34*) and then developed by Mai and Cotterell (*35-37*) to characterize plane-stress fracture toughness of ductile materials. The EWF methodology offers an attractive means to separate the fracture energy involved in the development of the process zone into the specific essential work of fracture, w_e, and the specific non-

essential work of fracture, w_p. There is a positive linear dependence between the specific total work of fracture and ligament length. The positive intercept (w_e) which indicates the crack resistance of the material, and the slope indicates the capability of the material to dissipate energy plastically. The European Structure Integrity Society (ESIS) has proposed a protocol specifying test conditions for the EWF test in 1997 (*38*).

Although the EWF method has been widely applied to studying the fracture mechanics of many ductile materials, its application to polymer thin films is still problematic due to the films' limited geometric stability under tensile loading. Previous studies indicated that elastic film with high length-to-thickness ratio would exert a region of compressive stress in the specimen and causes an out-of-plane buckling under in-plane tensile loading (*36*). The buckling would likely alter the stress distribution within the ligament zone (*41*) and lead to inaccurate EWF results. In this paper, we demonstrate the effectiveness of a custom-built film fixture to minimize the buckling of m-LLDPE thin films evaluated using the double-edge-notched tension (DENT) setup for the EWF analysis.

Consistent and reproducible results in the EWF analysis are expected since the out-of-plane buckling in the DENT experiments is eliminated. This EWF approach is employed to investigate mode-I fracture toughness of m-LLDPE films and to validate its usefulness and capability of fracture toughness characterization. The effects of testing speed, gauge length, specimen width, orientation and film thickness on the EWF parameters are examined. The implication of the present study for structure-property correlation of m-LLDPE blown films is discussed.

21

2.1 Essential Work of Fracture

The fundamental concept of the EWF method is based on the energy partition, which separates the total fracture energy (W_f) into two components: the essential work of fracture (W_e) and the non-essential works of fracture (W_p):

$$W_f = W_e + W_p = w_e tL + \beta w_p tL^2 \tag{2.1}$$

$$W_e = w_e tL \tag{2.2}$$

$$W_p = \beta w_p tL^2 \tag{2.3}$$

Where W_e represents the energy dissipated in the inner fracture process zone (IFPZ), which is responsible for creation of the fracture surface; W_p is the energy dissipated in the outer plastic deformation zone (OPDZ), not related to the creation of the fracture surface; β is a shape factor associated with the volume of the plastic deformation zone; L is the ligament length; and t is the thickness of the specimen. The specific total work of fracture (w_f) can be expressed as:

$$w_f = \frac{W_f}{Lt} = w_e + \beta w_p L \tag{2.4}$$

Therefore, there is a linear relationship between w_f and L, where w_e, the specific essential work of fracture, can be obtained from the y-axis intercept and βw_p, the specific non-essential work of fracture, can be obtained from the slope of the curve. The ESIS protocol for EWF recommends the following criterion for a valid range of the ligament length:

$$(3t \sim 5t) \leq L \leq \min \left(\frac{W}{3}, 2R_p \right) \tag{2.5}$$

W is the width of the specimen, and R_p is the radius of the plastic zone. The ESIS criterion ensures the specimen tested in plane-stress conditions and the ligament were fully yielded before crack propagation for the EWF analysis. Its upper limit also keeps the specimen away from edge effects. The detailed description of the EWF method could be found elsewhere (*34, 35*).

2.2 Materials and Experimental Details

2.2.1 Materials and Sample Preparation

m-LLDPE (Exceed[TM] PE 1018) blown films were provided by ExxonMobil Chemical. Exceed 1018 is a metallocene ethylene-hexene copolymer. It has a density of 0.918 g/cm^3, a melt index of 1.0 g/10 min and a peak melting temperature at 119°C. Three different thicknesses (0.019, 0.030, and 0.076 mm) of m-LLDPE blown films with a blow-up ratio (BUR) of 2.5 were chosen for this study. The EWF test specimens with width and length dimensions of 153 x 280 mm were prepared from the film stock prior to being assembled in a customized film fixture.

2.2.2 Film Fixture and Tensile Test

There were three major features of the customized film fixture that exerted sufficient in-plane constraints on the sides of the test specimen and eliminated out-of-plane buckling. These features include: increase of the specimen's width/height ratio, introduction of a pair of customized U-clamps to hold the film flat, and inclusion of U-clamps with additional masking tapes (Figure 2.2).

23

(a) Fixture Alone

(b) Fixture + U-Clamps

(c) Fixture + U-Clamps + Masking Tape

(d) Masking Tape

(e) Observation with Cross-Polarizer

1 2 3

4 5 6
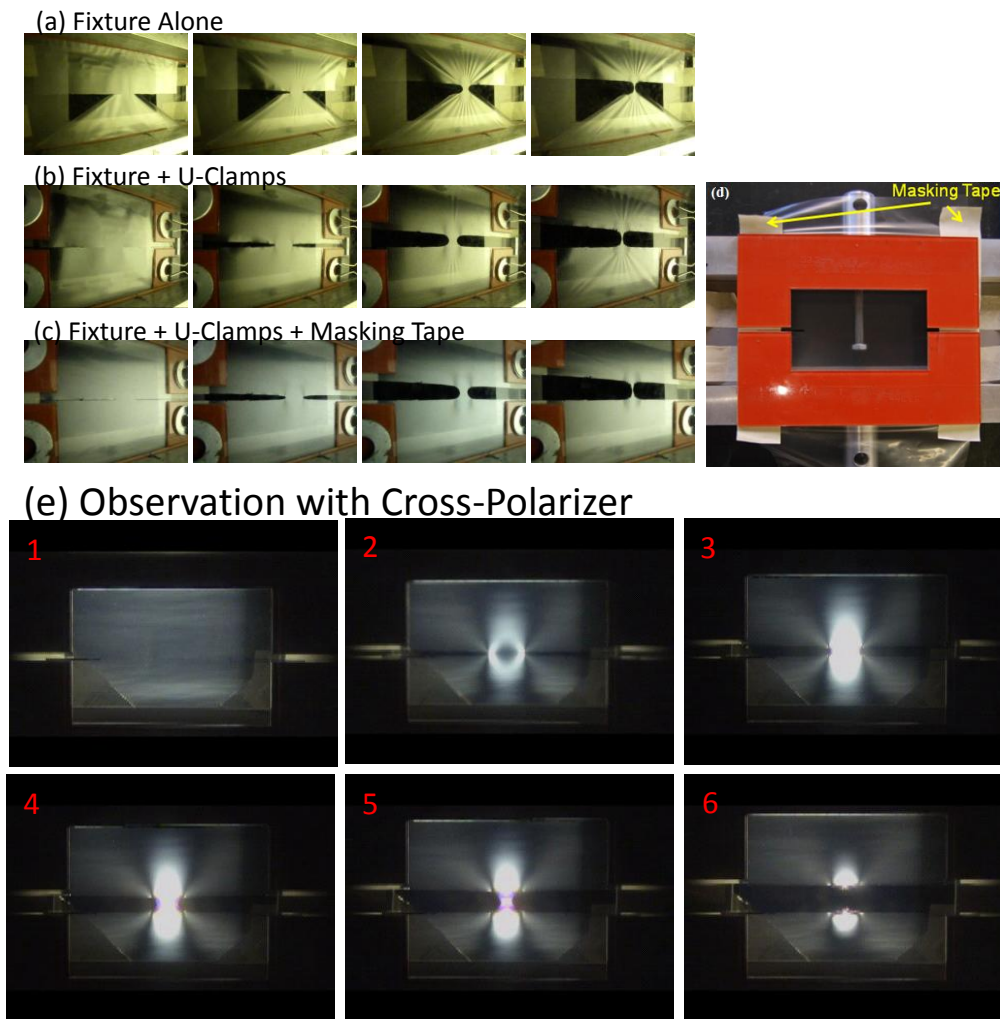
Figure 2.2. Observation of film buckling and stress distribution on DENT LLDPE films with different film fixture modifications. (a) Fixture alone; (b) Fixture with U-clamps; (c) Fixture with U-clamps and additional side constraints; (d) Experimental setup with film fixture, U-clamps, and masking tape; (e) Photoelastic observation of the experimental setup in (c).

After assembling the m-LLDPE thin film in the custom-built film fixture, a fresh razor blade was used to prepare notches in every DENT specimen. The ligament lengths were chosen to be 10 mm, 16 mm, 20 mm, 26 mm, and 30 mm. Three sets of tests were carried out for each test condition and specimen geometry for statistical purposes. All tests were performed on a custom-built tensile tester with a load cell capacity of 445 N operated at room temperature.

Several factors can possibly affect the EWF test result: fixture, crosshead speed, specimen width, film orientation, film thickness, film location and etc. To evaluate the effects of specimen geometry and testing condition, the following experiments were conducted. A) To check the consistency and reproducibility of the EWF analysis, 0.030 mm-thick m-LLDPE film made with a 2.5 BUR were tested in the MD under a crosshead speed of 10 mm/min and a gauge length of 110 mm with and without using the new film fixture. B) The effect of crosshead speed on the film's EWF was evaluated using 0.030 mm-thick film made with a 2.5 BUR at room temperature with crosshead speeds of 2, 10 and 50 mm/min. C) The effect of the gauge length was also studied using 0.030 mm-thick film made with a 2.5 BUR for the gauge length varying from 20 mm to 110 mm. D) The influence of the specimen width on EWF parameters was studied using a 0.030 mm-thick film made with a 2.5 BUR for the specimen widths varying from 50 mm to 117 mm. E) To evaluate the influence of film orientation on EWF, 0.030 mm-thick m-LLDPE films made with a 2.5 BUR were tested for crack propagation in both MD and transverse direction (TD). F) m-LLDPE films with thicknesses of 0.019 mm, 0.030 mm, and 0.076 mm with a 2.5 BUR were used to characterize the effects of the

25

film thickness on the EWF behavior. All of the samples were tested at a crosshead speed of 10 mm/min unless otherwise specified.

2.2.3 In-situ Film Deformation Analysis

Photoelasticity is a nondestructive, whole-field graphic stress-analysis technique based on the stress-optical property of birefringence. Birefringence is the decomposition of light into rays when it passes through anisotropic materials. Tensile loading can induce molecular orientation, thus anisotropy of m-LLDPE films. Under cross-polarizer observation, stressed material usually exhibits birefringence patterns related to differences between the principal stresses in a plane normal to the light propagation direction. The birefringence measurement setup consists of a light source, a polarizer, the specimen of interest and an analyzer that is always crossed with respect to the polarizer. The technique provides a reliable full-field stress distribution analysis of the DENT specimen under tensile loading. A Sony camcorder was used to record the birefringence development of the DENT specimens, crack propagation and the size of OPDZ.

2.3 Results and Discussion

2.3.1 EWF Tests and Reproducibility

On tensile loading, m-LLDPE thin films would become highly undulated without additional geometric constraints to the films. This out-of-plane buckling would greatly alter the stress distribution within the ligament zone of the films and lead to

inconsistency in the EWF analysis (*43, 44*). Figure 2.2 shows how the out-of-plane

buckling can be eliminated by applying additional side constraints to the m-LLDPE thin

film. An increase in specimen width alone can only reduce buckling slightly. If the film

is not mechanically strong, the setup will still cause additional stress complexity and

mixed mode fracture in the ligament zone (Figure 2.2a). With utilization of a pair of

customized U-shaped clamps to hold the film flat, a significant reduction in out-of-plane

buckling is obtained even when the film's width is reduced from 153 mm to 117 mm

(Figure 2.2b). The–buckling can be fully eliminated by reinforcing the clamp with

masking tape applied to both sides of the film prior to the assembly of the film fixture

(Figure 2.2d). Figure 2.2c shows that the out-of-plane buckling is completely eliminated

and the film remains flat during testing. The above setup is then used to study the effects

of testing condition, specimen geometry, and film orientation on the EWF fracture

toughness of m-LLDPE thin films. The observation using a cross-polarization setup

shows development of two symmetric birefringent patterns from both notches of the

DENT specimen, which clearly suggests that the above experimental setup is adequate

for mode-I fracture toughness characterization of ductile polymeric thin films (Figure

2.2e).

To check the consistency and reproducibility of the EWF analysis using the new

film fixture, the plots of w_f versus L within the ligament length range of 5 mm $\leq L \leq$ 30

mm are shown in Figure 2.3. The new fixture setup greatly reduces test variability and

minimizes the scattering of data compared to not using the custom-built U-shape fixture.

In addition, the EWF parameters are reproducible between three separate tests on three

separate occasions with the new film fixture setup. This finding demonstrates that the film fixture employed in this study is adequate and suitable for mode-I EWF fracture toughness measurements of ductile polymeric thin films.
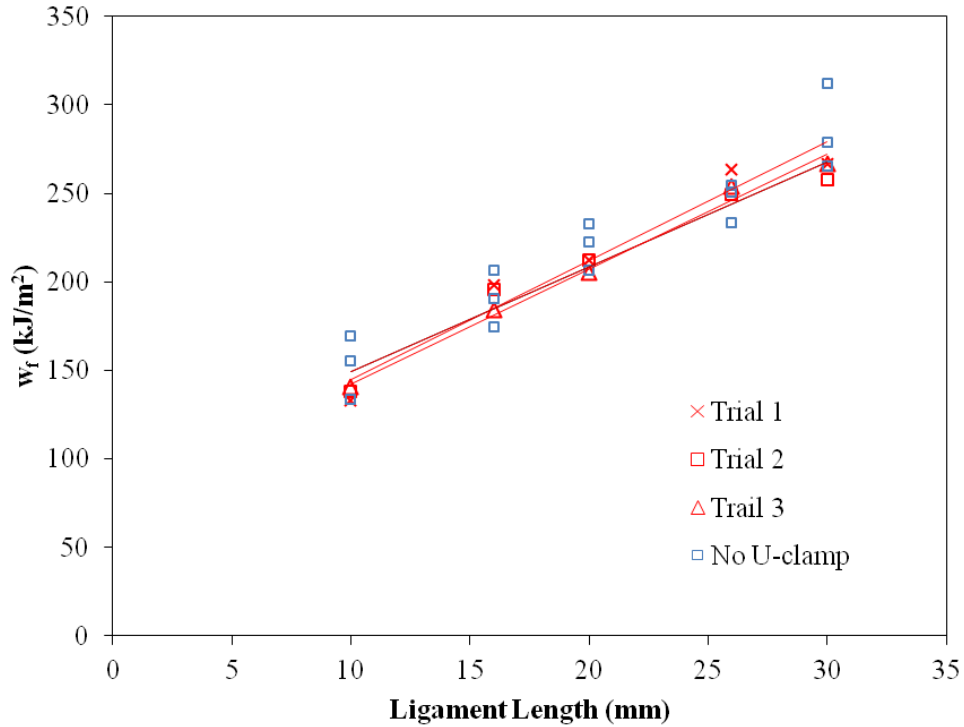
Trial	w_e (kJ/m^2)	βw_p (MJ/m^3)	R^2
New Fixture	54.3 ± 5.1	4.26 ± 0.24	0.98
No U-clamp	59.1 ± 8.3	4.26 ± 0.38	0.95

Figure 2.3. Consistency and reproducibility of the EWF analysis with the newly-modified film fixture (Figure 2.1c).

From detailed analyses of the load-displacement curves of 0.030 mm-thick film made with a 2.5 BUR, both the maximum crosshead displacement and maximum load were found to increase linearly with an increase in the ligament length (Figure 2.4). The DENT specimens with larger ligament lengths withstand higher loads before yielding

and stretches longer before film breakage. Further, photoelastic observation of the fracture process was performed on m-LLDPE blown films made with a BUR of 2.5 and thicknesses of 0.019, 0.030, and 0.076 mm. The photoelastic characterizations of m-LLDPE blown films were also carried out in both MD and TD. The maximum crosshead displacement was higher for thicker films and for crack propagation in the TD (Figure 2.5a). The thicker films possess larger OPDZ areas than thinner films, and films with crack propagation in the TD also have larger OPDZ areas than those with crack propagation in the MD (Figure 2.5b).
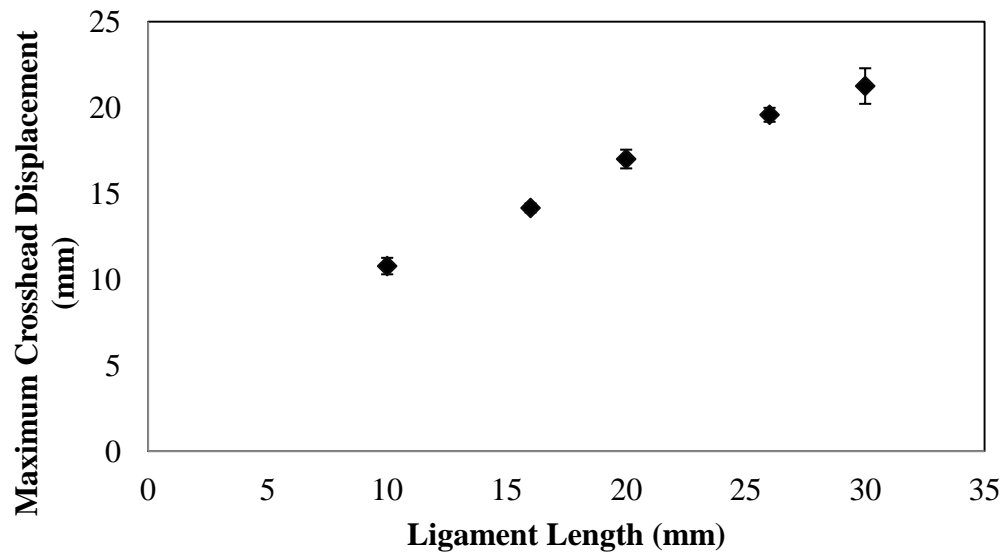
(a)
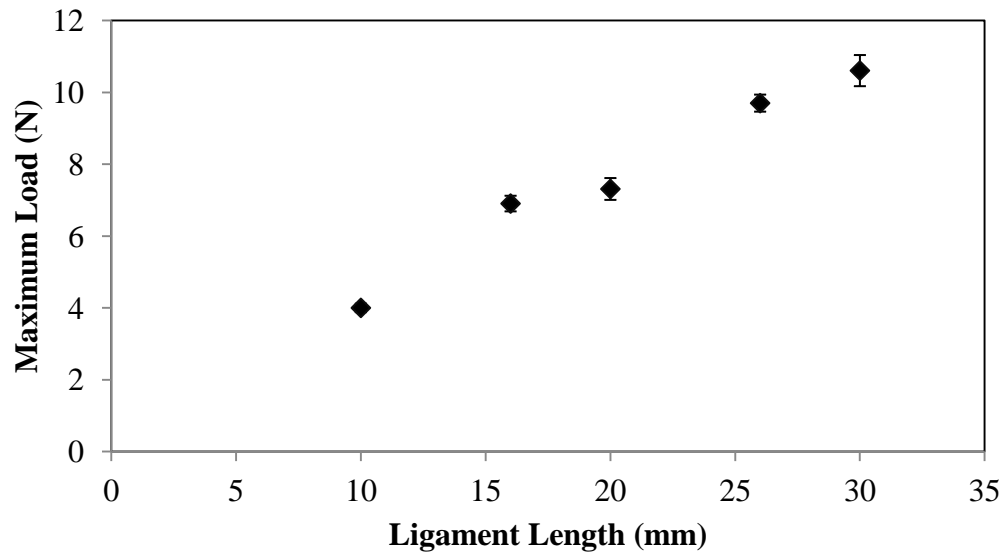
(b)

Figure 2.4. (a) Maximum crosshead displacement versus ligament length. (b) Maximum load versus ligament length.
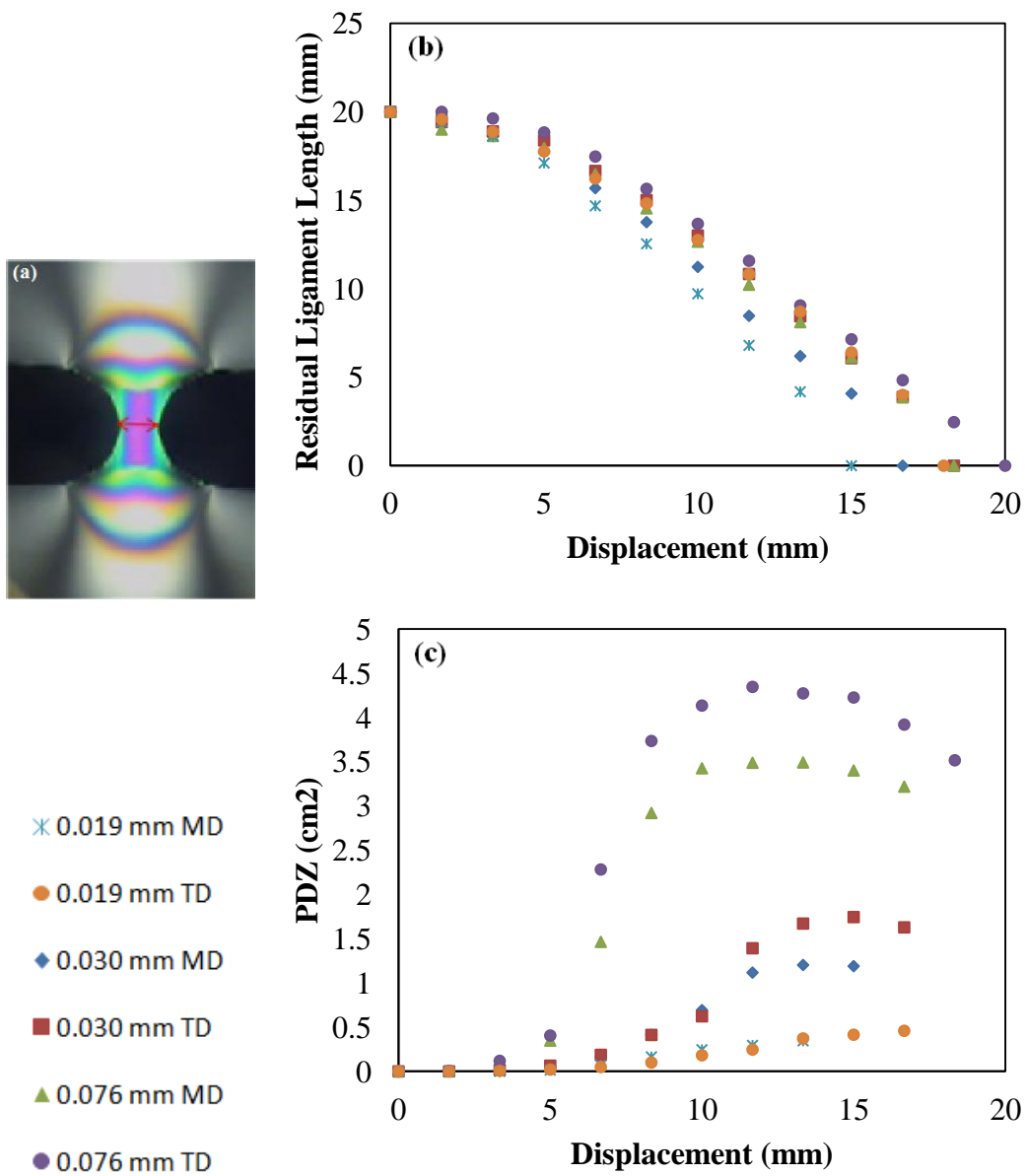
Figure 2.5. (a) Photoelastic observation of crack propagation and OPDZ; (b) Observation of crack propagation at different crosshead displacements; (c) OPDZ areas of DENT LLDPE films at different crosshead displacements.

31

2.3.2 Crosshead Speed Effect

The effect of crosshead speed on EWF behavior was evaluated. Plots of w_f versus L for different crosshead speeds within the valid ligament length range of 5 mm $\leq L \leq$ 30 mm are shown in Figure 2.6. All samples failed in a ductile manner. Both w_e and βw_p were insensitive to the crosshead speed within the chosen range tested (Figure 6). In the literature, there have been conflicting findings on the effect crosshead speed has on w_e and βw_p. Some reports showed consistent result (*33, 45*), as shown here. Others showed reports showed either w_e (*41, 46, 47*) and/or βw_p (*40-42, 47-51*) depends on crosshead speed. The inconsistent findings can be attributed to either the viscoelastic nature of polymers or the plane stress-plane strain transition in fracture behaviors of ductile materials. Although an extremely high loading rate can lead to brittle fracture and may affect both EWF parameters, the loading rate within the chosen range of crosshead speeds does not influence the EWF results for the m-LLDPE films investigated here.
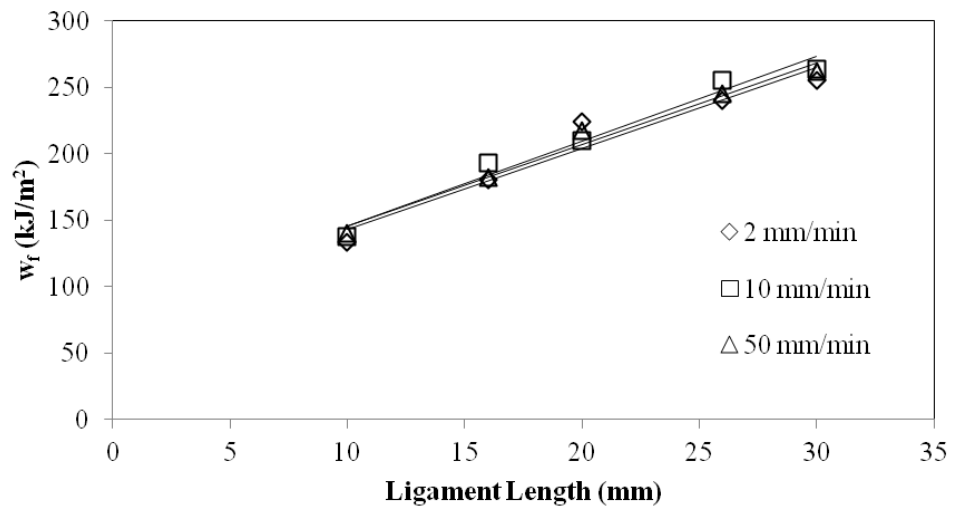
Testing Rate (mm/min)	w_e (kJ/m^2)	βw_p (MJ/m^3)
2	82.6	6.08
10	81.5	6.39
50	84.1	6.15

Figure 2.6. Specific work of fracture versus ligament length at different loading rates.

2.3.3 Gauge Length Effect

The effect of the gauge length was studied and plots of w_f versus L for different gauge lengths are shown in Figure 2.7. Linear regression lines were obtained by using data inside the valid ligament length range (5 mm $\leq$ L $\leq$ 30 mm). From the results shown, both w_e and βw_p are insensitive to the gauge length within the chosen range investigated (Figure 2.7).

Arkhireyeva et al., Ching et al., Maspoch et al., and Hashemi all have indicated that both w_e and βw_p are independent of the gauge length for various polymeric materials (*40-42, 44, 50*). The results suggest that implementing the new fixture shows no influence of the gauge length on the EWF behavior. Ching et al. indicated that brittle fracture might occur for specimens with longer gauge length, and the minimum ligament length at which ductile/brittle transition took place decreased with increasing gauge length (*48*). The gauge length needs to be large enough to minimize its influence on the plastic deformation zone (PDZ) but small enough to prevent excess stress accumulation and brittle fracture at the ligament region. Our observation with cross-polarizers indicates that the film fixture for gauge length < 50 mm interferes with the birefringent deformation zone, but the interference does not seem to affect the measured EWF parameters.
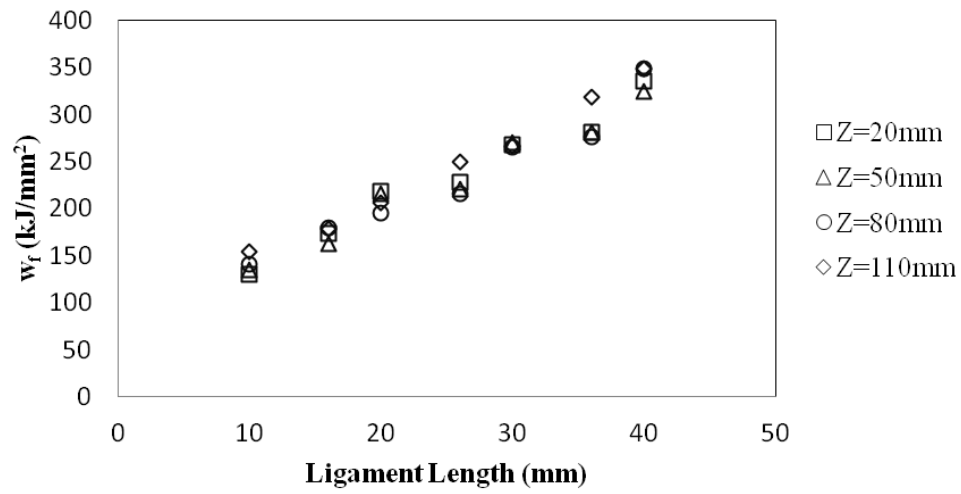
Gauge Length (mm)	βw_p (MJ/m^3)	w_e (kJ/m^2)
110	6.59	78.3
80	6.29	72.1
50	6.11	74.8
20	6.22	75.3

Figure 2.7. Specific work of fracture versus ligament length at different gauge lengths.

2.3.4 Specimen width Effect

The influence of the specimen width on EWF parameters was studied, and plots of w_f versus L for different specimen widths are shown in Figure 2.8. Both w_e and βw_p are insensitive to the specimen width within the chosen range investigated (Figure 2.8). Hence, the chosen range of specimen width does not cause a boundary effect to interfere with the plastic zone formation using the new fixture setup.

Previous studies showed different responses of EWF parameters on the specimen width. Chan et al. showed that w_e increases with specimen width, but βw_p decreases with increasing width for PE sheets (*33*). Arkhireyeva et al. found that w_e and βw_p are independent of specimen width for plane stress condition (*42*). Hashemi showed that there is no effect of the specimen width on the EWF parameters of polybutylene terephthalate (PBT) film (*52*). However, the specimen width does influence both EWF parameters for high impact polystyrene sheets, with w_e increasing and βw_p decreasing with sheet width (*40*). It should be noted that ESIS has set an upper limit of the ligament criterion to prevent the specimen boundary effect on EWF parameters. Many previous studies with various ductile materials have shown that the upper limit of the ligament criterion set by ESIS is too restrictive (*33, 39, 41, 53*). They find that the plots of w_f vs. L generally follow the linear regression line even when the ligament length is beyond the upper limit. Overall, the new fixture introduced here does not show any influence of the specimen width to the EWF parameters.
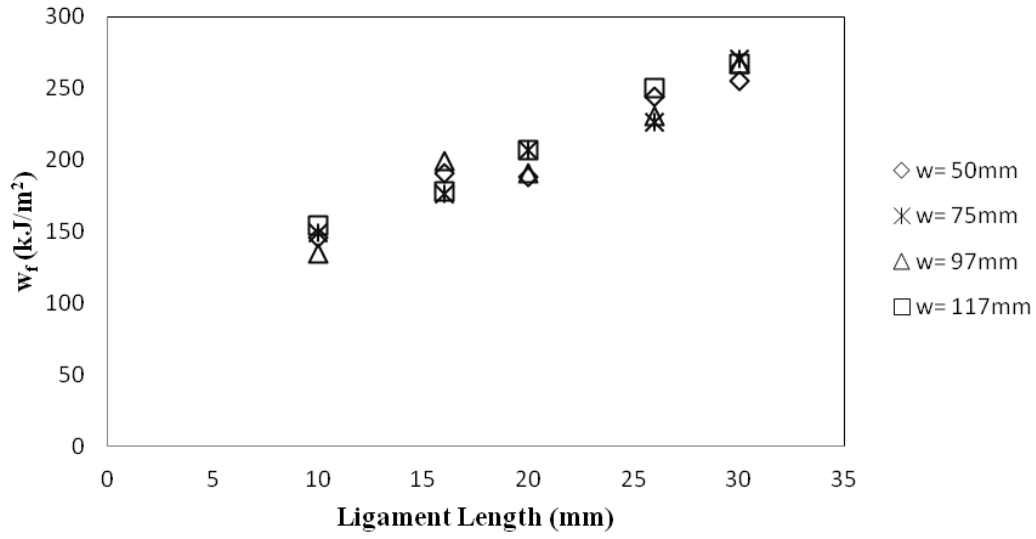
Figure 2.8. Specific work of fracture versus ligament length at different specimen widths.

2.3.5 Film Thickness Effect

The effect of film thickness on the EWF behavior was determined using m-LLDPE films with thicknesses of 0.019 mm, 0.030 mm, and 0.076 mm made using a 2.5 BUR. Plots of w_f vs. L for three different film thicknesses are shown in Figure 2.9. Linear regression lines were obtained by using data inside the ligament length range (5 mm $< L <$ 30 mm). Figure 2.10 shows w_e significantly increased with decreasing film thickness, but no clear trend in the change of βw_p. The literature has shown conflicting findings regarding the effect of film thickness on the EWF parameters. Maspoch, et al., found a decrease in w_e with an increase in film thickness for isotactic PP (iPP) films, with no clear trend of change for βw_p (*41*). Ching, et al., Maspoch, et al., and Hashemi discovered that w_e is relatively independent of specimen thickness, but βw_p changes with increasing specimen thickness (*46, 47, 52*). Zhang, et al., found m-LLDPE blown film

37

made with a greater draw down ratio (DDR) tends to have more a-axis orientation in the MD and small b-axis orientation perpendicular to the MD (*54*). This finding explains why thinner films exhibit higher resistance to crack initiation and propagation in the MD.
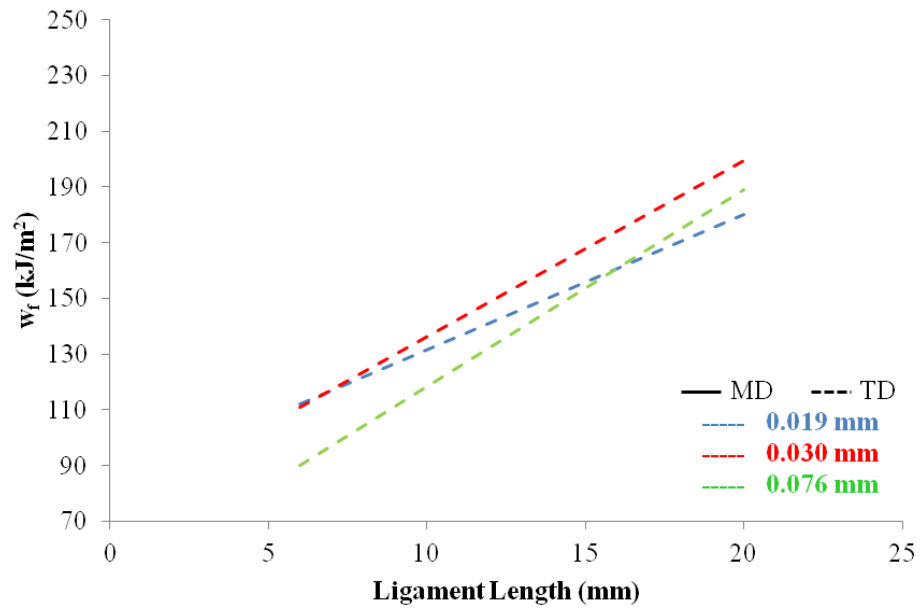
Figure 2.9. Specific work of fracture versus ligament length at different film thicknesses for crack propagation along TD.
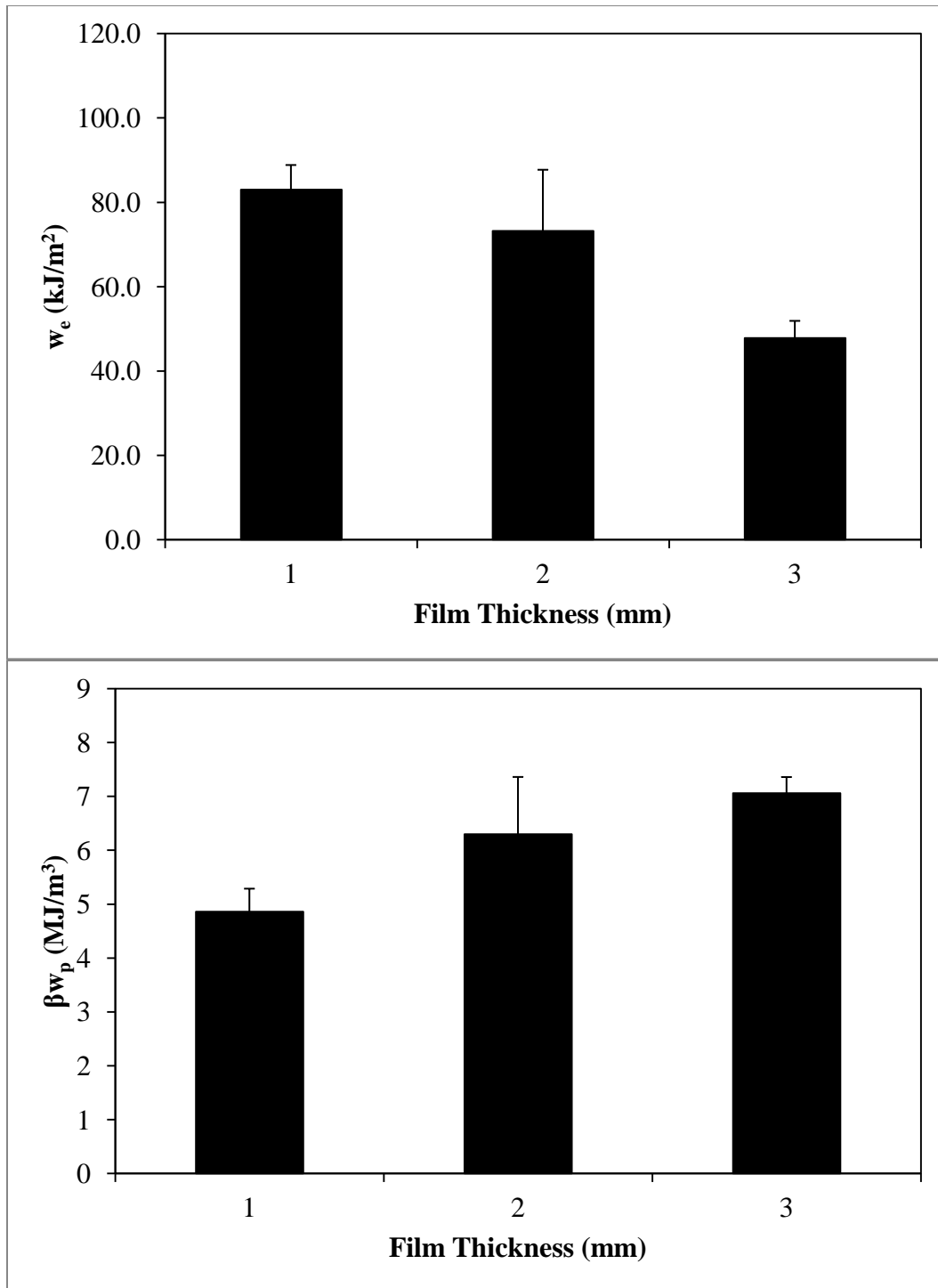
Figure 2.10. (a) Specific essential work of fracture and (b) non-specific essential work of fracture of Exceed^{TM} 1018 m-LLDPE blown film with different thicknesses for for crack propagation along TD.

2.3.6 Film Orientation Effect

To evaluate the influence of film orientation on EWF results, plots of w_f versus L for crack propagation in both MD and TD were examined (Figure 2.11). The EWF parameters, w_e and βw_p, are significantly greater in the TD than in the MD. Maspoch, et al., found w_e is greater in the MD than in the TD, and βw_p is independent of the molecular orientation for iPP films (*41*). Previous studies have shown that m-LLDPE blown films have more crystal and amorphous phase orientation along the MD, which correlates with greater MD strength and TD tear resistance (*54, 55*). This observation is consistent with our current finding that the films in the TD have a greater resistance in crack initiation and propagation and dissipate more energy in the plastic deformation zone. Thus, films tested in the TD possess higher fracture toughness values.

The application of the EWF method to ductile polymeric thin films has been tentative due to lack of mechanical stability under tensile loading. The out-of-plane buckling and out-of-pane collapse under an in-plane tensile loading may lead to stress complexity, inconsistent data, invalid testing results and mixed mode fracture. Our newly modified film fixture eliminates out-of-plane buckling and ensures mechanical stability in ductile polymeric thin films under Mode-I fracture. It greatly improves the consistency and reproducibility of valid EWF analysis on polymeric thin films. The crosshead speed, gauge length, and specimen width exhibit no effect on the EWF results within the ranges tested. While different film thicknesses for the same BUR achieved by different DDR exhibit different degrees of preferential crystalline orientation, w_e is significantly higher for thinner films. Furthermore, film in the TD has higher fracture

resistance and can dissipate more energy in OPDZ than in the MD because of higher

degrees of crystal and amorphous phase orientation along the MD.
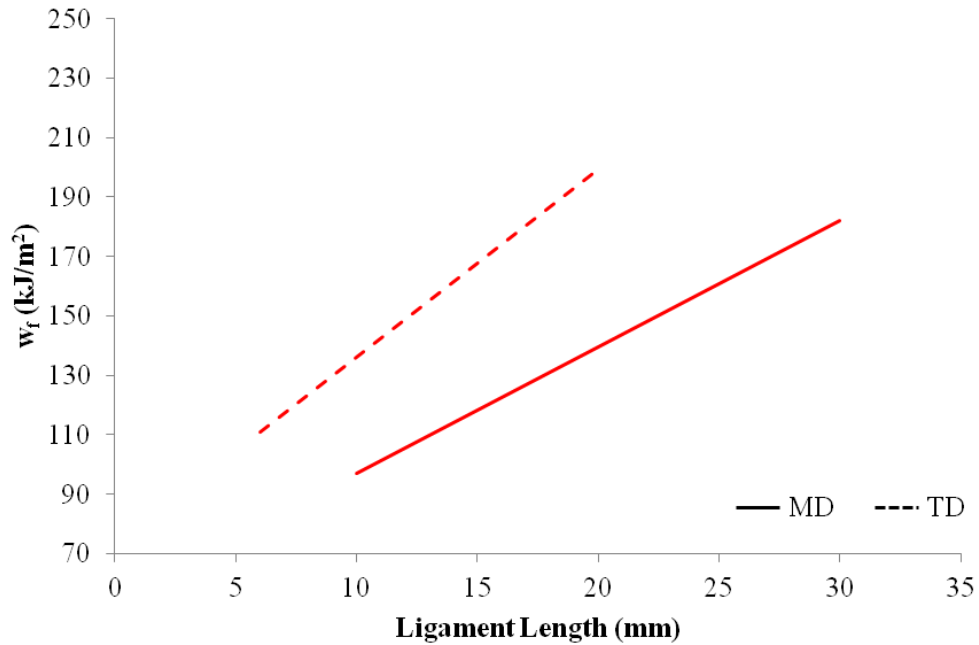
Figure 2.11. Specific work of fracture versus ligament length for different film orientations of Exceed[TM] 1018 m-LLDPE blown film with thickness of 0.030 mm.

In summary, the newly modified film fixture successfully provides a reliable

solution to the problematic characterization of Mode-I fracture toughness of ductile

polymeric thin films, and to greatly improve consistency and reproducibility in the EWF

analysis. Combination of the EWF and new fixture setup is capable of accurately

determining the fracture toughness of ductile polymeric thin films having different

material properties and morphological characteristics without concerning the influence

of testing condition and specimen geometry. The observed accuracy and reproducibility

41

of the EWF analysis is essential for our further study on process-structure-property relationships of ductile polymeric thin films, which will be reported in a separate paper.

2.4 Conclusions

A newly modified film fixture capable of eliminating out-of-plane buckling has been constructed to ensure mechanical stability of polymeric thin films during Mode-I EWF testing. The effects of specimen geometry and testing conditions, such as crosshead speed, gauge length, specimen width, film thickness, of m-LLDPE thin films were investigated and found to have no significant influence to the EWF parameters within the chosen ranges tested. However, film orientation and film thickness were found to have a significant influence on EWF results. Furthermore, the film in the TD has higher fracture toughness than that in the MD. The effectiveness of the EWF analysis and new fixture setup combination for determining the fracture toughness of polymeric thin films was demonstrated.

CHAPTER III

EFFECT OF PROCESSING PARAMETERS ON ESSENTIAL WORK OF

FRACTURE TOUGHNESS OF LLDPE BLOWN FILMS

Linear low-density polyethylene (LLDPE) is the most widely used material for film due to its diverse applications such as packaging for snack foods, produce, medical and pharmaceutical products, and stretch and shrink-wraps. The high ductility, strength, durability, and relatively low cost make it attractive for various applications, with 70% of the commercial LLDPE films being produced through the blown film extrusion process (*4-6*). Although there has been wide usage of the blown films, only few investigations focused on the films' fracture mechanics and processing-structure-property relationships to-date (*11, 40-42*).

In the blown film process, molten polymer is extruded through an annular die. Air is fed through an inner tube at the center of the die causing the extruded melt to inflate into a film bubble with diameters several times the die's diameter, accompanied by a decrease in film thickness. A concentric air ring cools the film bubble just above the die. The temperature of the melt decreases with increasing distance from the die. The temperature reduction increases the viscosity of the melt, induces crystallization, and leads to film solidification (*22*). The distance from the die face to where solidification takes place is called the frost-line-height (FLH). At the frost line, the bubble is at its maximum diameter and there is effectively no further stretching. Guide rolls located above the FLH flatten and collapse the film into a double-layer flat film as nip rolls

43

apply tension to the film and pull it in the machine direction (MD) away from the die. A single die can make films with many different thicknesses and sizes by controlling the processing conditions of the blown film process. Typically, the expansion ratio between the die diameter and that of the final film bubble is defined as the blow-up-ratio (BUR). The draw-down-ratio (DDR) is an indicator of the elongation that occurs in the MD, and it is defined as the ratio of die gap to the film's thickness.

The blown film process offers a high level of flexibility for producing a wide variety of high performance films for demanding applications with processing variables significantly influencing the film's morphology and performance. In addition to the resin's molecular structure, many processing factors, including the melt temperature, speed of cooling, drawing speed, DDR, and BUR, greatly influence the film's morphology and properties. Blown films generally have a good balance of mechanical properties. Various aspects of the blown film extrusion process have been studied from both modeling and experimental perspectives (*12-15*). Many studies have also attempted to correlate the mechanical properties and microstructures of the polymer film as a function of processing parameters (*56, 57*).

In packaging application, the plastic film generally experiences mode-I and/or mode-III fracture upon loading, where mode-I fracture is usually a weaker mode of fracture. Therefore, it is critical to characterize and improve the film resistance to mode-I fracture. The essential work of fracture (EWF) analysis is a simple, straightforward technique that has been widely utilized for determining the toughness of various ductile polymeric materials, especially for samples in film or sheet forms (*31-33*).

44

The EWF method was originally suggested by Broberg (34) and then developed by Mai and Cotterell (35-37) to characterize plane-stress fracture toughness of ductile materials. The fundamental concept of the EWF method is based on the partition of energy, which separates the total fracture energy (W_f) into two components: the essential work of fracture (W_e) and the non-essential work of fracture (W_p):

$$W_f = W_e + W_p = w_e tL + \beta w_p tL^2 \tag{3.1}$$

$$w_f = {W_f}/{Lt} = w_e + \beta w_p L \tag{3.2}$$

where W_e represents the energy dissipated in the inner fracture process zone (IFPZ), which is responsible for creation of the fracture surface; W_p is the energy dissipated in the outer plastic deformation zone (OPDZ); β is a shape factor associated with the volume of the plastic deformation zone; L is the ligament length; t is the thickness of the specimen (39).

The specific total work of fracture (w_f) can be obtained by normalizing W_f with the cross-sectional area of the ligament where w_e is the specific essential work of fracture and w_p is the specific non-essential work of fracture. There is a positive linear dependence between w_f and ligament length. The positive intercept (w_e) indicates the resistance to crack propagation, and the slope indicates the capability of the material to dissipate energy plastically. The European Structure Integrity Society (ESIS) proposed the following criterion for a valid range of the ligament length for the EWF test :

$$(3t\sim5t) \leq L \leq min\ (\frac{W}{3}, 2R_p) \tag{3.3}$$

The detailed description of the EWF method can be found elsewhere (*34, 35, 39*).

      The EWF application to polymer thin films is problematic due to the limited geometric stability of the film under tensile loading, which leads to an out-of plane buckling under in-plane tensile loading (*13, 14*). The buckling would alter the stress distribution within the ligament zone (*6*) and lead to inaccurate and scattering of EWF measurements. Previously, a custom-built film fixture was developed to minimize the buckling of m-LLDPE thin films evaluated using the double-edge-notched tension (DENT) setup and to achieve good stability, consistency, and reproducibility for the mode-I EWF toughness characterization (*58*). Both w_f and w_p were found to be independent of the crosshead speed, gauge length (distance between upper and lower clamps), and specimen width within the ranges tested (*58*).

      In this study, morphological observations, EWF analyses, and Elmendorf testing were performed on m-LLDPE films made with different processing conditions. The film thinning process within the necked zone during EWF testing was carefully characterized. The effects of FLH, DDR, BUR, and haze-zone region on the EWF parameters of m-LLDPE films were determined. Correlations between EWF parameters and the tear resistance of m-LLDPE blown films were also made. The usefulness of the EWF for investigating ductile polymeric blown films fracture performance is discussed.

3.1 Experimental

3.1.1 Materials

A series of m-LLDPE (Exceed™ 1018) blown films were provided by ExxonMobil Chemical. Exceed 1018 is a metallocene ethylene-hexene copolymer. It has a density of 0.918 g/cm^3, a melt index of 1.0 g/10 min, and a peak melting temperature of 119°C. Three different thicknesses (0.019, 0.030, and 0.076 mm) combined with two different BURs (3 and 2.5) of m-LLDPE blown films were chosen for this study. The material information is listed in Table 3.1. The m-LLDPE films were carefully examined under cross-polarized light to determine the haziness along the transverse direction of the film stocks. Since the film bubble was collapsed into a double-layer flat film stock at the end of the blown film process, the folding line (FDL), which was on the side of the operator, was used as the reference location along the transverse direction.

Table 3.1. Thicknesses of m-LLDPE blown films and their corresponding processing parameters.

BUR$^{\%}$	3			2.5		
Thickness (mm)	0.076	0.03	0.019	0.076	0.03	0.019
Stretch Rate (s^{-1})	0.3	0.85	1.46	0.37	1.06	1.72
TD Draw	20	20	20	24	24	24
MD Draw	6.7	16.7	26.7	8	20	32
Total Draw	20	50	80	20	50	80
Draw Down Ratio	5	14	22	6	17	27

3.1.2 Microscopic Observations

The surface morphologies of all specimens were assessed using two different microscopic techniques: a scanning electron microscope (SEM) (JEOL JSM-6400) and an atomic force microscope (AFM) (Bruker, Dimension Icon). The SEM was operated at 7000x, with an accelerating voltage of 25kV and a working distance of 8 mm. The surfaces of all specimens were carefully preserved to minimize any contamination or artifact before the characterization. Prior to the examination by SEM, the specimens were attached to aluminum stubs by conductive carbon tape and gold sputter coating under argon to render them electrically conductive. Before the observation with AFM, the samples were attached to metal stubs by double-sided tape. The AFM was operated at the tapping mode with a RFESP cantilever (Bruker).

3.1.3 EWF Test and Film Deformation Analysis

The m-LLDPE films with the width and length dimensions of 280 mm x 153 mm were prepared from the chosen transverse locations of the film stocks, which were determined by the local haziness and FLH, prior to being assembled in a customized film fixture. The DENT test of m-LLDPE thin films was conducted with the custom-built film fixture [24]. After putting the m-LLDPE thin film in the fixture, a fresh razor blade was used to prepare the notches in the specimen (117 mm x 95 mm). Because of the custom-built film fixture, the specimen had a gauge height of 110 mm and width of 117 mm. The ligament lengths chosen for this study were between 6 mm to 30 mm. All tests were performed on a custom-built tensile tester with a load cell capacity of 445 N

operated at a crosshead speed of 10 mm/min at room temperature. The mode-I EWF toughness characterization was performed using the ESIS protocol for EWF. The experimental setting and procedure for the DENT test on m-LLDPE thin films can be found elsewhere (*58*). The tear tests were done on an Elmendorf testing apparatus according to ASTM D-1922 at ExxonMobil.

Photoelastic imaging technique is a nondestructive, whole-field, graphic stress-analysis technique based on the stress-optical property of a material. The fringe patterns are related to the difference between the principal stresses in a plane normal to the light propagation direction. Photoelastic technique was utilized to provide a reliable, visual full-field stress distribution analysis of the DENT specimen under tensile loading with a set of cross-polarizers (*58*). A Canon EOS Rebel T3i camera was used to record the DENT tests conducted on the LLDPE thin films. A Mitutoyo Digimatic Micrometer was used to measure the film thicknesses.

3.2 Results and Discussion

3.2.1 Morphological Observations of m-LLDPE thin films

As mentioned above, during the blown film extrusion process, the molten polymer was extruded and cooled while being pulled away from the die. From the infrared thermograph of the film bubble, the film's temperature varied around the die exit where the brighter regions indicate the film sections with higher temperatures (Figure 3.1). The film temperature also varies along the film bubble away from the die exit as it cools. The temperature variation leads to differences in FLHs along the

circumference of the film bubble and cause the differences in the film's morphology. These differences can be observed visually as haze bands and clear zones across the film.

To characterize the morphology of the m-LLDPE films with different thicknesses and BURs, SEM was utilized to study the surfaces of the films. From the SEM observation, spherulitic structures can be directly observed on the surfaces of the m-LLDPE films (Figure 3.2). The sizes of spherulites are larger in thicker films than in thinner films. Spherulites were also found to form throughout the thickness of the films (Figure 3.3). The characteristics of the spherulites are different in the haze region and the clear zone with distinct spherulitic superstructures forming in the haze region (compare Figure 3.2 and Figure 3.3c). There is no significant size difference for the spherulites in the haze and clear regions.
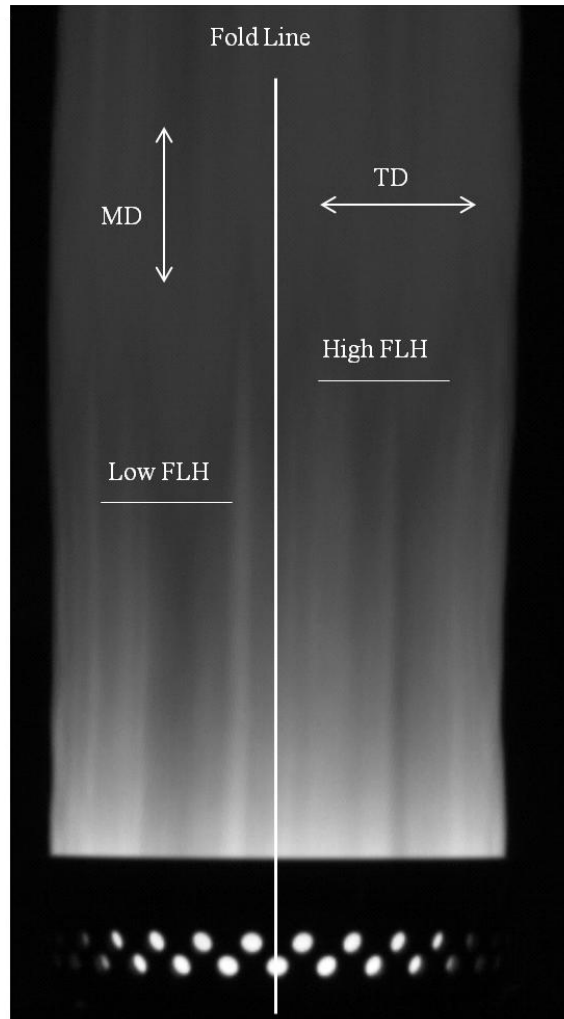
Figure 3.1. Infrared image of 0.019 mm thick, 2.5 BUR m-LLDPE blown film.
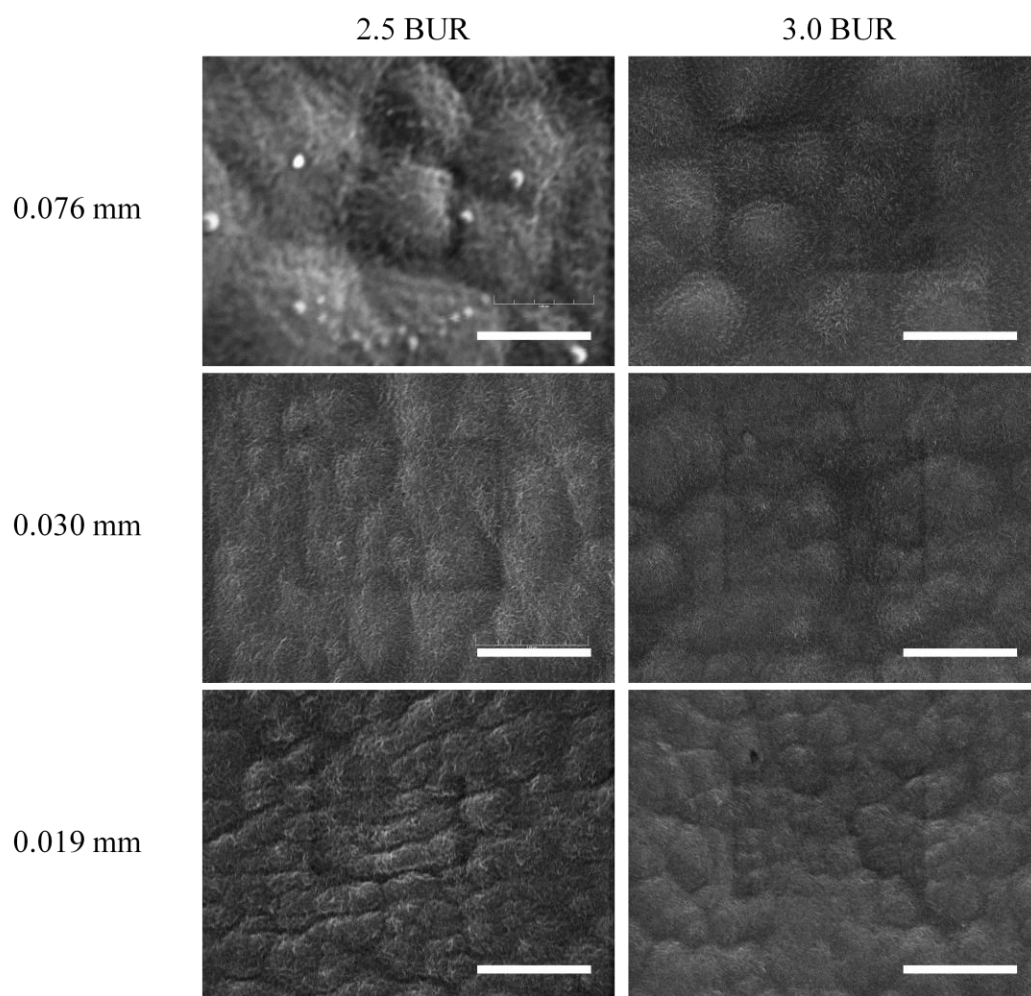
Figure 3.2. SEM images of m-LLDPE films with different thicknesses and BURs (scale bar = 5 μm).
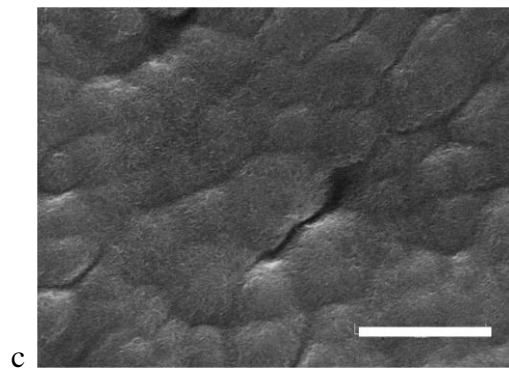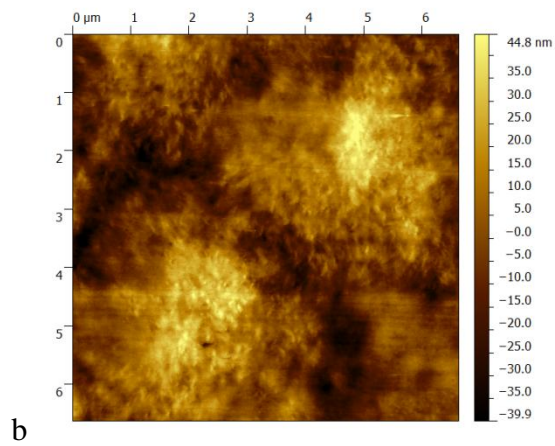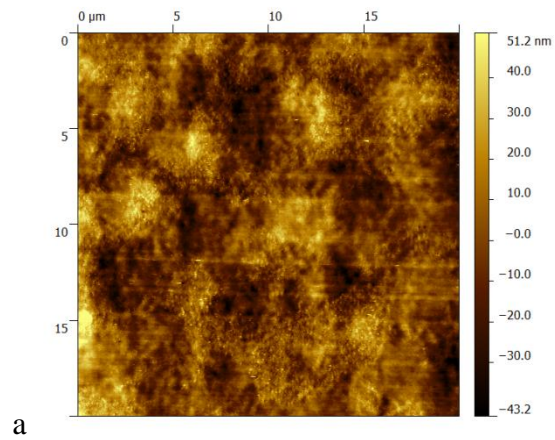
Figure 3.3. AFM images ((a) 20μm X 20μm; (b) 6.5μm X 6.5μm) of 0.076 mm, 2.5 BUR m-LLDPE film at the cross section, and SEM image of 0.030 mm, 2.5 BUR m-LLDPE blown film in the haze band region (c). (scale bar = 5 μm).

3.2.2 Deformation Observation of DENT Film Specimens

  The load-displacement curves of the m-LLDPE films were shown in Figure 3.4, and the geometric similarity of the load-displacement curves, which is one of the prerequisites for the application of the EWF method, can be observed. The whole-field stress distribution of the DENT m-LLDPE specimens was observed using the photoelastic technique (*58*). During the DENT test, intensified fringe patterns due to stress build-up can be clearly seen (Figure 3.5). From the photoelastic observation, the fringe development starts at both ends of the crack tips. Upon further loading, the two birefringent fringe fronts of the DENT specimen begin to grow in size and merge with each other. After two fringe fronts merge, the process zone (i.e., necking) that is enclosed by the fringes start to propagate and develop in the loading direction. The necking process in polymers is known to be due to a 1-D geometric constraint in the width direction when the specimen width is much greater than its thickness. This constraint leads to the thinning of the polymer in the thickness direction upon deformation beyond yielding. Then, the polymer strain softening behavior allows the necking to propagate within the gauge length region until strain hardening begins to dominate the deformation. It is noted that the fringe pattern did not disappear after the film failure and separation (Figure 3.5), suggesting non-recoverable deformation is present in the failed DENT specimen.
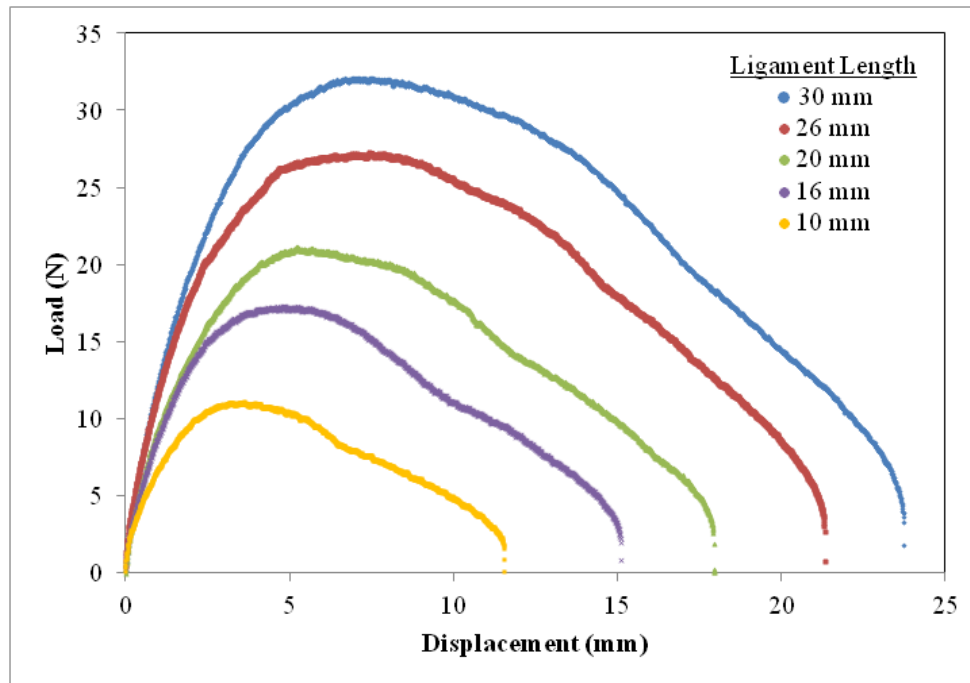
Figure 3. 4. Load-displacement curves of 0.076 mm thick, 2.5 BUR m-LLDPE blown film with the crack propagation in MD.

The thickness of the DENT specimen was measured post-mortem from the tip of the fracture point to the top of the residual fringe pattern boundary (Figure 3.6a). Significant reduction in film thickness was observed near the top of the fringe boundary (Figure 3.6b). The film thickness reaches a plateau level after a dramatic reduction in the film thickness and remains at the plateau thickness until failure (Figure 3.6b). Regardless of the original ligament lengths, the DENT specimens reach the same plateau value in film's final thickness (Figure 3.6b). It is noted that thinner films can reach a lower plateau film thicknesses compared to that of the thicker films. But BUR and film orientation have no effect on the plateau film thickness (Figure 3.7a). Moreover, regardless of film thicknesses, film orientation, and BUR, the thickness of post-mortem

55

DENT specimen reaches a plateau thickness at about 40% of their original thicknesses (Figure 3.7b). The fundamental cause(s) behind the post-mortem DENT m-LLDPE specimens dropping to 40% of their original thicknesses in the process zone regardless of film thicknesses, film orientation, and BUR is still unknown. It could be related to their similar strain hardening behavior and their ultimate strain to failure characteristics. In-depth research is now underway to confirm the above conjecture.
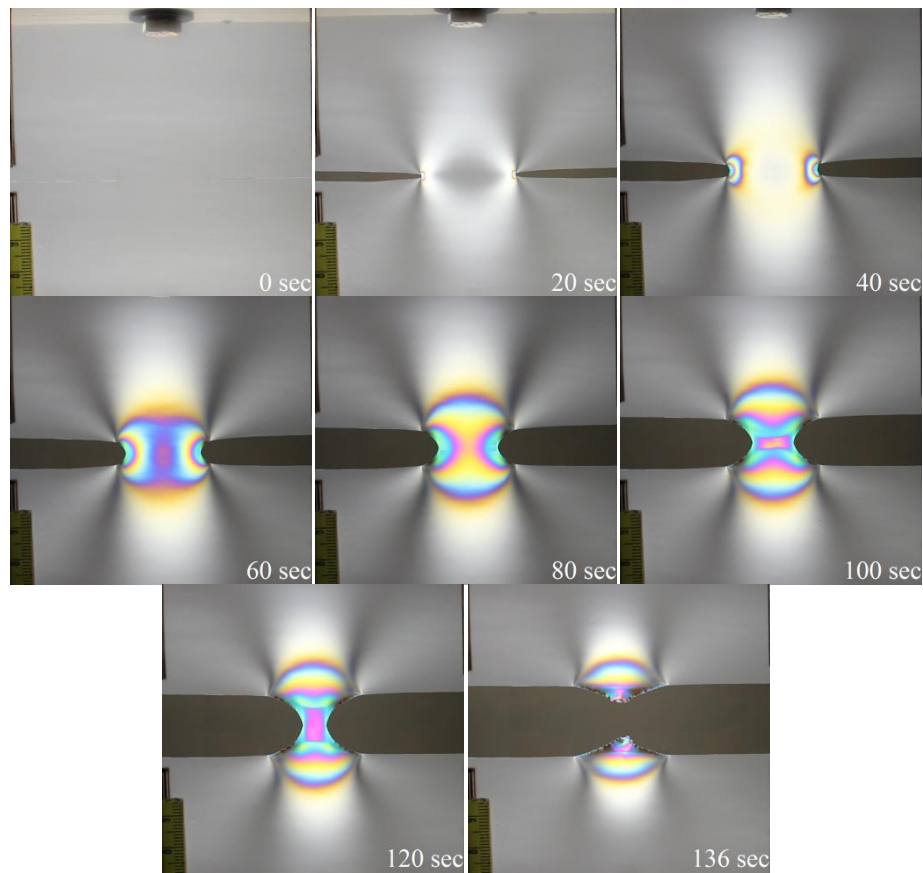
Figure 3.5. Photoelastic observation of 0.076 mm thick, 2.5 BUR m-LLDPE blown film with 30 mm ligament length and crack propagation in MD.
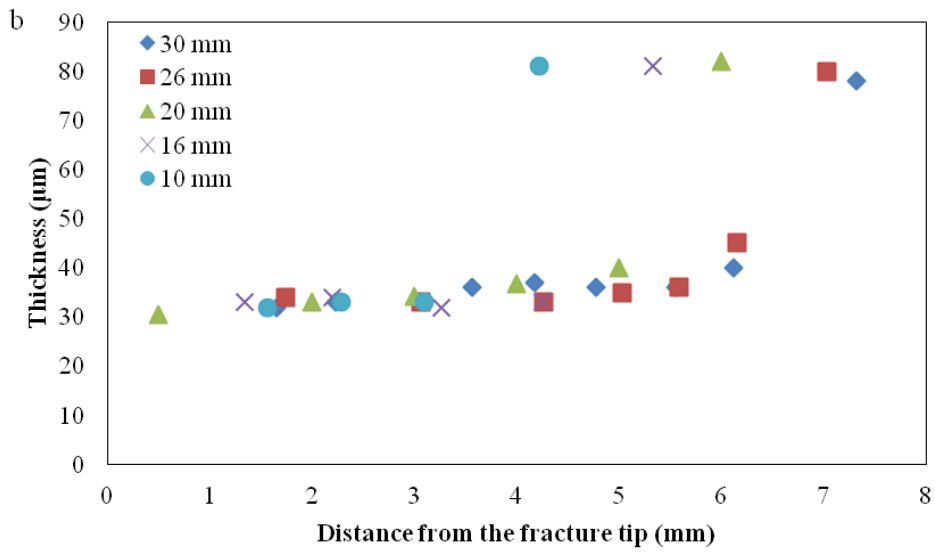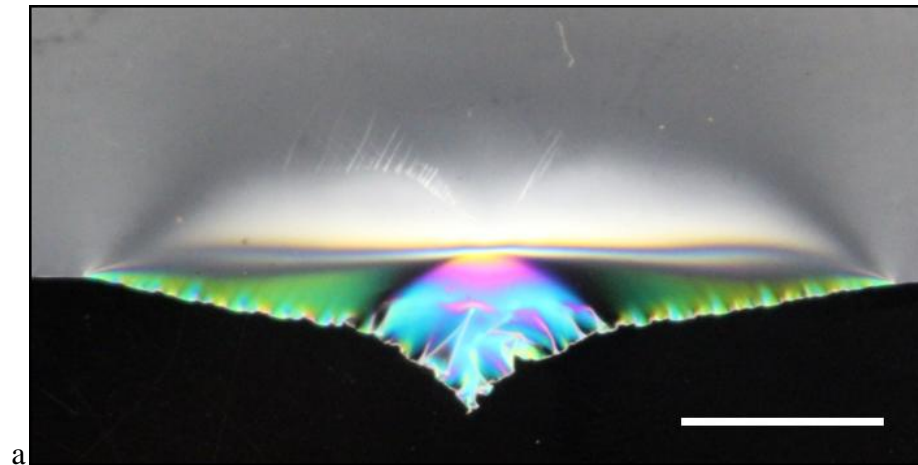
Figure 3. 6. (a) Photoelastic observation of post-mortem 0.076 mm 2.5 BUR m-LLDPE blown film. (scale bar = 5 mm) (b) Measurements of film thickness at the tip of the PDZ zone with different ligament lengths.
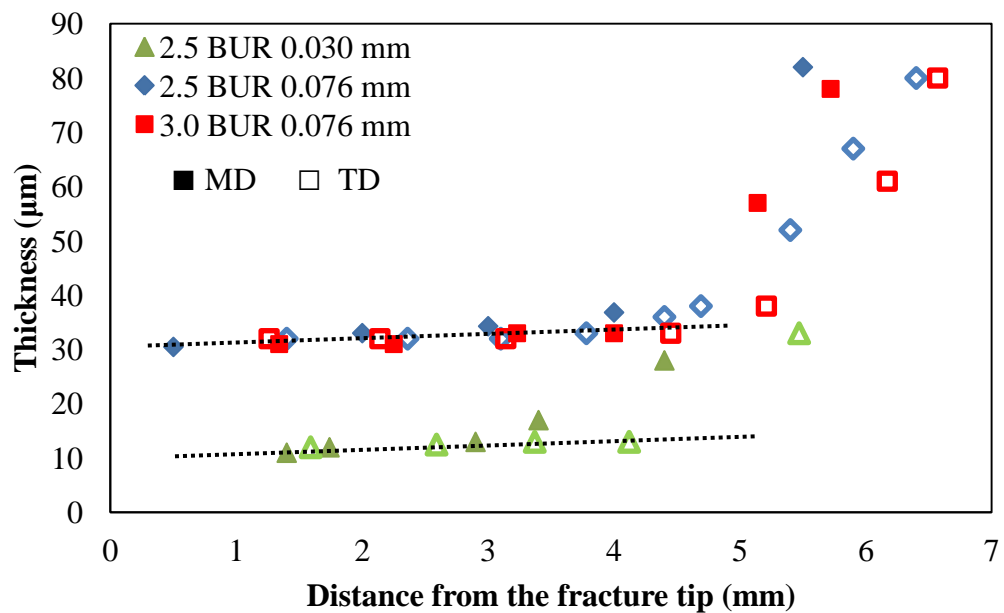
a
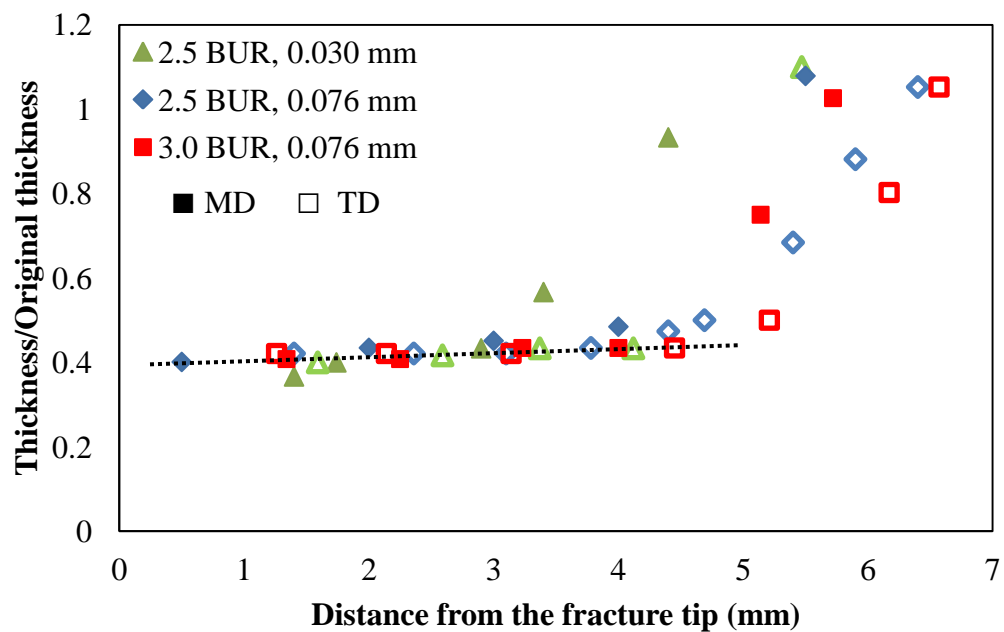
b

Figure 3. 7. (a) Film thicknesses and (b) normalized film thicknesses in the deformation zones of post-mortem m-LLDPE blown films with different BURs.

3.2.3 Effect of FLH and Haze

The effect of FLH and haze on the EWF behavior was determined using m-LLDPE films with thicknesses of 0.030 mm made using 2.5 BUR. The w_e and βw_p values are summarized in Table 3.2. All samples failed in a ductile manner. The w_e is lower for the specimen with higher FLH, while βw_p is insensitive to the FLH (Figure 3.8). It should be noted that the haze band regions have lower FLH. In the haze band region, βw_p is significantly lower than that in the clear zone, but its w_e is higher than that in the clear zone (Figure 3.8). The differences in the EWF parameters between the haze region and the clear region are attributed to localized morphological differences, variations in cooling, solidification, or crystallization rates.

Table 3.2. EWF parameters and clarity of 0.030 mm, 2.5 BUR m-LLDPE blown film with different FLHs.

0.030 mm, 2.5 BUR m-LLDPE blown films							
FLH (m)	Location relative to FDL (m)	Morphology	Orientation	w_e (kJ/m^2)	Sdwe (kJ/m^2)	βw_p (MJ/m^3)	SD$_{\beta wp}$ (MJ/m3)
0.203	0.494 Left	Haze	MD	60.0	10.1	3.27	0.37
			TD	69.3	13.1	5.52	0.96
0.429	0.419 Left	Clear	MD	60.4	5.6	5.00	0.26
			TD	44.8	7.3	6.12	0.53
0.483	0.165 Left	Clear	MD	54.3	5.1	4.26	0.24
			TD	73.2	11.6	6.30	0.85
0.635	0.165 Right	Clear	MD	44.5	7.6	4.64	0.35
			TD	42.8	6.3	6.62	0.46
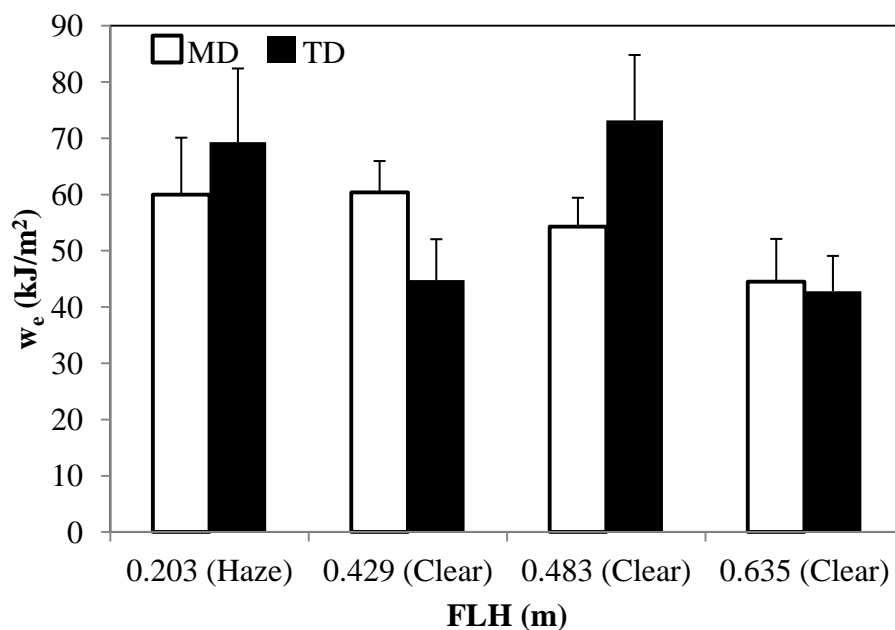
a
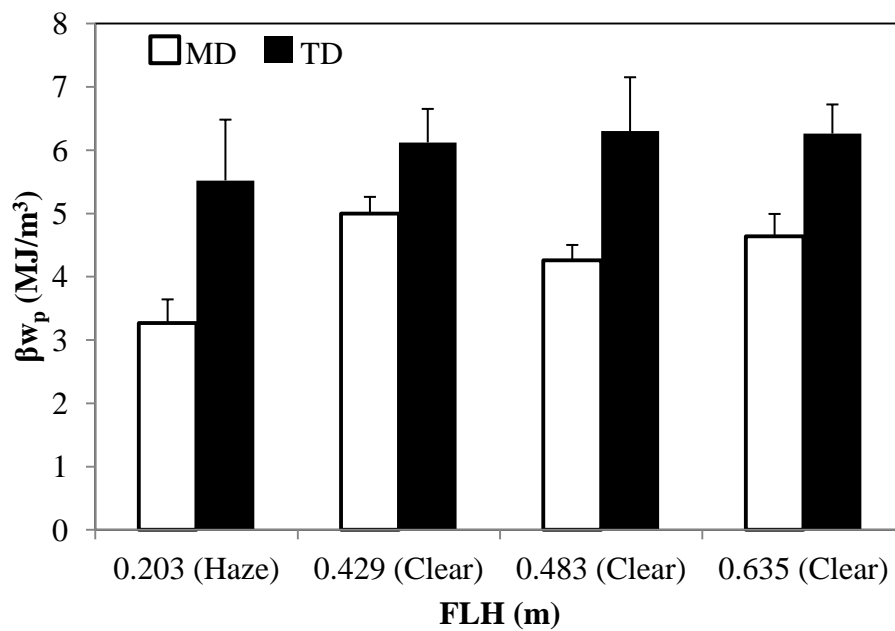
b

Figure 3.8. (a) Specific essential work of fracture and (b) non-specific essential work of fracture of 0.030 mm in thickness, 2.5 BUR m-LLDPE blown films with different FLHs for crack propagation in both MD and TD.

3.2.4 Effects of Film Thickness, Film Orientation, and BUR

The effects of film thickness, film orientation, and BUR on the EWF parameters of the m-LLDPE films are summarized in Table 3.3. All test specimens selected for the DENT testing had a FLH of 0.483 m, except as indicated in Table 3.2. The ligament lengths for the specimens' ranged between 6 mm and 30 mm. Plots of w_f vs. L for different film thicknesses made using 2.5 BUR are shown in Figure 3.9, and plots of w_f vs. L for different film thicknesses made using 3 BUR are shown in Figure 3.10. In general, w_e is greater for thinner films than for thicker films, indicating crack propagation in thinner films requires more energy. Further, βw_p is greater in thicker films, suggesting more energy is dissipated in the plastic deformation zone of thicker films. In general, the crack propagation in TD has higher fracture toughness than that in the MD, which leads to greater w_e and βw_p. The differences in the EWF parameters between MD and TD diminish as film thickness increases. This change is attributed to a decrease in the film anisotropy as the film's thickness increases. Thicker films have lower DDR (Table 3.1) resulting in less orientation dependence for thicker films. The m-LLDPE blown films have more crystal and amorphous phase orientation along the MD, which correlates with greater MD strength and TD tear resistance (*6, 54*). The above findings are consistent with the literature findings (*59-61*).

BUR is related to the degree of stretching in TD of the film's bubble during the blown film process. Increasing BUR creates more orientation in TD. In general, greater BUR diminishes differences of w_e between MD and TD (Figure 3.11). m-LLDPE films made using a greater BUR have lower βw_p in both MD and TD (Figures 3.10 & 3.11)

with the differences in βw_p for different BURs decreasing with a decrease in the films thickness (Figures 3.10 & 3.11). This change is attributed to an increase in the orientation within the film as the film become thinner.

Table 3. 3. EWF parameters of m-LLDPE blown films.

BUR	Thickness (mm)	Location relative to FDL (m)	Morphology	Orientation	w_e (kJ/m^2)	Sdwe (kJ/m^2)	βw_p (MJ/m^3)	$SD_{\beta wp}$ (MJ/m^3)
3	0.076	0.165 Left	Clear	MD	61.7	4.48	4.89	0.21
				TD	62.0	5.47	5.42	0.40
	0.030	0.165 Left	Clear	MD	77.8	8.03	3.34	0.37
				TD	67.9	6.08	5.02	0.44
	0.019	0.165 Left	Clear	MD	67.1	7.24	3.58	0.34
				TD	75.7	5.81	5.35	0.42
2.5	0.076	0.165 Left	Clear	MD	48.5	6.63	6.04	0.31
				TD	47.8	4.57	7.06	0.33
	0.030	0.165 Right	Clear	MD	44.5	7.61	4.64	0.35
				TD	42.8	6.29	6.26	0.46
		0.165 Left	Clear	MD	54.3	5.12	4.26	0.24
				TD	73.2	11.60	6.30	0.85
		0.419 Left	Clear	MD	60.4	5.55	5.00	0.26
				TD	44.8	7.25	6.12	0.53
		0.494 Left	Haze	MD	60.0	10.10	3.27	0.37
				TD	69.3	13.10	5.52	0.96
	0.019	0.165 Left	Clear	MD	66.9	4.57	3.58	0.21
				TD	83.0	9.44	4.86	0.69
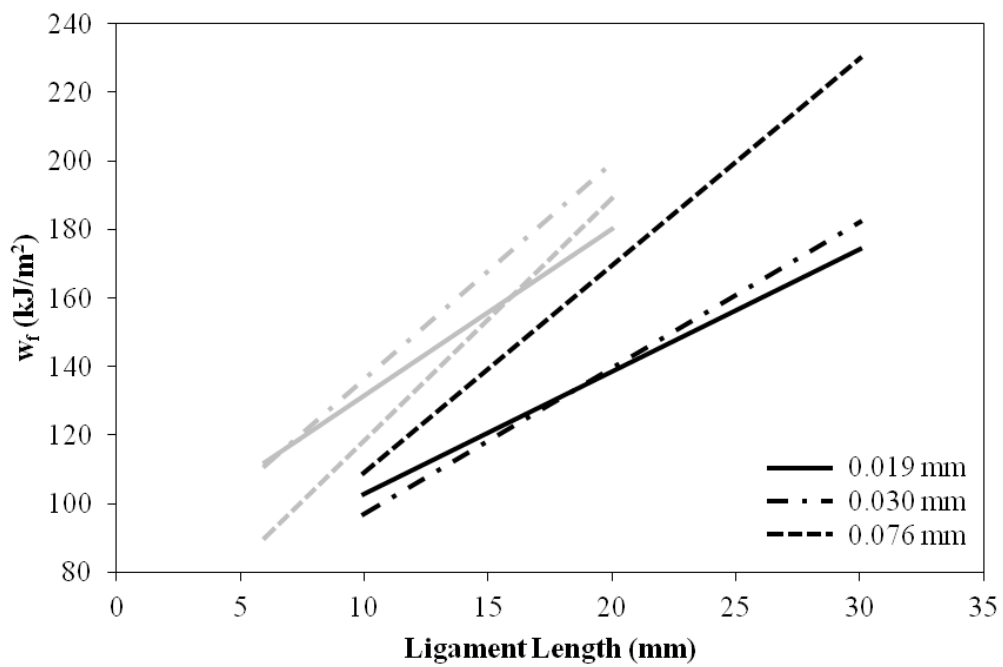
Figure 3.9. Specific work of fracture versus ligament length for 2.5 BUR m-LLDPE blown films with different thicknesses and film orientations. Black lines are for the crack propagation in the MD, and the grey lines are for the crack propagation in the TD.
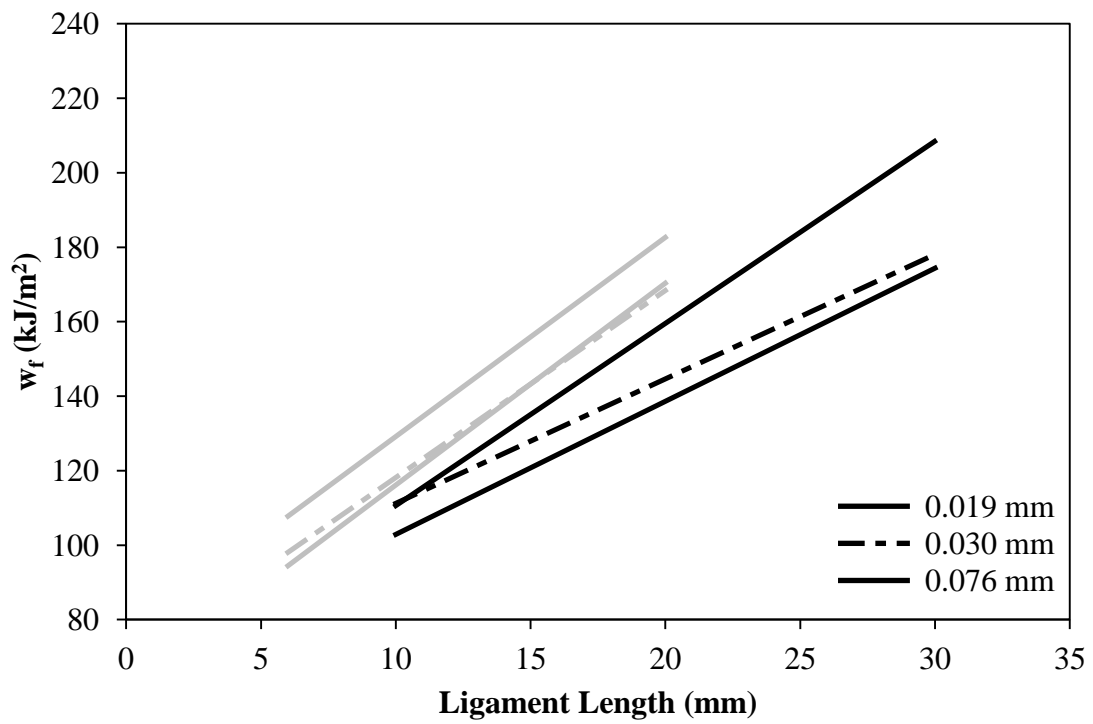
Figure 3.10. Specific work of fracture versus ligament length for 3 BUR m-LLDPE blown films with different thicknesses and film orientations. Black lines are for the crack propagation in the MD, and the grey lines are for the crack propagation in the TD.
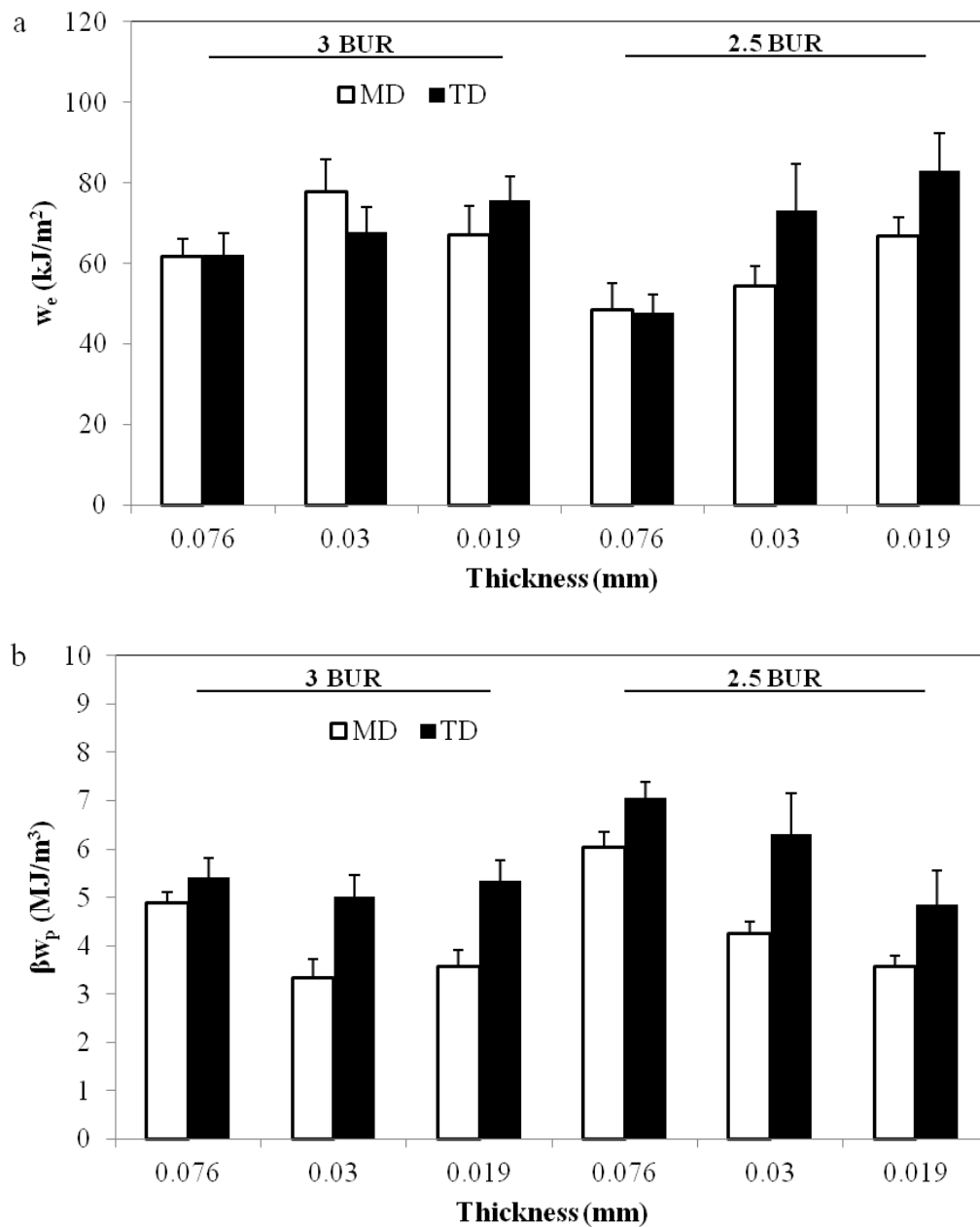
Figure 3.11. (a) Specific essential work of fracture and (b) non-specific essential work of fracture of m-LLDPE blown film with different thicknesses, BURs, and film orientations.

3.2.5 Elmendorf Tear and EWF Parameters

The Elmendorf tear test is an industrial test for determining the relative tear (mode-III) resistance of polymeric materials. The test itself involves the loading and stretching of the Elmendorf arms, which absorb mechanical energy, and the deformation and mode-III fracture of the material around the crack. In actuality, the Elmendorf test involves both mode-III tear and mode-I stretching during the test, especially for thin ductile films (*39, 44, 62, 63*). As a result, the Elmendorf test cannot be easily correlated with material properties. Unlike the Elmendorf tear test, the EWF tests involve a known applied mechanical energy to cause deformation and fracture of the films near the crack under a purely mode-I loading condition. Consequently, the correlation between the two types of the tests, if any, will be material dependent and cannot be made universal.

The Elmendorf tear strengths of m-LLDPE films are summarized in Table 3.4. The Elmendorf tear resistance is greater for thicker films, and in TD (Figure 3.12a). The normalized Elmendorf tear resistance in TD increases with decreasing film thickness, but the normalized Elmendorf tear resistance in MD increases with increasing film thickness (Figure 3.12b). The normalized MD / TD Elmendorf tear ratio increases with increasing film thickness. The correlation between the normalized Elmendorf tear resistance and EWF parameters of m-LLDPE blown films is shown in Figure 3.13. The normalized Elmendorf tear resistance decreases with w_e in MD and increases with w_e in TD, but the normalized Elmendorf tear resistance increases with βw_p in MD and is constant with βw_p in TD. The Elmendorf tear resistance of m-LLDPE films correlates

well with the molecular orientation due to the DDR and BUR of the blown film process, as is in the case for w_e.

Table 3. 4. Elmendorf Tear Performance of m-LLDPE blown films.

BUR	Thickness (mm)	Location relative to FDL (m)	Morphology	Orientation	Elmendorf Tear* (g)	(g/mm)
	0.076	0.165 Left	Clear	MD	871	11461
				TD	996	13105
3	0.030	0.165 Left	Clear	MD	287	9567
				TD	428	14267
	0.019	0.165 Left	Clear	MD	164	8632
				TD	277	14579
	0.076	0.165 Left	Clear	MD	916	12053
				TD	1020	13421
		0.165 Right	Clear	MD	314	10464
				TD	453	15104
2.5	0.030	0.165 Left	Clear	MD	327	10900
				TD	446	14867
		0.419 Left	Clear	MD	302	10064
				TD	410	13669
		0.494 Left	Haze	MD	253	8448
				TD	546	18192
	0.019	0.165 Left	Clear	MD	162	8526
				TD	304	16000
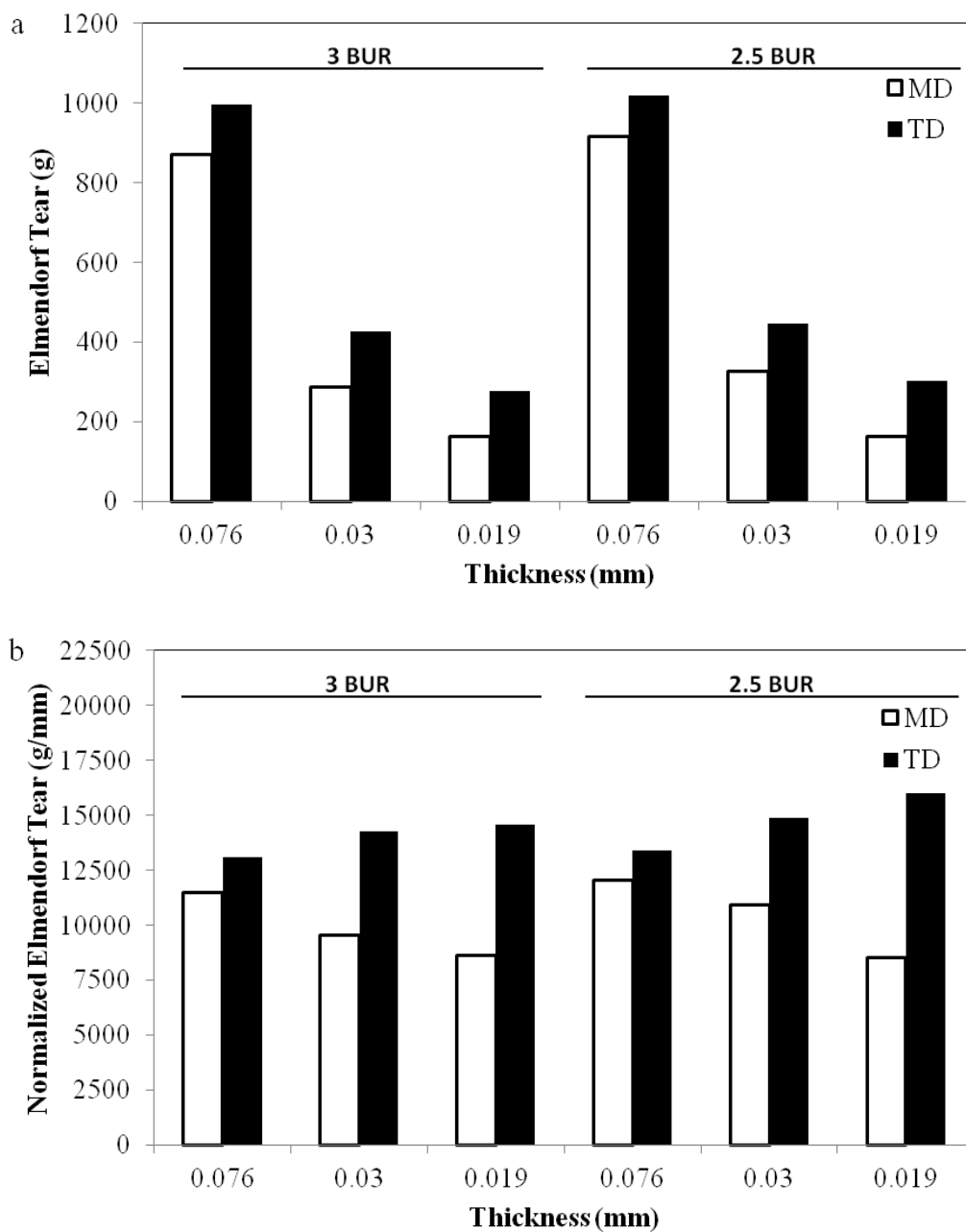
Figure 3. 12. (a) Elmendorf tear resistance and (b) normalized Elmendorf tear resistance of m-LLDPE blown films.
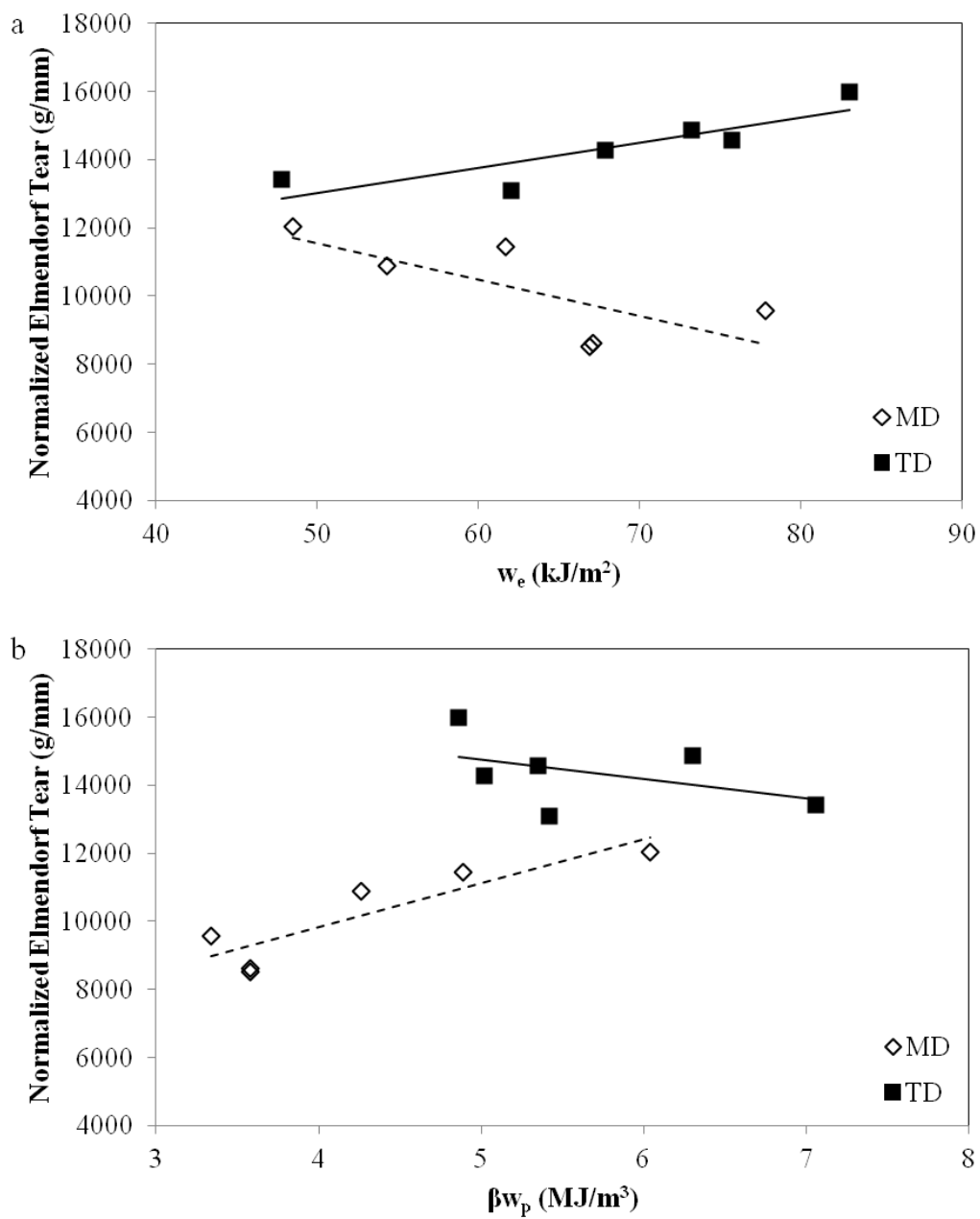
Figure 3. 13. Correlations between normalized Elmendorf tear resistance and EWF parameters of m-LLDPE blown films.

As pointed out earlier, the Elmendorf tear test involves a mix-mode fracture process. For ductile films, mode-I facture usually becomes dominant during the late stage of deformation and fracture (*62*). Under such a high speed testing, the microstructure in m-LLDPE thin films does not have sufficient time to participate in or respond to the high rate of deformation, which will likely happen during a low speed EWF test. As a result, the EWF test is expected to be more sensitive to both microstructure and processing condition in fracture toughness characterization. Furthermore, for the Elmendorf tear test in TD, the crack propagation is perpendicular to the MD, so the crack propagation will likely require the breakage of the molecular chains oriented in MD. Thinner films have more molecular chains oriented in MD due to the greater difference between DDR and BUR, which leads to higher tear resistance in TD. The correlation between w_e to the normalized Elmendorf tear resistance in TD can thus be observed (Figure 3.13). For the Elmendorf tear test in MD, the crack propagation is parallel to the MD. The resistance for the crack propagation is highly correlated to the disentanglement of polymer chains which is related to the ability of films to deform plastically in TD. Since βw_p corresponds to nonessential plastic deformation, the tear resistance in MD is highly correlated to βw_p in the EWF analysis. As a result, good correlation between the normalized Elmendorf tear resistance and EWF parameters is expected. It should be noted that the EWF parameters are material parameters that offer fundamental insights toward how the mechanical energy is consumed and partitioned during the fracture process. Therefore, the EWF test is preferred over the Elmendorf test for characterizing fracture toughness of polyolefin films.

The present study has demonstrated the usefulness and sensitivity of the EWF test methodology in determining how the blown film processing conditions can influence mode-I fracture toughness of m-LLDPE thin films. The film gage, FLH, DDR, BUR, and film inhomogeneity all are found to greatly affect the fracture behavior. Therefore, the EWF test carried out here should be an effective tool for gaining fundamental understanding on how the polyolefin molecular structure and processing conditions influence m-LLDPE film morphology and their corresponding fracture behavior, especially when *in-situ* film morphology development and deformation process are being monitored. The fundamental knowledge generated will then likely facilitate efficient design and development of high performance polyolefin films for a vast variety of film packaging applications.

3.3 Conclusions

Blown film process is one of the most common processes to produce wide variety of high performance polyolefin films. In this study, effects of different processing parameters on the morphology and fracture behavior of m-LLDPE films were investigated. The FLH reflects the film's thermal history, which leads to the difference in morphology and the fracture resistance of the m-LLDPE films. The effects of processing conditions, DDR and BUR, and the film orientation on the fracture resistance of m-LLDPE films correspond well to the molecular orientation characteristics and the microstructural deformation mechanisms. Significant film thinning is a clear indication of the neck formation in the process zone of m-LLDPE film prior to film ultimate

fracture. The present study has demonstrated that the EWF test methodology is a powerful tool for fundamental understanding of fracture behavior of ductile polyolefin films and for better design of tougher films for a vast variety of film packaging applications.

CHAPTER IV

EFFECT OF SHORT-CHAIN BRANCH CONTENT ON THE ESSENTIAL WORK

OF FRACTURE TOUGHNESS AND TENSILE PROPERTIES OF LLDPE BLOWN

FILMS

In 2012, the global market value of packaging films was estimated to be approximately \$89 billion, and had a predicted compound annual growth rate of 5.8 % over the next 5 years (*1*). The United States demand for plastic film is expected to grow 1.9 % every year, requiring 16 billion pounds of film with a predicted market value of \$19 billion by 2016 (*1*). Linear low density polyethylene (LLDPE) will be one of the most widely used films in the future because of its capability to be used in many diverse applications, due to its ductility, strength, durability, and low cost. It is expected to represent almost 50 percent of the demand for polymer films by 2016 (*1*). 70 % of commercial LLDPE films are produced through the blown film extrusion process (*4-6*).

LLDPEs are made by the copolymerization of ethylene and varying amounts of α-olefin comonomers, such as 1-butene, 1-hexene, or 1-octene. The α-olefin comonomer introduces short chain branches, such as ethyl, butyl, or hexyl branches, on the polyethylene backbone which influences the crystallization and lamellae formation of the resulting polyethylene molecule (*9*). Thus, the presence of these branches has an effect on the bulk copolymer's end product properties.

Controlling branch distribution is mainly done by changing the catalyst used or altering the reaction conditions during polymerization (*7, 8, 10*). LLDPE resins that are

produced using Ziegler-Natta (ZN) heterogeneous catalysts have a heterogeneous distribution of short-chain branching and are considered to be a mixture of polyethylene copolymers with a wide range of molecular weights and short-chain branch content. With single site metallocene catalysts, LLDPEs with narrower molecular weight distributions and considerably more homogenous short-chain branching distributions can be produced. The single-site metallocene catalyst prevents the formation of high- and low-molecular-weight tails, which reduce the variability in the physical properties of the resulting copolymers. Consequently, metallocene-LLDPEs (m-LLDPEs) have a more controlled structure.

The physical properties of LLDPE films are generally known to be influenced by molecular structural parameters such as average molecular weight, molecular weight distribution, and the type, amount, and distribution of short chain branches (*16-19*). In addition to the molecular structure, the processing conditions can also greatly affect the material's morphological features, such as preferred orientation, lamellae morphology, degree of crystallinity, surface roughness, and intercrystalline connectivity, all of which have major effects on the mechanical properties of blown LLDPE films (*16, 17, 19-21*). Although many researchers have investigated the effects of short chain branching on the crystallization behavior and mechanical properties of ZN-LLDPEs, there are only limited studies on m-LLDPEs. Because m-LLDPEs are generally believed to have homogeneous branching distributions and narrow MWDs, m-LLDPEs provide an opportunity to investigate the roles of short-chain branching on the mechanical properties of polymers.

74

In this work, the objective was to investigate the effect of branch content on the tensile properties and fracture toughness of m-LLDPE films. The blown films used in this work were made from m-LLDPE resins, which are composed of metallocene copolymers of ethylene and 1-hexen. While the films had similar molecular weight and molecular weight distribution values, they differed in their short-chain branch content. Deformation observations, photoelastic observations, EWF analyses, tensile testing, and Elmendorf testing were all performed on the m-LLDPE films. The film thinning process that occurred within the necked zone during EWF testing was also characterized. The true stress-strain curves of the m-LLDPE films were obtained, and the effect of branch content on the tensile properties was characterized. The effect of branch content on the EWF parameters of m-LLDPE films was determined, and a correlation between the EWF parameters and the tear resistance of m-LLDPE blown films was also made. The purpose of this work is to present some trends that may shed light on the effects of branch content on the mechanical properties of m-LLDPE blown films and to discuss the usefulness of EWF analysis when investigating a ductile polymer blown film's fracture performance.

4.1 Experimental

4.1.1 Materials

Three different series of Exceed™ m-LLDPE blown films m-LLDPE made of different resin densities were provided by ExxonMobil Chemical. Exceed™ resin is a metallocene ethylene-hexene copolymer. For each resin density, m-LLDPE films with

two different film thicknesses (0.019 mm and 0.076 mm) were chosen for this study. All films were made with a blow-up ratio (BUR) of 2.5. More material information is listed in Table 4.1.

Table 4.1. Material properties of m-LLDPE blown films.

Resin	Exceed 1023		Exceed 1018		Exceed 1012	
Density (g/cm³)	0.923		0.918		0.912	
Melt Index	1		1		1	
Hexene Content (mol%)	< 1.5		1.5		3	
BUR	2.5		2.5		2.5	
Thickness (mm)	0.076	0.019	0.076	0.019	0.076	0.019

4.1.2 Microscopic Observations

The surface morphologies of all specimens were assessed using an atomic force microscope (AFM) (Bruker, Dimension Icon). The surfaces of all specimens were carefully preserved to minimize any contamination or artifact accumulation before the characterization. The AFM was operated in tapping mode with a RFESP cantilever (Bruker).

4.1.3 Essential Work of Fracture

Essential work of fracture (EWF) analysis has been widely used for determining the toughness of various ductile materials, especially for samples in film or sheet forms (*31-33*). The fundamental concept behind the EWF method is based on the partition of

76

energy, which separates the total fracture energy (W_f) into two components: the essential work of fracture (W_e) and the non-essential work of fracture (W_p):

$$W_f = W_e + W_p = w_e tL + \beta w_p tL^2 \tag{4.1}$$

$$w_f = \frac{W_f}{Lt} = w_e + \beta w_p L \tag{4.2}$$

where W_e represents the energy dissipated in the inner fracture process zone (IFPZ), which is the energy responsible for the creation of the fracture surface; W_p is the energy dissipated in the outer plastic deformation zone (OPDZ); β is a shape factor associated with the volume of the plastic deformation zone; L is the ligament length; t is the thickness of the specimen.

The specific total work of fracture (w_f) can be obtained by normalizing W_f with the cross-sectional area of the ligament where w_e is the specific essential work of fracture and w_p is the specific non-essential work of fracture. There is a positive linear dependence between w_f and ligament length. The positive intercept (w_e) indicates the resistance to crack propagation, and the slope indicates the capability of the material to dissipate energy plastically. The European Structure Integrity Society (ESIS) proposed the following criterion for a valid range of the ligament length for the EWF test in 1997 (*38*):

$$(3t \sim 5t) \leq L \leq \min\left(\frac{W}{3}, 2R_p\right) \tag{4.3}$$

The detailed description of the EWF method can be found elsewhere (*34, 35*).

77

4.1.4 EWF Test and Film Deformation Analysis

The custom-built film fixture which was designed in the previous study was utilized to perform the double edge notched tension (DENT) test of m-LLDPE thin films (*58*). A fresh razor blade was used to prepare the notches in the specimen after installing the m-LLDPE thin film specimen in the fixture. All DENT tests were performed on a custom-built tensile tester with a load cell capacity of 445 N operated at a crosshead speed of 10 mm/min at room temperature. The mode-I EWF toughness characterization was performed using the ESIS protocol for EWF (*38*). The experimental setting and procedure for the DENT test on m-LLDPE thin films can be found elsewhere (*58*). The tear tests were done on an Elmendorf testing apparatus according to ASTM D-1922 at ExxonMobil.

Photoelastic imaging technique, which is based on the stress-optical property of a material, can provide a nondestructive, whole-field, graphic stress-analysis. The fringe patterns appear because the loaded materials become optically anisotropic and are related to the difference between the principal stresses in a plane normal to the light propagation direction. Photoelastic technique was utilized to provide a reliable, visual full-field stress distribution analysis of the DENT specimen under tensile loading with a set of cross-polarizers (*58*). A Canon EOS Rebel T5i camera was used to record the DENT tests conducted on the LLDPE thin films. A Mitutoyo Digimatic Micrometer was used to measure the film thicknesses.

4.1.5 Tensile Testing

A traditional tensile testing was performed to obtain the engineering stress-strain curves for the m-LLDPE blown film samples in both machine (MD) and transverse directions (TD). The film specimens were made 25.4 mm wide and 80 mm long. The distance between two grips was 76.2 mm apart at the beginning of the test, so the test area was 25.4 mm wide by 76.2 mm long. The tensile test was conducted at 0.5 m/min. The tensile tests for the engineering stress-strain curves were done at ExxonMobil.

4.2 Results and Discussion

4.2.1 Morphological observations of m-LLDPE thin films

To characterize the morphological differences between m-LLDPE films made from different resin densities, AFM was used to observe the spherulitic structure of the films. Although there is no significant difference in the average spherulite size for these films, the lamellar structure of the spheulites changes depending on which resin density the film was made from (Figure 4.1). The lamellae are thicker for the m-LLDPE films made from the higher density resin when compared with the films made from lower density resin. Because resin density is highly correlated with the amount of comonomer in the system, changes in the resin density strongly affect the short-chain branch content and the degree of crystallinity. The m-LLDPE structure has a linear backbone and short, uniform branches that prevent the polymer chains from packing closely together. A higher short-chain branch content correlates with lower resin density. The short-chain branch content also has significant effect on the crystallization kinetics of m-LLDPEs

since these side chains do not crystallize and are rejected into the amorphous or interfacial regions (*21, 64*). Thus, the short-chain branch content can strongly influence lamellae thickness, tie-molecule concentration, and the degree of lamella imperfection, resulting in different material morphologies and macroscopic behavior (*18, 65-67*).
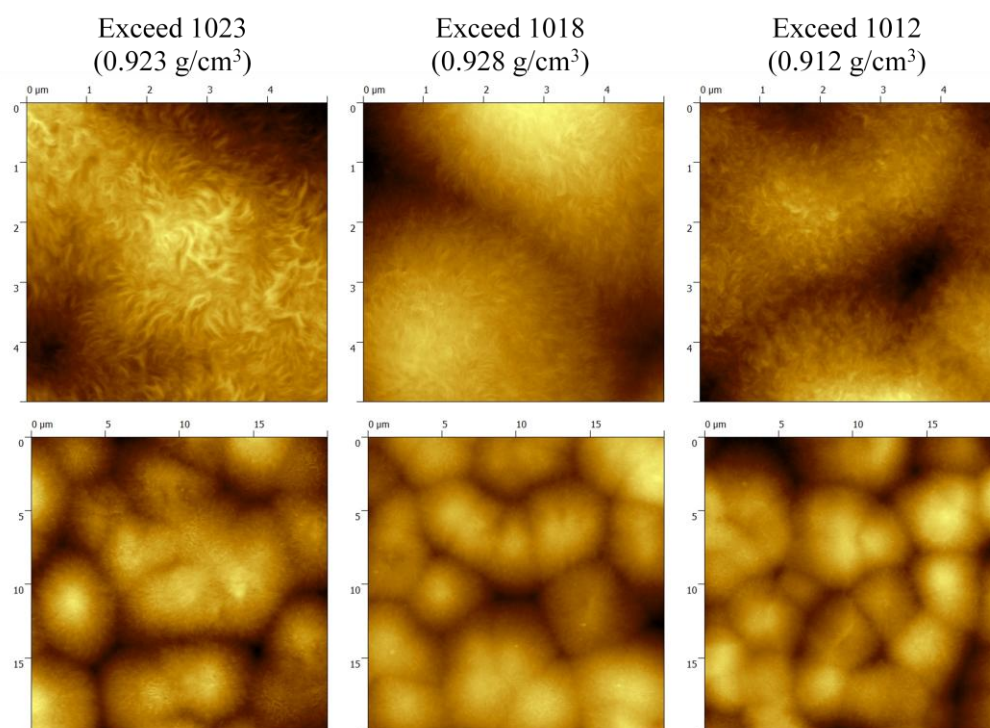
Figure 4.1. AFM images of 0.076 mm thick, 2.5 BUR m-LLDPE films made of different resin densities.

4.2.2 Tensile Properties of m-LLDPE thin films

The engineering stress-strain curves of the m-LLDPE films made of different resin densities are shown in Figure 4.2, and the tensile properties obtained from the engineering stress-strain curves are summarized in Table 4.2. The elastic modulus is higher for the m-LLDPE film made of higher resin density (Figure 4.3a). Several studies have found the elastic modulus decreases with increasing short chain branching content [D/13, 22]. The modulus of m-LLDPE film correlates to its crystalline which is highly influenced by the short chain branching content. But the effect of crystallinity on the modulus is complex [D/4, 5]. Slight increase in the elongation at yield for the m-LLDPE thin films with increasing short chain branching content (Figure 4.3b). With higher short chain branching content, it becomes more difficult for m-LLDPE polymer chains to pack closely together and to crystallize. The reduction in crystallinity leads to the increase in the amorphous region, which dominates the deformation before yielding. But the yield strength is higher for the m-LLDPE film made of higher resin density (Figure 4.3c). The yielding of the semicrysatlline polymer, such as m-LLDPE, involves the disruption of crystalline lamellae structure [D/6-33 37]. Since the m-LLDPE film made of higher resin density tends to have higher crystallinity, it makes sense for the m-LLDPE film having higher yield strength to deform the crystalline lamellae have to allow higher straining upon further stretching. The strain hardening modulus is higher for m-LLDPE film made of lower resin density (Figure 4.2). The elongation at break in TD is higher than that in MD. For 0.076 mm thick m-LLDPE films, the elongation at break is higher for the films made with higher resin density, but no significant difference in the elongation at break

for the 0.019 mm thick films. But the m-LLDPE films made of lower resin density haves lightly higher tensile strength than those made of higher resin density. The main feature of copolymers is the presence of branching which reduces crystallinity and increases tie molecule concentration (*68*). The drawing ability and strength of the fibrils depend on the rate of disentanglement of the fibrils and are influenced by the tie-molecules (*69*). It suggests that these copolymers with different short chain branching content have different strain energy density to deform. Although the effects of resin density to strain hardening, the elongation at break and the tensile strength can be observed, the phenomenon behind is not understood and further investigation is warranted. Since the short chain branching content can greatly influence material morphology, molecular motions, crystallization kinetics, and microstructural deformation, the tensile properties are different for m-LLDPE films made of different resin densities.

Table 4.2. Tensile properties of m-LLDPE blown films.

Resin	Thickness (mm)	Orientation	Elastic Modulus (MPa)	Yield Strength (MPa)	Elongation @ Yield (%)	Tensile Strength (MPa)	Elongation @ Break (%)
Exceed 1023	0.076	MD	161.01	10.45	5.6	55.27	775
		TD	141.76	11.05	5.5	54.92	823
	0.019	MD	129.93	10.11	5.6	50.90	449
		TD	130.72	10.40	4.9	50.46	667
Exceed 1018	0.076	MD	133.81	8.80	5.9	59.15	717
		TD	144.14	9.96	8.1	60.00	779
	0.019	MD	135.28	9.38	7.0	76.47	488
		TD	135.66	9.07	5.3	60.44	665
Exceed 1012	0.076	MD	63.71	6.43	6.6	60.05	673
		TD	78.38	6.50	6.4	59.09	716
	0.019	MD	55.98	6.56	7.1	69.43	426
		TD	62.50	6.32	6.4	63.84	652
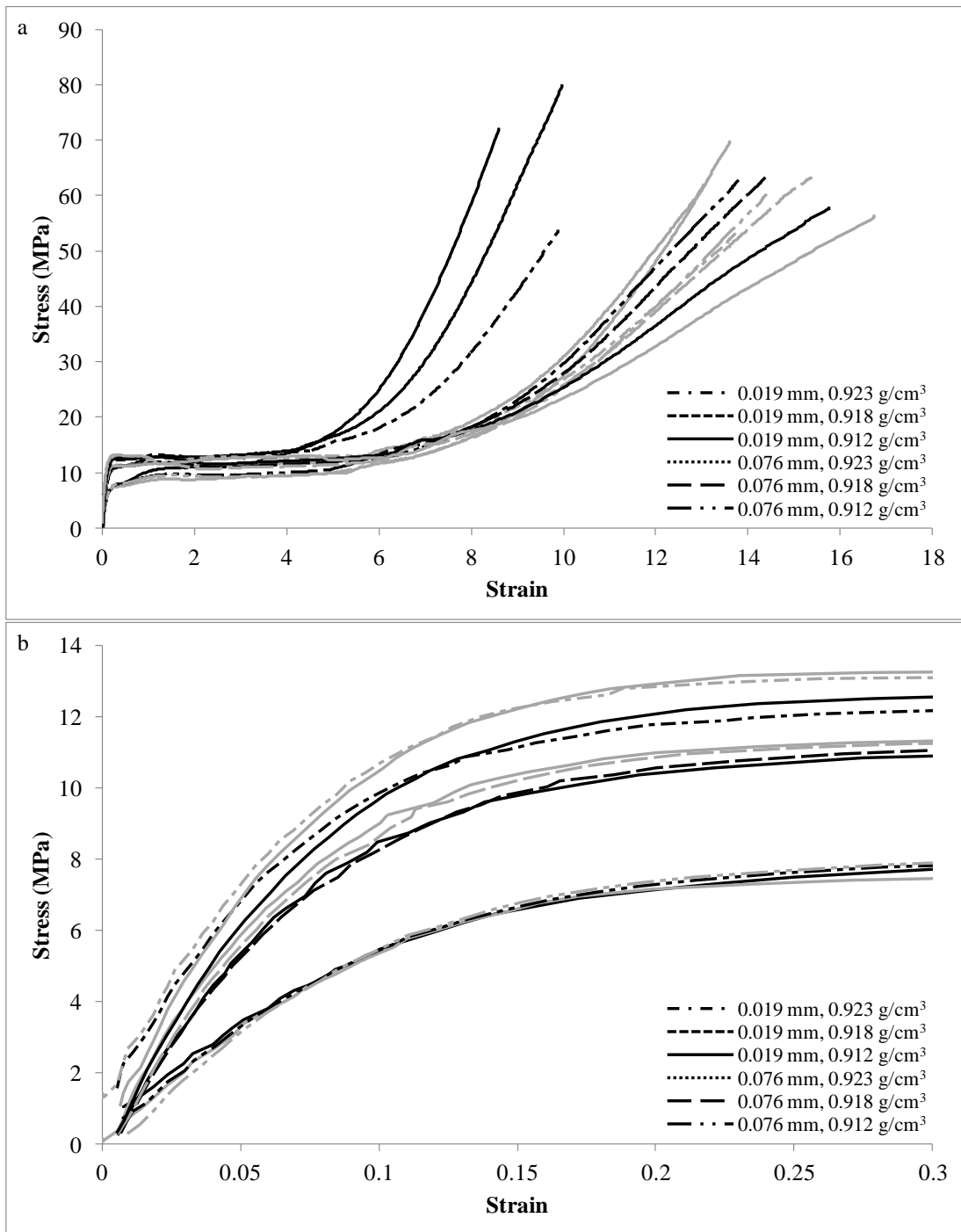
Figure 4.2. (a) The engineering stress-strain curves of 2.5 BUR m-LLDPE films with different resin densities and film thicknesses. (b) An enlarged view of the elastic portion of the stress-strain curves. Black lines are the tensile test results for the MD, while grey lines are for the TD.
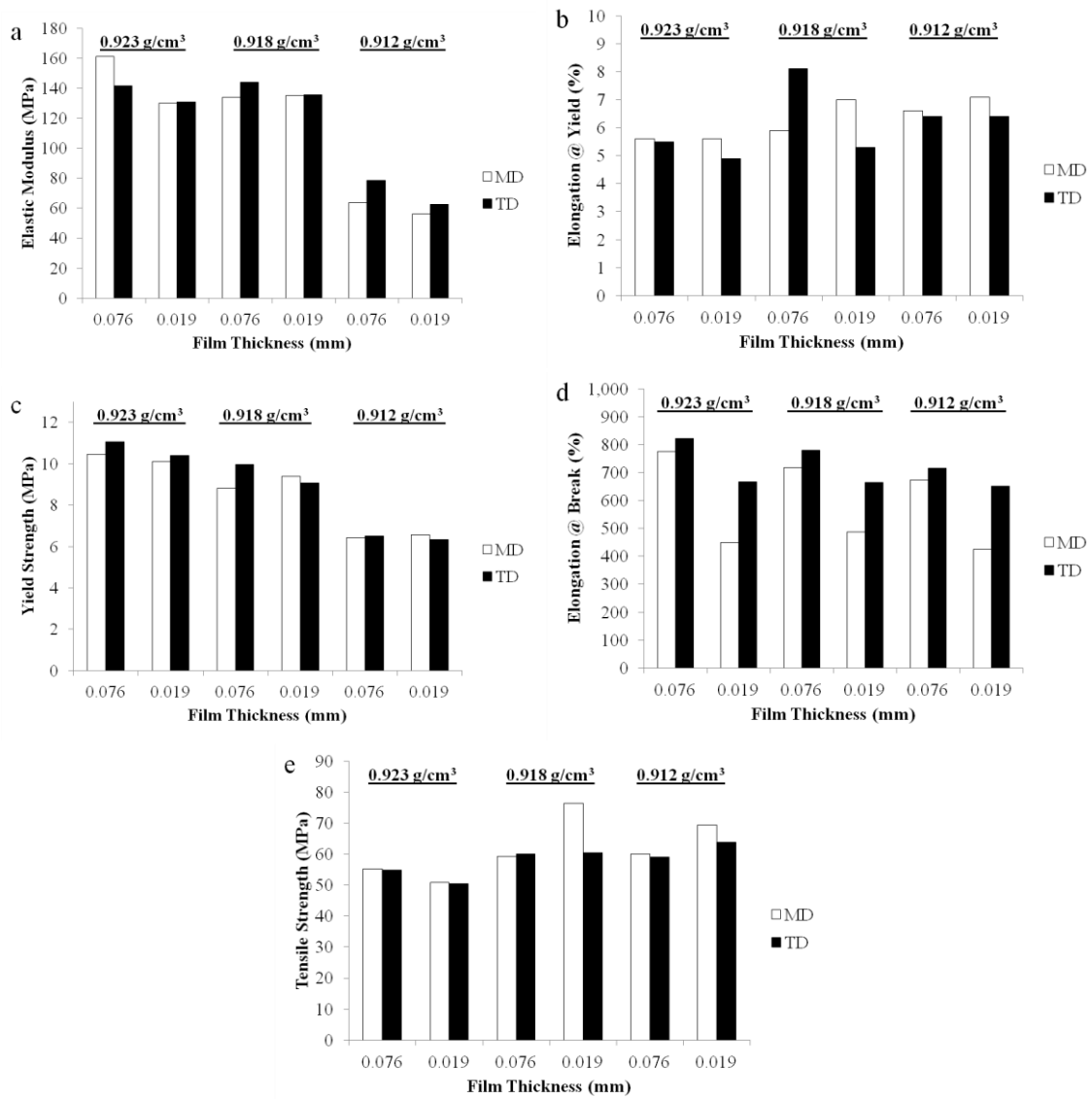
Figure 4.3. The tensile properties of 2.5 BUR m-LLDPE films with different resin densities and film thicknesses.

85

4.2.3 Deformation in the DENT film specimens

The photoelastic technique was used to observe the whole-field stress distribution of the DENT m-LLDPE specimens. During the DENT test, fringe patterns developed and intensified due to stress build-up. The fringe development starts at the crack tips, which are the areas of highest stress concentration, then the two fringe fronts grow in size, and propagate toward the center of the ligament, finally merging with each other upon sufficient loading. After two fringe fronts merge, they start to propagate and develop in the loading direction. However, the fringe patterns change in the DENT m-LLDPE specimens depending on the resin density they were made out of, which indicates different stress states occur during the fracture process. Necking development can be observed for the DENT m-LLDPE specimens under mode-I fracture, but the stress states within the necking deformation zone are significant for the DENT m-LLDPE specimens made from different resin densities. The fringe pattern did not disappear after the film's failure and separation, suggesting non-recoverable deformation is present in the failed DENT specimen.

The thickness of the DENT specimen was measured post-mortem from the tip of the fracture point to the top of the residual fringe pattern boundary. A large reduction in film thickness was observed near the top of the fringe boundary (Figure 4.4). The film thickness reaches a plateau level after a dramatic reduction in the film thickness near the fringe boundary (Figure 4.4). The film's orientation had no effect on the plateau film thickness. Large film thinning is a clear indication of necking formation in the process zone of m-LLDPE film prior to film's ultimate fracture. The thinning behaviors at the

plateau region are among DENT m-LLDPE specimens made of different resin densities. The DENT specimen made of higher resin density reaches slightly lower plateau value in film's final thickness. The film thickness at the plateau region stays constant for the DENT specimen made of higher resin density, but the film thickness gradually increase at the plateau region for the DENT specimen made of lower resin density. The reasons behind the differences in the plateau thicknesses and the thinning behaviors for the DENT specimens may be due to the differences in the short-chain branch contents, which prevent the polymer chains from packing closely together and influence the microstructural deformation.
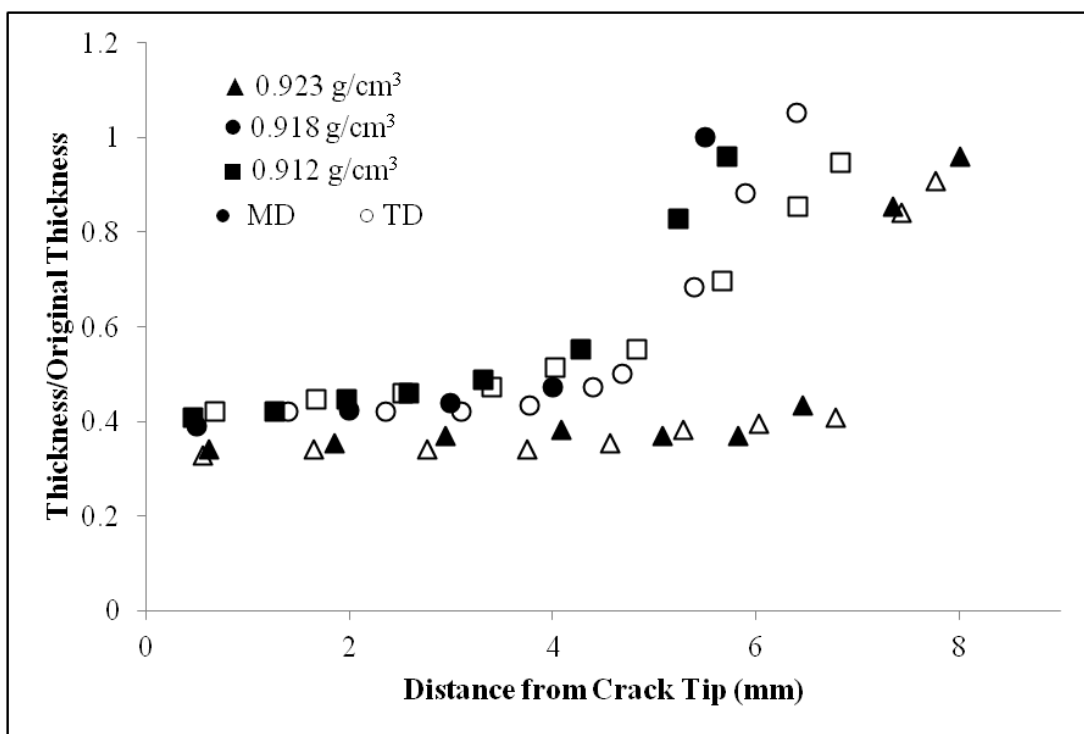
Figure 4.4. Normalized film thicknesses in the plastic deformation zone of post-mortem m-LLDPE blown films made of different resin densities.

4.2.4 The Effect of Resin Density on the EWF Analysis

The EWF parameters of the m-LLDPE films made of different resin densities are summarized in Table 4.3. All test specimens selected for the DENT testing had a FLH of 0.483 m. The ligament lengths tested for the specimens' EWF testing ranged from 6 mm to 30 mm. Plots of w_f vs. L for m-LLDPE films made of different resin density made using 2.5 BUR are shown in Figure 4.5. In general, the crack propagation in the TD has higher fracture toughness than that in the MD for thinner films, which leads to greater w_e and βw_p, but the differences in the fracture toughness between the MD and the TD diminish for thicker films. Thinner films have more crystal and amorphous phase orientation along the MD, which correlates with greater MD strength and TD tear resistance (*6, 54*). But thicker films, which are made under more balanced processing conditions between the draw down ratio and the blow-up ratio, have less film anisotropy, resulting in less orientational differences in their fracture toughness.

Table 4.3. EWF parameters of m-LLDPE blown films.

Resin	Thickness (mm)	Orientation	w_e (kJ/m²)	βw_p (MJ/m³)
Exceed 1023	0.076	MD	27.3	6.67
		TD	46.6	6.09
	0.019	MD	51.6	5.12
		TD	71.8	7.01
Exceed 1018	0.076	MD	49.2	4.82
		TD	42.1	5.13
	0.019	MD	67.1	3.58
		TD	75.7	5.35
Exceed 1012	0.076	MD	40.4	3.61
		TD	39.7	4.27
	0.019	MD	50.1	2.23
		TD	76.7	3.20
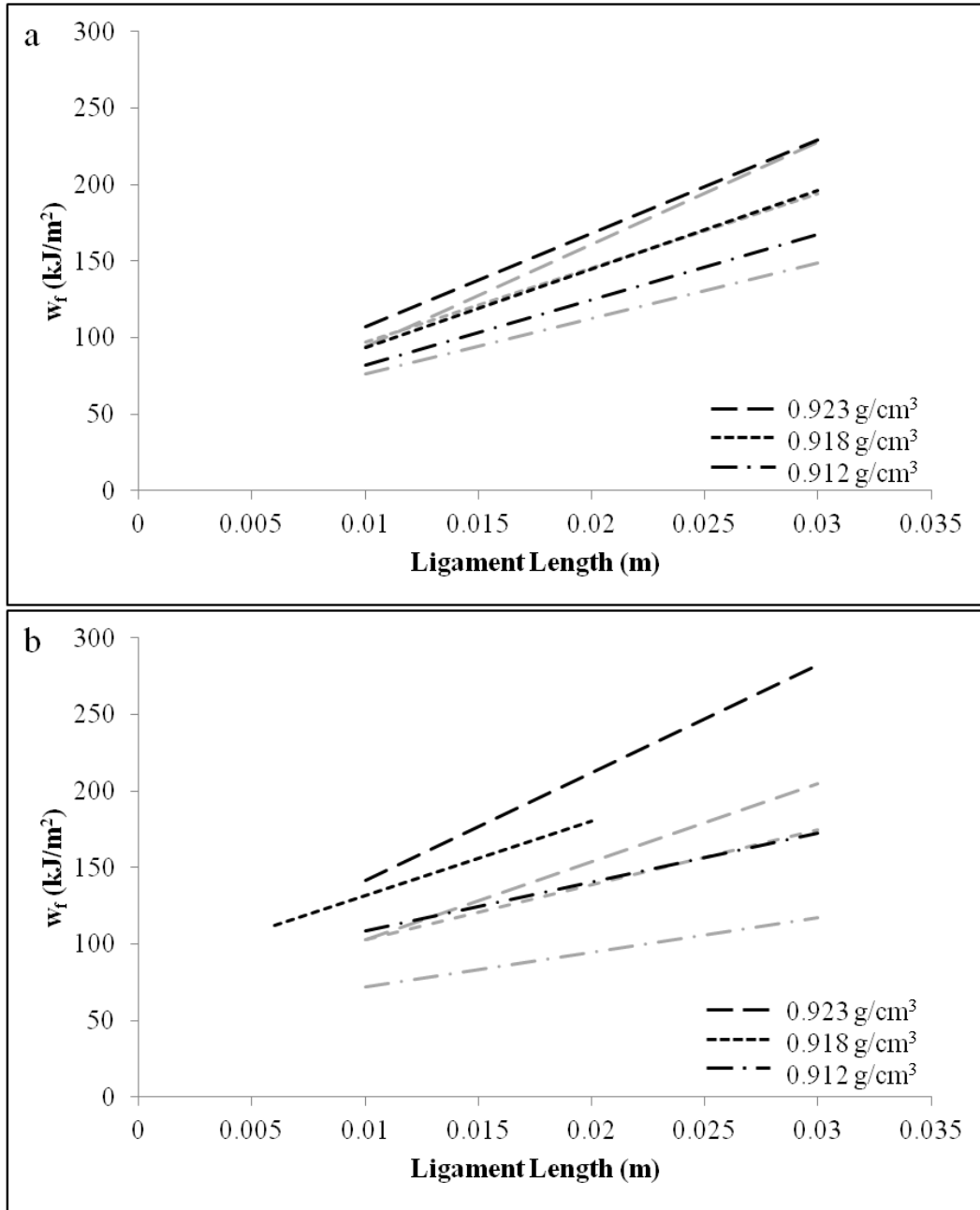
Figure 4.5. Specific work of fracture versus ligament length for 2.5 BUR m-LLDPE blown films with different thicknesses and film orientations. Black lines are for the crack propagation in the MD, and the grey lines are for the crack propagation in the TD.
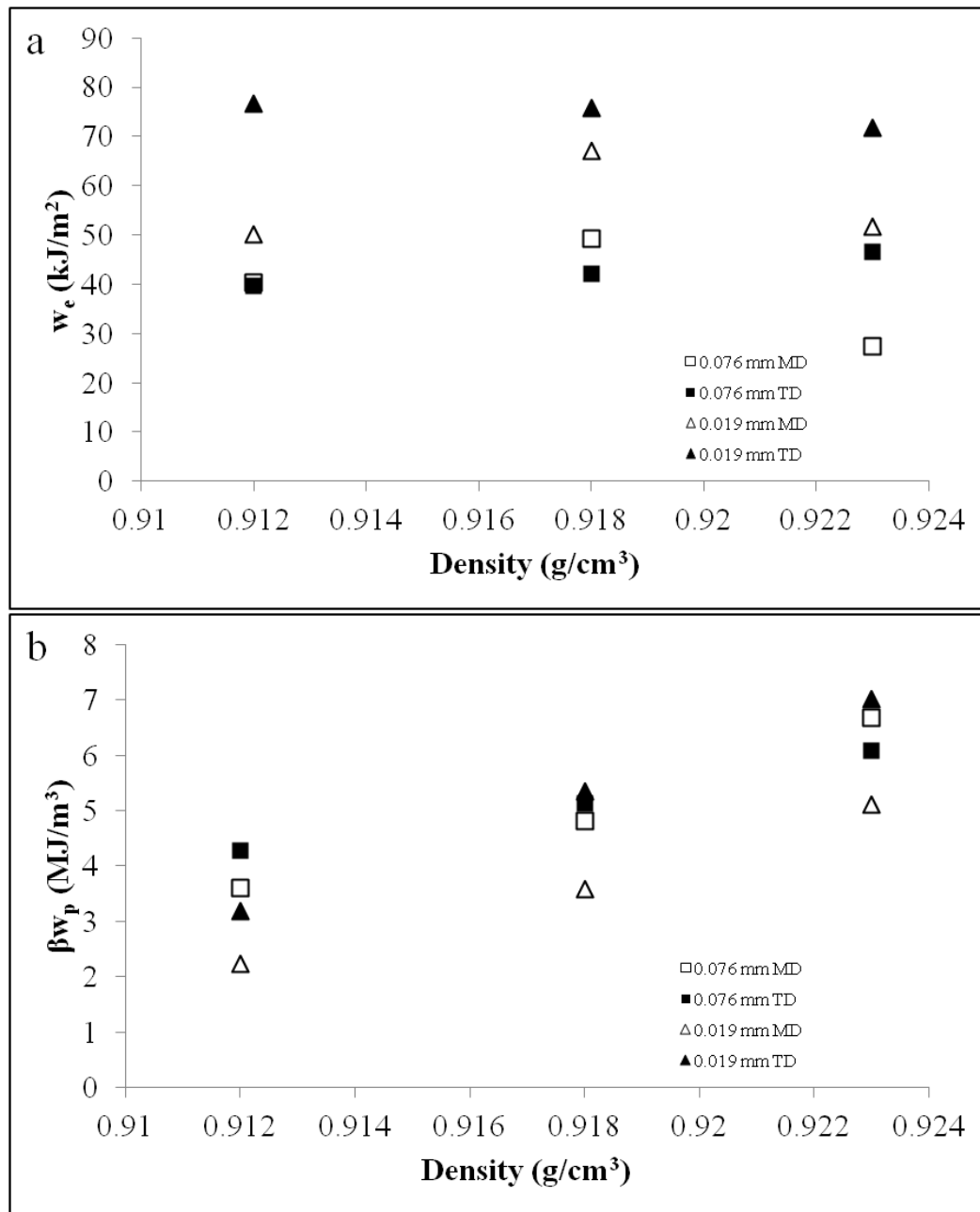
Figure 4.6. (a) Specific essential work of fracture and (b) non-specific essential work of fracture of m-LLDPE blown films with resin densities.

91

The correlations between the EWF parameters and the resin density are shown in Figure 4.6. Resin density has no significant effect on w_e for m-LLDPE films. However, βw_p is higher for the films made from higher resin density regardless of thickness and orientation, which are mainly controlled by the processing conditions, such as draw down ration and blow-up ratio. The cause of resin density's relationship with βw_p is most likely due to the short-chain branch content changes between resin densities. The film made of higher resin density has lower short-chain branch content and higher crystallinity and requires more energy to yield and to deform beyond yielding, which leads to greater βw_p value.

4.2.5 Elmendorf Tear

The Elmendorf tear test is an industrial test for determining the relative tear (mode-III fracture) resistance of polymeric materials. The Elmendorf tear strengths of m-LLDPE films are summarized in Table 4.4. The Elmendorf tear resistance is greater for thicker films, and in TD (Figure 4.7a). The normalized Elmendorf tear resistance in the TD increases with decreasing film thickness, but the normalized Elmendorf tear resistance in the MD increases with increasing film thickness (Figure 4.7b). The effect of thickness and orientation on the Elmendorf tear resistance of m-LLDPE films correlates well with the molecular orientation due to the blown film processing conditions. The film made of higher resin density has greater Elmendorf tear resistance regardless of film thickness, but the effect is more profound for the tear resistance in the TD. The crystallization kinetics and the molecular thermodynamics due to the short-chain branch

content could be the main reason for the film made of higher resin density requiring more fracture energy.

Table 4.4. Elmendorf tear performance of m-LLDPE blown films.

Resin	Thickness (mm)	Orientation	Elmendorf Tear	
			(g)	(g/mm)
Exceed 1023	0.076	MD	835	10992
		TD	1236	16257
	0.019	MD	196	10324
		TD	418	22004
Exceed 1012	0.076	MD	916	12059
		TD	1020	13423
	0.019	MD	162	8514
		TD	304	16021
Exceed 1012	0.076	MD	753	9912
		TD	905	11912
	0.019	MD	120	6331
		TD	260	13676
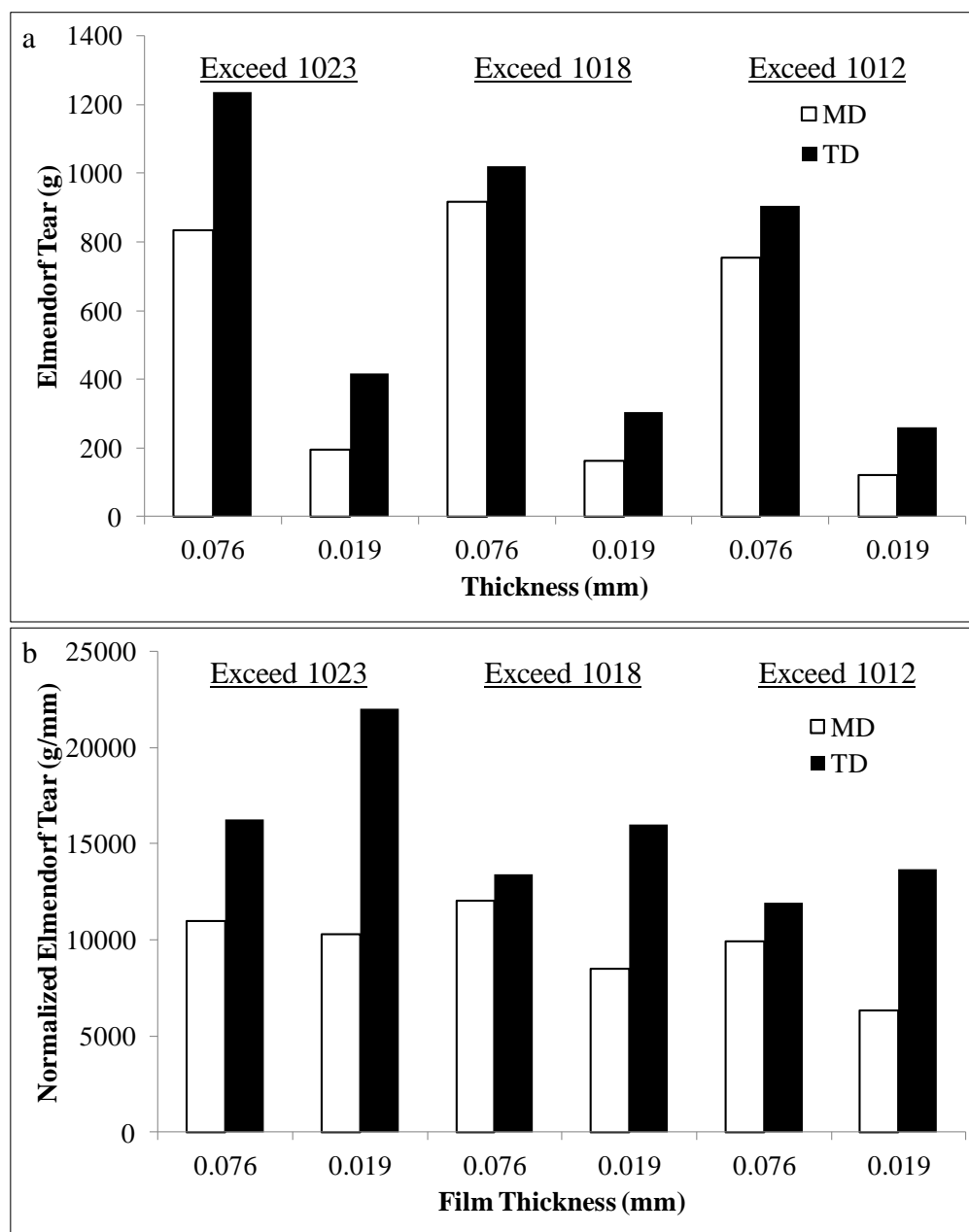
Figure 4.7. (a) Elmendorf tear resistance and (b) normalized Elmendorf tear resistance of m-LLDPE blown films with different resin densities.

4.3 Conclusions

The effect of resin density the morphology and fracture behavior of m-LLDPE films were investigated in this study. The resin density is highly correlated to the short-chain branch content, which can greatly influence the material morphology, molecular motions, crystallization kinetics, and microstructural deformation. The effect of resin density on the spherulitic morphology was observed under the AFM. The tensile properties of m-LLDPE films made of different resin densities were also quantified, and their true stress-strain curves were obtained with the application of the custom-built film fixture, two-half-circle-cutoff-shaped specimen, Sharpie speckle pattern technique, the video recording technique, and the DIC system. The photoelastic technique was utilized to provide the visual full-field stress distribution analysis of the DENT film specimen with different resin densities, and the significant film thinning was observed in the process zone of the DENT film specimen prior to film ultimate fracture. The effect of resin density on the EWF parameters and the Elmendorf tear resistance was characterized. The short-chain branch content, which can greatly influence material morphology, molecular motions, crystallization kinetics, and microstructural deformation, is believed to be the main cause of the different tensile properties and fracture toughness for m-LLDPE films made of different resin densities. Unfortunately, the phenomenon behind is not fully understood and further investigation is needed.

CHAPTER V

EXPERIMENTAL ASSESSMENT AND PHYSICAL INTERPRETATION OF

ESSENTIAL WORK OF FRACTURE PARAMETERS BASED ON M-LLDPE

BLOWN FILMS

The essential work of fracture (EWF) method, applicable when fracture occurs under stable crack growth through a yielded zone, is originated from the post-yielding fracture mechanics (PYFM) concept by K.B. Broberg (*34, 70*). Universal equations for the EWF method was then developed by Cotterel, Mai, and their co-workers (*35, 37*). The EWF method has gained significant attention and acceptance as a tool to characterize the fracture toughness of ductile polymers, toughened polymer blends, and composites because of its simplicity in experimental procedure and data processing (*39, 49, 71, 72*). The EWF method is unique for its concept of partitioning the total fracture energy (W_f) consumed during the post-yielding fracture of a pre-cracked specimen into two distinct zones of energy consumption (Figure 5.1). W_f can be calculated from the integral of the load-displacement (L-d) curve for each specimen. The inner fracture process zone (IFPZ) is directly responsible for the formation of two new fracture surfaces. The essential work of fracture (W_e) indicates the energy associated with the inner process zone and is proportional to the cross-sectional area of the ligament region. The non-essential work of fracture (W_p) represents the energy consumed in plastic deformation and other dissipative processes in the outer plastic deformation zone (OPDZ), and is proportional to the volume of the outer plastic deformation zone.

Therefore, the total fracture energy (W_f) is the sum of the essential work of fracture (W_e) and the non-essential work of fracture (W_p):

$$W_f = W_e + W_p \tag{5.1}$$

When dividing W_f by the cross-sectional area of the ligament, a positive linear dependence between the specific total work of fracture (w_f) and ligament length (L) can be obtained:

$$w_f = W_f/tL = w_e + \beta w_p L \tag{5.2}$$

where y-intercept is the specific essential work of fracture (w_e), the slope is the specific non-essential work of fracture (βw_p), β is a shape factor associated with the volume of the plastic deformation zone, and t is the thickness of the specimen. Theoretically, only w_e is geometry independent and therefore can be a material parameter, and it has been found to be equivalent to the J-integral critical value, J_{1c} (39, 43, 73, 74). In addition, the βw_p term provides a highly morphology-sensitive parameter, which is useful for evaluation of fracture toughness in thin specimens. In the EWF analysis, there are a few key assumptions (39, 75, 76). Firstly, the load–displacement curves should be self-similar among all specimens tested in a series of different ligament lengths to confirm a common geometry of fracture. Secondly, the ligament length is fully yielded before the crack propagation. Thirdly, the volume of the OPDZ is proportional to L^2. Finally, the fracture occurs under plane stress conditions, thus both w_e and βw_p are independent of ligament length. The European Structural Integrity Society (ESIS) TC-4 committee standardized the EWF method(77, 78) and set the following criterion for ligament lengths for a valid EWF test:

$$(3t{\sim}5t) \le L \le min\ (\tfrac{W}{3}, 2R_p)$$
(5.3)

where W is the width of the specimen and R_p is the radius of the plastic zone at the crack

tip.
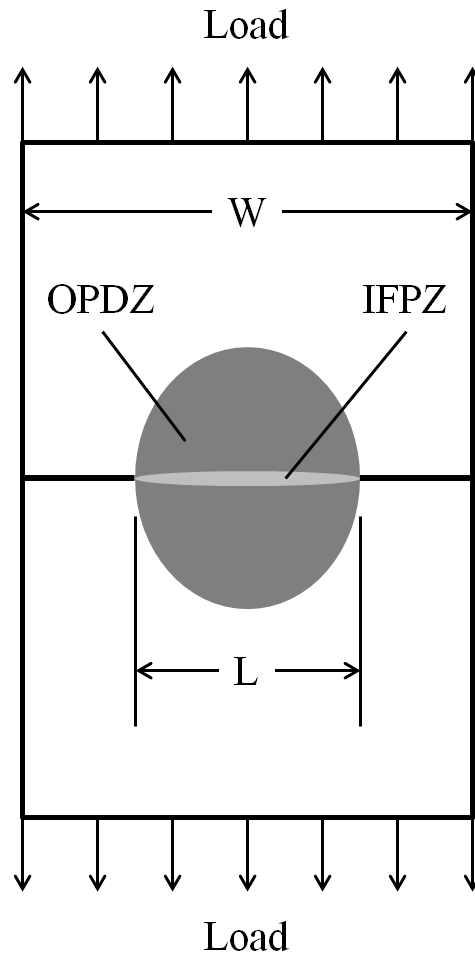
Figure 5.1. Double-edge-notched tensile specimen. (W is the width of the film specimen; L is the ligament length; OPDZ is the outer plastic deformation zone; IFPZ is the inner fracture process zone)

Although the EWF method is based on the energy partitioning concept, many studies have attempted to further elucidate the deformation mechanisms and corresponding fracture energy by partitioning the total work at either the maximum load or the onset of necking or crack propagation (*39, 79-83*). The yielding work approach (Figure 5.2a) was proposed by Karger-Kocsis (*79-81*). It partitions the total fracture energy at the maximum load of the L-d curve into two components, the work of yielding the ligament area (W_y) and the work of fracture of subsequent necking and tearing (W_n):

$$w_f = w_{f,y} + w_{f,n} = \left(w_{e,y} + \beta w_{p,y}L\right) + \left(w_{e,n} + \beta w_{p,n}L\right) \tag{5.4}$$

where $w_{e,y}$ has been shown to be independent of molecular weights (*80, 84*) and strain rate (*49, 80*) for copolyester materials. Previous works have suggested that $w_{e,y}$ is a material parameter because it is closely related to the plane-strain essential work of the fracture ($w_{e,IC}$) (*79, 80, 84, 85*), which represents an inherent material toughness parameter. Mai and Cotterell (*39, 43, 82, 83, 86, 87*) defined another energy partitioning concept, the initiation work method, which is related to crack initiation, whereby the elastically stored energy in the specimen was taken into account (Figure 5.2b). The energy partition criterion is taken after the necking of the ligament area. W_f is separated into two components: W_I (irreversible initiation process involving yielding, necking and crack-tip blunting) and W_{II} (crack propagation and extended necking in the plastic zone):

$$w_f = w_{f,I} + w_{f,II} = \left(w_{e,I} + \beta w_{p,I}L\right) + \left(w_{e,II} + \beta w_{p,II}L\right) \tag{5.5}$$

where the absorbed elastic energy in the necked specimen is supposed to be released during the W_{II} process, and it is not included in the initiation work. The concept is based

99

on two reasons: firstly, it corresponds to a clear transition of the process, which is the onset of crack propagation; secondly, the transition coincides with a clearly distinguishable point on the curve, which makes the data treatment easier and unambiguous. The energy splitting has been done parallel to the slope of the elastic range curve with the purpose of leaving out the elastic energy that is initially stored, which is not actually dissipated since it is theoretically released later as energy available for the fracture processes.
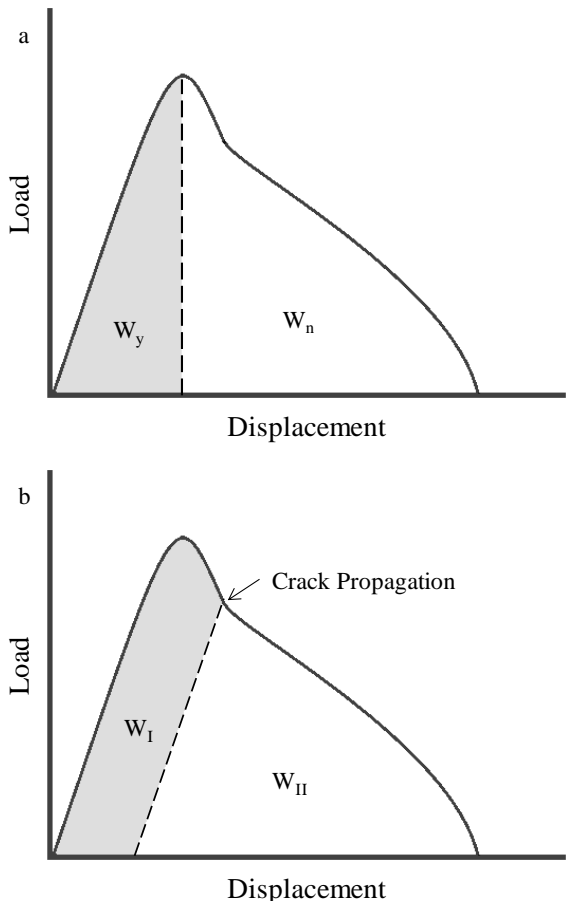
Figure 5.2. Energy partitioning methods, schematically illustrated according to (a) the yielding and (b) the initiation concepts.

Although both of the above energy partitioning criteria, which are based on the analysis of the L-d curve and corresponding fracture process, have been widely applied in the EWF characterization of various materials, they lack direct experimental confirmation of those specific energy density terms with the actual deformation process.

The EWF method is applicable to fracture processes in which the plastic deformation zone is fully developed before the crack growth commences, and the non-essential part of the energy consumption scales with L^2. These assumptions may not be met for the fracture process of some polymeric materials (*88, 89*) and should be validated. The validity of the EWF approach is questioned even if regression analysis shows good linear correlation in w_f vs. L curve. Although βw_p from the EWF approach can serve as an indication of the material capacity for plastic deformation, uncertainty on β value has limited its usefulness. As a result, the EWF approach is mainly used to determine the w_e that represents the essential material property for resistance to fracture in a given loading condition.

Instead of the EWF method, a mechanistic approach for determining the fracture resistance of polyethylene in the plane stress condition was proposed by Jar et al (*88, 89*). The approach uses the energy balance principle to develop an equation that considers all the mechanisms involved in the plane stress fracture process of a DENT specimen at the neck propagation stage where the constant crack growth occurs:

$$w_f = w_e + w_{p,ng} + w_{p,s} \tag{5.6}$$

where the corresponding specific energy densities for crack surface formation, necking, and plastic deformation are represented by w_e, $w_{p,ng}$, and $w_{p,s}$, respectively. The approach

provides an interesting energy partitioning concept for the three mechanisms involved in the fracture process at the neck propagation stage, but it lacks the capability to evaluate the entire fracture process and experimental validation for each energy term.

In this study, a new experimental approach has been developed to directly quantify and partition the total fracture energy under mode-I DENT EWF test. The approach partitions the total fracture energy into three components, the work associated with necking and crack propagation (W_e), the work consumed by plastic deformation (W_p), and the work related to recoverable viscoelastic deformation (W_v). The experimental determination of energy dissipation was carried out based on an integration of strain energy density over the volume of each deformation zone. The summation of W_e, W_p, and W_v terms was then validated through comparison with the mechanical energy input to the film, i.e., the area under the L-d curve. Physical correlation between the EWF parameters and film deformation zones could then be established. The usefulness and implication of the present approach for establishing structure-property relationship in polyethylene blown films is discussed.

5.1 Experimental

5.1.1 Material

Exceed™ 1018 and 1023 resins are metallocene linear low density polyethylene (m-LLDPE) copolymers. Two sets of model m-LLDPE blown films with a 2.5 blow-up ratio (BUR) and film thickness of 0.076 mm were prepared by ExxonMobil.

5.1.2 Tensile true stress-strain curve

Tensile testing was conducted with a custom-built film fixture which was originally designed for EWF testing on polymeric thin films. The modified film fixture can eliminate any surface wrinkling on the thin film specimen. A tapered tensile specimen was prepared to create controlled stress concentration at a location of interest and to prevent multiple necking regions, which are observed in a typical dogbone-shaped specimen, during tensile testing of polymeric films. A digital image correlation (DIC) system from Correlated Solutions is a non-intrusive method for *in-situ* deformation measurement. A Canon EOS Rebel T5i camera was used to record the DENT and tensile tests conducted on the m-LLDPE thin film. Combining a Sharpie speckle pattern technique, video recording, and the DIC system, local deformation of the tensile specimen can be measured and a true stress-strain curve can be generated.

5.1.3 Mode-I DENT Test

The DENT test of m-LLDPE thin film was performed using the custom-built film fixture designed in our previous study . A fresh razor blade was used to prepare the notches in the specimen after installing the m-LLDPE thin film specimen in the fixture. The DENT test was performed on a custom-built tensile tester with a load cell capacity of 445 N operated at a crosshead speed of 10 mm/min at room temperature.

5.1.4 Photoelastic Observation

Photoelastic imaging, which is based on the stress-optical properties of a material, can provide a nondestructive whole-field, *in-situ* graphical stress analysis of the blown films. Fringe patterns appear under polarized light because the loaded materials become optically anisotropic in a way that is related to the difference between the principal stresses in a plane normal to the light propagation direction. The photoelastic technique was used to provide a reliable, visual full-field stress distribution analysis of the DENT specimen under tensile loading using a set of cross-polarizers.

5.2 Results and Discussion

Photoelastic technique was used to observe the whole-field stress distribution of the DENT m-LLDPE specimen. Upon DENT test, birefringent patterns develop and intensify during loading (Figure 5.3). Two birefringent patterns develop symmetrically near the two crack tips which grow in size, then propagate toward the center of the ligament and merge with each other upon further loading. After the two fringe fronts merge, the birefringent pattern starts to propagate and develop in the loading direction. The birefringent pattern does not disappear after the film fracture and separation (Figure 5.3), suggesting non-recoverable deformation is present in the failed DENT specimen. Three distinctive process zones can be observed from the birefringent pattern (Figure 5.4). Mai et al. indicated that IFPZ, i.e., W_e, includes the cracking region where new surface is formed and may include a necking region if the material is ductile (*82*). In this study, it is found that necking occurs not only in the region adjacent to the crack surface but also propagates along the loading direction due to an unloading effect (*90*). It is

uncertain if the EWF methodology can account for the observed extensive necking formation and propagation.
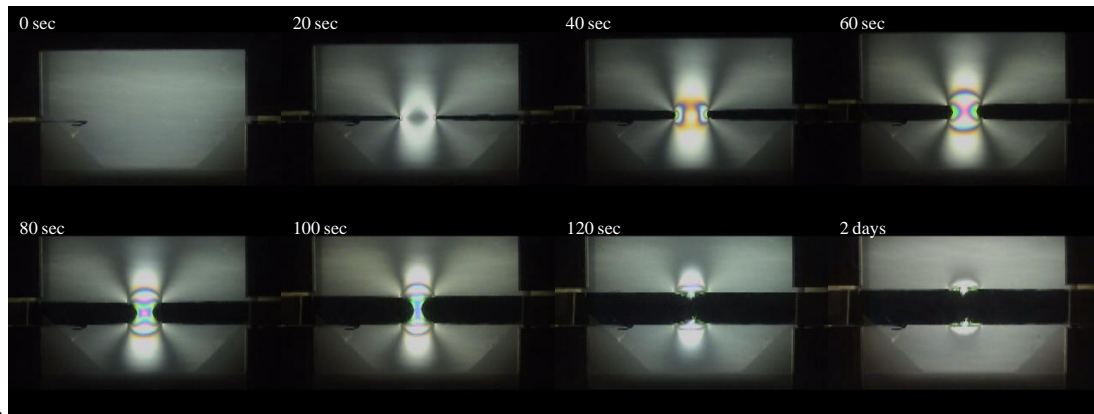
Figure 5.3. Photoelastic observation of 0.076 mm thick, 2.5 BUR m-LLDPE blown film with 20 mm ligament length.
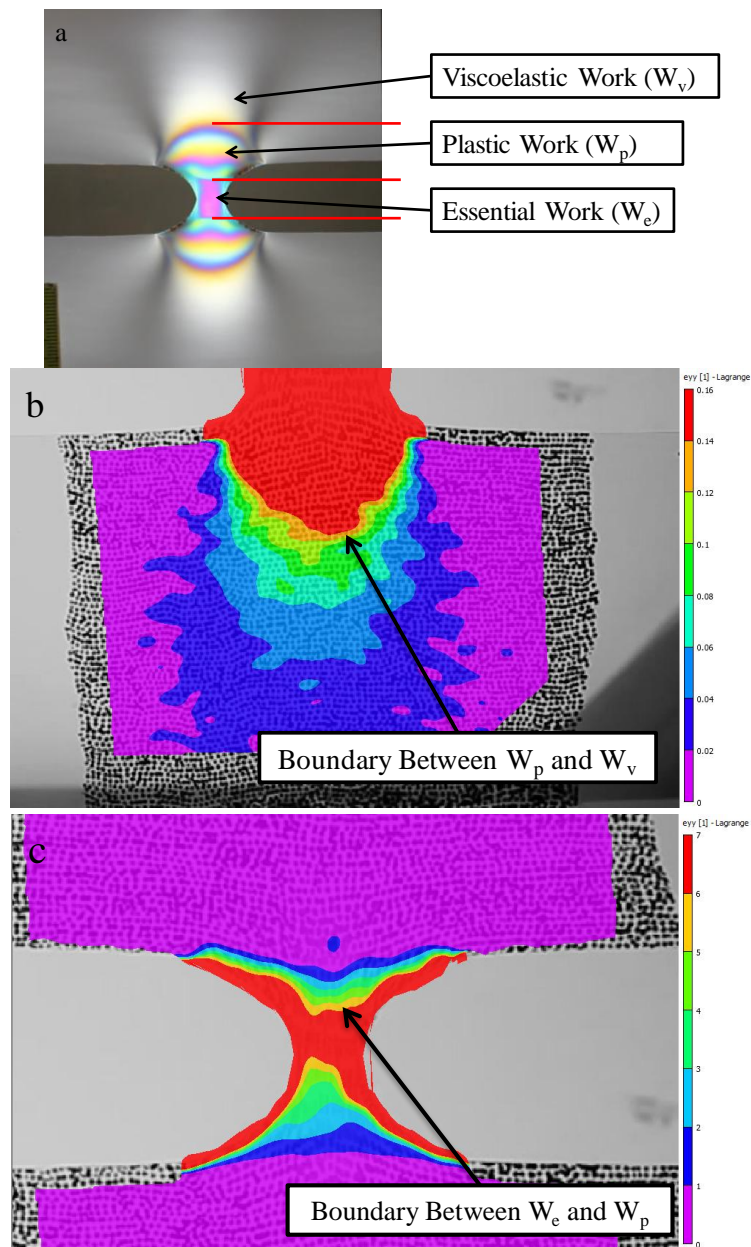
Figure 5.4. (a) Photoelastic observation for three energy components, work for necking and crack propagation (W_e), work for plastic deformation (W_p), and work for recoverable viscoelastic deformation (W_v). (b) Boundary between W_v and W_p and (c) boundary between W_p and W_e from the DIC analysis.

106

Besides the IFPZ and OPDZ, two additional large birefringent regions outside of the top and bottom plastic deformation zones are also observed (Figures 5.3 and 5.4). These large birefringent regions would greatly reduce in size when the film fracture occurs, which indicates some elastic recovery, and then diminishes in size further and eventually disappears over time, which indicates viscoelastic recovery (Figure 5.3). So, this deformation zone is considered as the recoverable viscoelastic deformation zone. The fundamental concept of the EWF method is based on the partitioning of W_f into W_e and W_p. It would be interesting to learn if W_v is significant enough to be included in the EWF energy partitioning. If so, the quantification of the W_v would become an important EWF parameter for the design and development of tough polymeric films. Here, we define that the total fracture energy includes the work done in the IFPZ, OPDZ, and the recoverable viscoelastic deformation zone:

$$W_f = W_e + W_p + W_v \tag{5.6}$$

To accommodate the measurement, a new experimental setup was developed to *in-situ* quantify and partition the total fracture energy into W_e, W_v, and W_p under mode-I DENT EWF test. The fracture energy was determined by strain mapping and integration of strain energy density over the entire deformation zone:

$$U_0 = \int_0^\varepsilon \sigma \, d\varepsilon \tag{5.7}$$

$$U = \int_V U_0 \, dV \tag{5.8}$$

where U_0 is the strain energy density, which represents the energy required for unit volume of the material to deform to a prescribed strain magnitude, and U is the strain energy of the volume of material involved in the deformation. In doing so, two major

pieces of information are still required to proceed in the experimental quantification and partitioning of the total fracture energy for the mode-I DENT specimen. One is the true stress-strain curve of the material and the other is the full-field strain mapping of the mode-I DENT specimen.
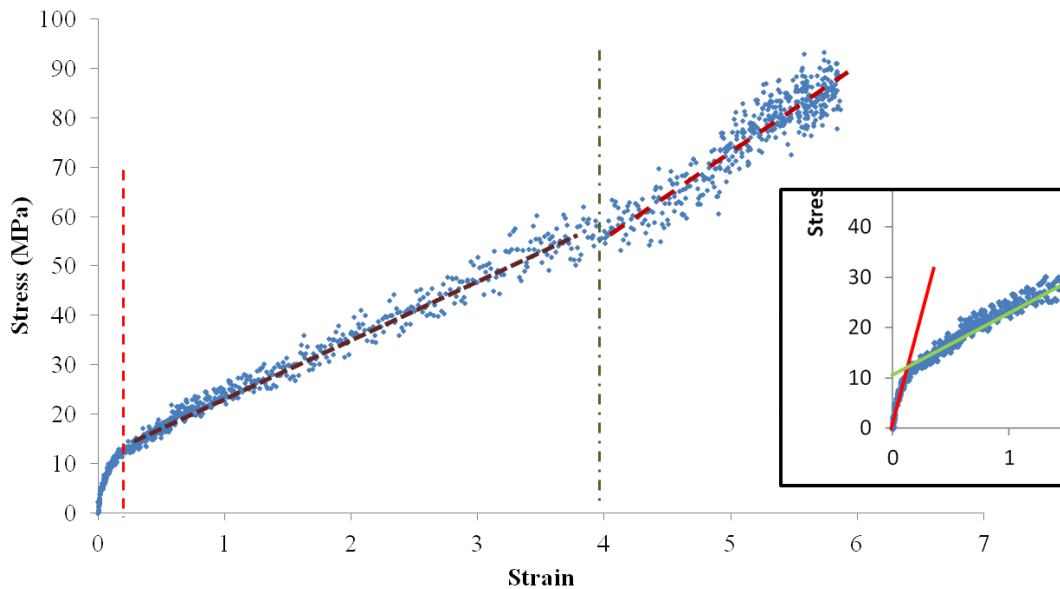
Figure 5. 5. True stress-strain curve and partitioning of strain energy density.

The m-LLDPE blown films are fragile, but ductile, and the films will typically experience substantial dimensional changes during tensile loading. As a result, to obtain true stress-strain curves, it is necessary to utilize non-contact DIC strain mapping to construct true stress-strain curves. The true stress-strain curve offers information about geometry-independent strain energy density of the film at any given location if strain mapping is conducted in full-field throughout the duration of the tensile test (Figure 5.5). The strain energy density can then be determined from the area underneath the true

stress-strain curve, and further divided into three parts for the purpose of energy partitioning. The deformation below the yielding point is considered as the recoverable viscoelastic deformation. Thus, the yielding point is used as the boundary to distinguish between W_v and W_p.

At a much higher strain level on the true strain-strain curve, a change in slope of the curve is observed for strain at around 400% for the m-LLDPE sample tested, which appears to be related to the necking of the material. Interestingly, the strain value at the boundary between the IFPZ and OPDZ observed from the DIC strain mapping during mode-I DENT test is also found to be about 400% (Figure 5.4). Therefore, the strain at the transitional slope on the true stress-strain curve is used as the strain boundary between W_e and W_p. The size of each deformation zone can now be identified from the full-field strain mapping by DIC with the assumption of the constant volume during deformation, which is considered a reasonable assumption since polymers are in general considered incompressible after yielding. The strain mapping provides the deformation information for the film per unit volume prior to fracture. The energy required per unit volume of material to the observed deformation can be determined through integration of the strain energy density over the entire volume of the necked region (Equation 5.7). Further, the energy consumed per unit volume is then integrated to obtain the energy terms of W_v and W_p according to the criteria described above.

It should be noted that the experimental approach to directly quantify and partition the total fracture energy of the mode-I DENT film specimen is done under the assumption of constant volume and the film deformation is monitored based on 2-D

imaging. Through the integration of the strain energy density and the size of each deformation zone, W_v and W_p can be quantified experimentally. Because the DIC provides the full-field strain mapping through the entire fracture process, the experimental approach not only determines the total energy for both W_v and W_p but also tracks the development of W_v and W_p throughout the entire deformation process.

The work done in the IFPZ involves both necking and crack propagation. From photoelastic observation and the full-field strain mapping, it clearly shows that W_e is involved within a finite volume instead of only the cross-sectional area of the ligament region due to necking. The finding is contrary to the original assumption of the EWF analysis, where W_e is considered proportional only to the cross-sectional area of the ligament region. The total work for W_e includes the work done due to both necking and crack propagation. Therefore, W_e can be estimated by integrating the strain energy density over the volume of the materials involved in the IFPZ (Figure 5.6). The development of W_e is found to be linearly proportional to the length of the crack growth (Figure 5.7). The initial reduction of the ligament length is due to the shrinkage by the Poisson's ratio effect, and a transitional change in the residual ligament length can be observed and is an indication of onset of the crack propagation. The linear crack propagation is observed until very end of the fracture process. The development of W_e can then be estimated through the fracture process (Figure 5.8).
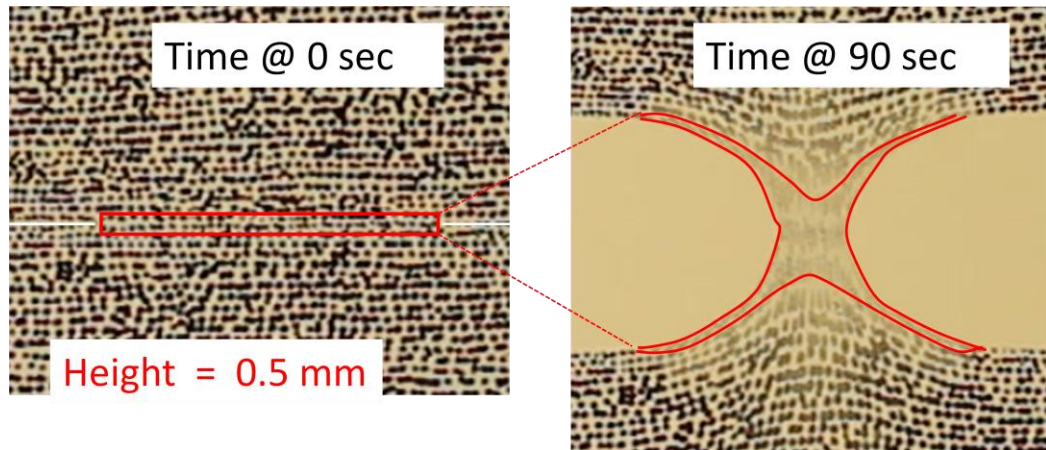
Figure 5.6. Deformation zone estimation of work for necking and crack propagation.
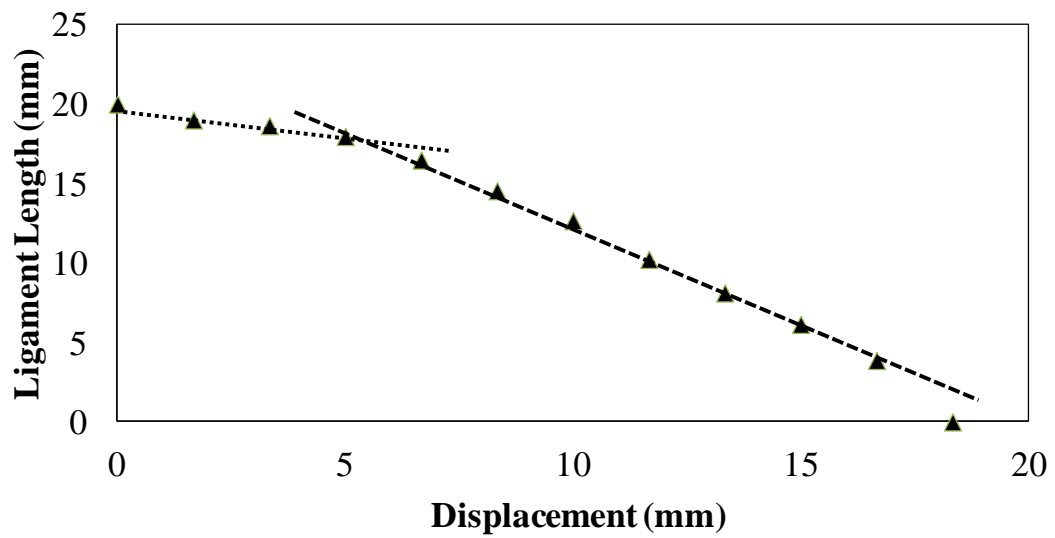
Figure 5.7. Observation of the crack growth.

111
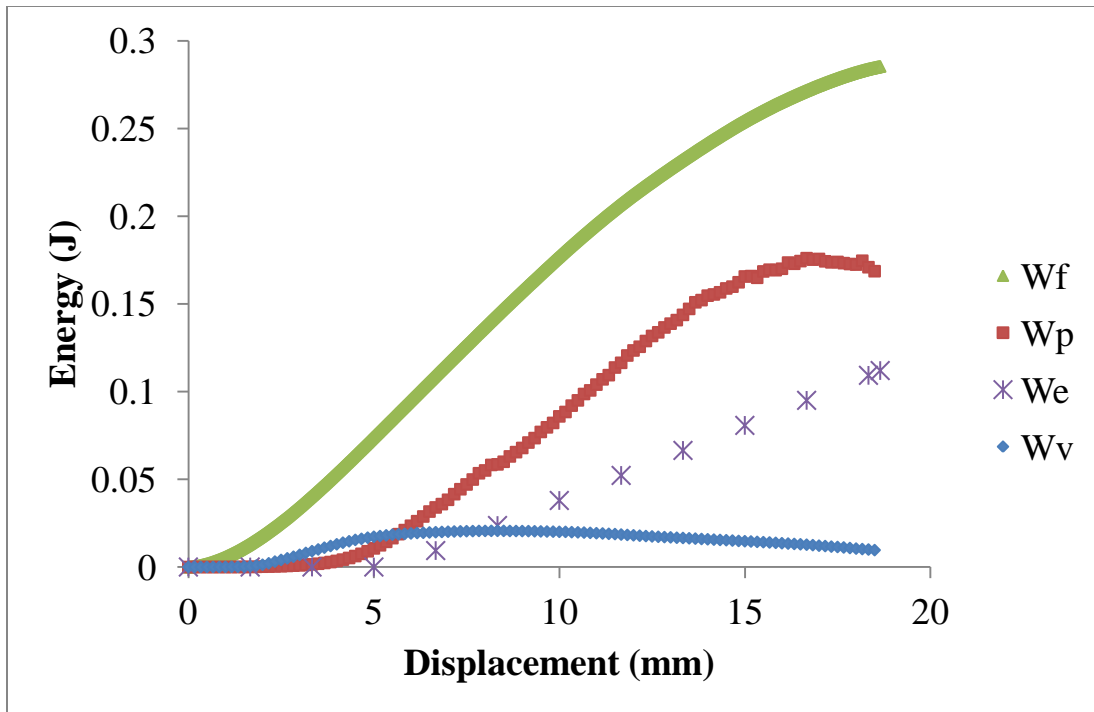
Figure 5.8. Quantification and partitioning of the total fracture energy through the fracture process.

Table 5.1. Summary of energy partitioning

	Exceed 1018, 0.076 mm, 2.5 BUR, L= 20 mm, TD		
	DIC Estimation (J)	EWF (J)	L-d Curve (J)
W_v	0.0096		
W_p	0.1686	0.2146	
W_e	0.1120	0.0727	
W_f	0.2902	0.2873	0.2854
	Exceed 1018, 0.076 mm, 2.5 BUR, L= 20 mm, MD		
	DIC Estimation (J)	EWF (J)	L-d Curve (J)
W_v	0.0090		
W_p	0.1182	0.1836	
W_e	0.1282	0.0737	
W_f	0.2554	0.2573	0.2625
	Exceed 1023, 0.076 mm, 2.5 BUR, L= 20 mm, TD		
	DIC Estimation (J)	EWF (J)	L-d Curve (J)
W_v	0.0168		
W_p	0.1546	0.1948	
W_e	0.1346	0.0745	
W_f	0.3060	0.2693	0.3219
	Exceed 1023, 0.076 mm, 2.5 BUR, L= 20 mm, MD		
	DIC Estimation (J)	EWF (J)	L-d Curve (J)
W_v	0.0146		
W_p	0.1154	0.2134	
W_e	0.1396	0.0437	
W_f	0.2696	0.2572	0.2629

The experimental estimation of the total fracture energy can be obtained from the summation of the experimental determination of W_e, W_p, and W_v. The experimental estimation of the total fracture energy is found to be surprisingly close to the mechanical energy input obtained from the L-d curve. The experimental approach for fracture energy quantification and partitioning was further applied to study the mode-I fracture of other model m-LLDPE films. The results are summarized in Table 5.1. The nearly ideal correlation of the experimentally obtained total fracture energy for all the model m-LLDPE films in comparison with the measured mechanical energy from the L-D curves indicate the approach presented here is likely to be valid. The minor discrepancies found between them might due to several reasons: (1) the specimen-to-specimen variations between the tensile test and mode-I DENT test although all specimen were prepared from the same film but local variations do exist among the samples, especially for blown films; (2) the true tensile stress-strain measurements and energy partitioning approach were based on a 2-D deformation observation and with the assumption of constant volume during deformation; (3) the stress state around the crack tip is bi-axial in nature and might not correspond to the uniaxial true stress-strain behavior directly.

It is noted that the W_p value obtained from the extrapolation of the EWF approach is much higher than the sum of W_p and W_v acquired from the experimental determination presented above. W_e from the experimental determination is greater than the value estimated from the direct EWF equation. This is likely due to the fact that W_e is physically associated within a finite volume of the material instead of only the cross-sectional area in the ligament region due to the significant necking formation. As a

114

result, W_e should be composed of the energy involved in the necking formation (W_n) and crack propagation (W_c):

$$W_e = W_c + W_n = w_c L_c t_c + \beta_n w_n L^2 t \tag{5.9}$$

where W_c should be proportional to the cross-sectional area of the necked material in the ligament region and W_n should be proportional to the volume of the necked material. The cross-sectional area of the necked material is different from the initial area of the ligament region due to the dramatic film thinning in the necking region and the shrinkage in the width of the ligament due to the Poisson's ratio effect. And, the shape factor of the necking region (β_n) is different from the β for the OPDZ. Therefore, Equation 5 can be further expressed as:

$$W_f = W_e + W_p + W_v = w_c L_c t_c + \beta_n w_n L^2 t + \beta w_p L^2 t + \beta_v w_v L^2 t \tag{5.10}$$

Consequently, the validation of the EWF analysis for ductile materials may become questionable when significant necking formation is involved in the fracture process. Furthermore, the EWF analysis assumes the ligament region is fully yielded before crack propagation, but the ligament region actually continues to deform after the crack propagation. Both scenarios above are contrary to the assumptions of the original EWF analysis, which leads to the significant discrepancies found between the experimentally determined energy quantification method and the EWF analysis using equations. In the case of W_v, even though its magnitude small in relation to W_p and W_e, it can still serve as a guide to differentiate among the m-LLDPE films for applications where time-dependent properties are of interest. It should not be ignored.

115

5.3 Conclusions

In this study, a new experimental approach was developed to directly quantify and partition the total EWF fracture energy parameters under the mode-I DENT test. The approach partitions the total fracture energy into three components: work for necking and crack propagation, work for plastic deformation, and work for recoverable viscoelastic deformation. The energy estimation is based on the integration of the strain energy density over the size of each deformation zone using *in-situ* DIC analysis. The approach is capable of experimentally estimate each energy component through the entire fracture process. In addition, W_e is caused by deformation within a finite volume instead of only the cross-sectional area of the ligament region, which is assumed in the EWF method. When comparing the result from the EWF method, W_p value from the original EWF approach is much higher than the sum of W_p and W_v from the experimental determination. And, W_e from the experimental estimation is greater than the value estimated from the EWF equation. The physical causes leading to the above discrepancies were proposed and discussed.

CHAPTER VI

CONCLUSIONS AND CONSIDERATIONS FOR FUTURE RESEARCH

6.1 Conclusions

The main objective of this research is to gain understanding about the fracture mechanics and the processing-structure-property relationships of ductile polymeric thin film. Due to the deficiencies of the current experimental methods, a new experimental method, incorporating a custom-built film fixture and the EWF analysis, was established to provide reliable and meaningful characterization on the mode-I fracture toughness of polymeric thin films. The modifications on the film fixture mainly focuses on eliminating the out-of-plane buckling without interfering with the fracture process to provide sensitive, reproducible, and consistent measurements with minimal data scattering for the EWF analysis on the Mode-I DENT m-LLDPE film specimens. The out-of-plane buckling is due to the limited geometric stability of m-LLDPE films under tensile loading when using the traditional fixture, and it probably alters the stress distribution within the ligament zone. The new film fixture is designed to reinforce the mechanical stability of m-LLDPE films to counteract the Poisson effect, which leads to the out-of-plane buckling. The effects of testing conditions, including testing speed, gauge length, and specimen width on the EWF parameters, are examined to validate the effectiveness and capability of the EWF method for investigating the fracture performance of ductile polymeric blown films.

The experimental approach, which is based on the custom-built film fixture and the EWF method, is further utilized to study the effects of the film orientations, DDR, BUR, FLH, haze-zone region, and density on the mode-I fracture toughness of m-LLDPE films. The morphological observation and Elmendorf test are also performed on m-LLDPE films with different processing conditions. The film geometric development during the EWF test, especially within the necked zone, is carefully analyzed. Correlation between EWF parameters and the tear resistance of m-LLDPE blown films is also investigated. The fracture toughness of polymeric films are highly correlated with the corresponding molecular orientation and the microstructure in the films.

To gain further understanding about underlying physics and its correlation with EWF parameters, a new experimental approach was developed to directly quantify and partition the total EWF fracture energy parameters under the mode-I DENT test. The approach partitions the total fracture energy into three components: work for necking and crack propagation, work for plastic deformation, and work for recoverable viscoelastic deformation. The energy estimation is based on the integration of the strain energy density over the size of each deformation zone using *in-situ* DIC analysis. The approach is capable of experimentally estimate each energy component through the entire fracture process. In addition, W_e is caused by deformation within a finite volume instead of only the cross-sectional area of the ligament region, which is assumed in the EWF method. When comparing the result from the EWF method, W_p value from the original EWF approach is much higher than the sum of W_p and W_v from the experimental determination. And, W_e from the experimental estimation is greater than the value

estimated from the EWF equation. The physical causes leading to the above discrepancies were mainly due to the limitations of the original EWF method.

This research provides a useful and reliable technique, which is based on the EWF method and the newly developed film fixture, to characterize the fracture performance of ductile polymeric thin films. It also provides insights toward the fracture mechanics and the processing-structure-property relationships of m-LLDPE thin film and the physics behind the EWF method.

6.2 Future Works

Through the course of this research, many interesting findings in this study leads to more questions about the physics behind, which require further studies to decipher the puzzles and gain more understanding about the process-structure-property relationship of polymeric thin films. The suggested future works includes: 1) Developing the finite element model for the mode-I DENT testing of polymeric thin films, 2) investigating the effect of unstable crack propagation and deformation recovery in both EWF analysis and fracture energy partitioning, 3) identifying the correlations between the fracture toughness of polymeric thin films and their corresponding microstructures, 4) developing a new experimental method to provide nondestructive, whole-field measurement of the deformation along the direction of the Z-axis, 5) investigating the physics behind the necking in the IFPZ of the polymeric DENT specimens and the corresponding plateau thicknesses. The future works could provide many useful and

119

important insights and fundamental understanding about the fracture mechanics and the processing-structure-property relationships of polymeric thin film.

REFERENCES

1.   Research and Markets, *Packaging Film Market By Application & Type (LDPE, LLDPE, HDPE, CPP, BOPP, Polyester, PVC, Polyamide, EVOH, Cellulose, PLA, PVDC, PVOH & Others) - Global Trends & Forecast to 2018*. (2013). Available: http://www.researchandmarkets.com/ [Accessed August 2014].

2.   Research and Markets, *Plastic Films & Sheets Market, by Type (LLDPE, LDPE, HDPE, BOPP, CPP, PVC, PES, PA), Applications (Packaging & Non-Packaging) And Geography (North America, Asia-Pacific, Europe and RoW)-Global Trends & Forecast to 2019*. (2015). Available: http://www.researchandmarkets.com/ [Accessed January 2015].

3.   Freedonia, *Plastic Film - Industry Market Research, Market Share, Market Size, Sales, Demand Forecast, Market Leaders, Company Profiles, Industry Trends*. (2015). Available: http://www.freedoniagroup.com/ [Accessed January 2015].

4.   J. Ross, J. Adams, *The Polymeric Materials Encyclopedia*. (CRC Press, New York, 1996), pp. 5953-5965.

5.   W. A. Jenkins, K. R. Osborn, *Plastic Films: Technology and Packaging Applications*. (CRC Press, Boca Raton, FL, 1992), pp. 272 p.

6.   R. K. Krishnaswamy, A. M. Sukhadia, Orientation characteristics of LLDPE blown films and their implications on Elmendorf tear performance. *Polymer* **41**, 9205-9217 (2000).

7.   L. D. Cady, LLDPE Properties Tied to Branch Distribution. *Plastics Engineering* **43**, 25-27 (1987).

8.   T. Usami, Y. Gotoh, S. Takayama, Generation Mechanism of Short-Chain Branching Distribution in Linear Low-Density Polyethylenes. *Macromolecules* **19**, 2722-2726 (1986).

9.   J. M. Brady, E. L. Thomas, Effect of Short-Chain Branching on the Morphology of Lldpe-Oriented Thin-Films. *J Polym Sci Pol Phys* **26**, 2385-2398 (1988).

10.   R. A. Bubeck, Structure-property relationships in metallocene polyethylenes. *Mat Sci Eng R* **39**, 1-28 (2002).

11.   D. L. Cooke, T. Tikuisis, Addition of branched molecules and high molecular weight molecules to improve optical properties of LLDPE film. *Journal of plastic film and sheeting* **5**, 290-307 (1989).

12.   A. K. Doufas, A. J. McHugh, Simulation of film blowing including flow-induced crystallization. *J Rheol* **45**, 1085-1104 (2001).

13.   C. C. Liu, D. C. Bogue, J. E. Spruiell, Tubular Film Blowing .2. Theoretical Modeling. *Int Polym Proc* **10**, 230-236 (1995).

14.   A. GhanehFard, P. J. Carreau, P. G. Lafleur, Study of kinematics and dynamics of film blowing of different polyethylenes. *Polym Eng Sci* **37**, 1148-1163 (1997).

15.   T. Kanai, J. L. White, Kinematics, Dynamics and Stability of the Tubular Film Extrusion of Various Polyethylenes. *Polym Eng Sci* **24**, 1185-1201 (1984).

16.   C. L. P. Shan, J. B. P. Soares, A. Penlidis, Mechanical properties of ethylene/1-hexene copolymers with tailored short chain branching distributions. *Polymer* **43**, 767-773 (2002).

17.   K. Jordens, G. L. Wilkes, J. Janzen, D. C. Rohlfing, M. B. Welch, The influence of molecular weight and thermal history on the thermal, rheological, and mechanical properties of metallocene-catalyzed linear polyethylenes. *Polymer* **41**, 7175-7192 (2000).

18.   E. Kontou, M. Niaounakis, G. Spathis, Thermomechanical behavior of metallocene ethylene-alpha-olefin copolymers. *Eur Polym J* **38**, 2477-2487 (2002).

19.   J. Sacristan, R. Benavente, J. M. Perena, E. Perez, A. Bello, R. Rojas, R. Quijada, F. M. Rabagliati, Thermal and mechanical properties of polyethylenes synthesized with metallocene catalysts. *J Therm Anal Calorim* **58**, 559-568 (1999).

20.   J. T. Graham, R. G. Alamo, L. Mandelkern, The effect of molecular weight and crystallite structure on yielding in ethylene copolymers. *J Polym Sci Pol Phys* **35**, 213-223 (1997).

21.   A. G. Simanke, G. B. Galland, L. Freitas, J. A. H. da Jornada, R. Quijada, R. S. Mauler, Influence of the comonomer content on the thermal and dynamic mechanical properties of metallocene ethylene/1-octene copolymers. *Polymer* **40**, 5489-5495 (1999).

22.   C. D. Han, J. Y. Park, Studies on Blown Film Extrusion .1. Experimental Determination of Elongational Viscosity. *J Appl Polym Sci* **19**, 3257-3276 (1975).

23. D. Broek, *Elementary engineering fracture mechanics*. (Martinus Nijhoff; Distributed by Kluwer Boston, The Hague, Boston, MA, ed. 3rd, 1982), pp. 469 p.

24. A. C. Fischer-Cripps, *Introduction to contact mechanics*. (Springer, New York, ed. 2nd, 2007), pp. 248 p.

25. J. Collins, *Failure of materials in mechanical design*. (John Wiley & Sons, New York, NY, 1993), pp. 654 p.

26. T. H. Courtney, *Mechanical behavior of materials*. (Waveland Press, Long Grove, IL, 2005), pp. 733 p.

27. T. L. Anderson, *Fracture mechanics : fundamentals and applications*. (Taylor & Francis, Boca Raton, FL, ed. 3rd, 2005), pp. 621 p.

28. J. G. Williams, *Fracture mechanics of polymers*. Ellis Horwood series in engineering science (E. Horwood; Halsted Press, Chichester, NY, 1984), pp. 302 p.

29. J. R. Rice, A Path Independent Integral and Approximate Analysis of Strain Concentration by Notches and Cracks. *J Appl Mech* **35**, 379-386 (1968).

30. S. Hashemi, J. G. Williams, A Fracture-Toughness Study on Low-Density and Linear Low-Density Polyethylenes. *Polymer* **27**, 384-392 (1986).

31. E. C. Y. Ching, R. K. Y. Li, S. C. Tjong, Y. W. Mai, Essential work of fracture (EWF) analysis for short glass fiber reinforced and rubber toughened nylon-6. *Polym Eng Sci* **43**, 558-569 (2003).

32. S. Hashemi, Effect of temperature on fracture toughness of an amorphous poly(ether-ether ketone) film using essential work of fracture analysis. *Polym Test* **22**, 589-599 (2003).

33. W. Y. F. Chan, J. G. Williams, Determination of the Fracture-Toughness of Polymeric Films by the Essential Work Method. *Polymer* **35**, 1666-1672 (1994).

34. K. B. Broberg, Stable Crack Growth. *J Mech Phys Solids* **23**, 215-237 (1975).

35. Y. W. Mai, B. Cotterell, Effects of Pre-Strain on Plane-Stress Ductile Fracture in Alpha-Brass. *J Mater Sci* **15**, 2296-2306 (1980).

36. Y. W. Mai, B. Cotterell, Effect of Specimen Geometry on the Essential Work of Plane-Stress Ductile Fracture. *Eng Fract Mech* **21**, 123-128 (1985).

37.   B. Cotterell, J. K. Reddel, Essential Work of Plane Stress Ductile Fracture. *Int J Fracture* **13**, 267-277 (1977).

38.   ESIS, Testing Proposal for Essential Work of Fracture. *European Structural Integrity Society*, (1997).

39.   T. Barany, T. Czigany, J. Karger-Kocsis, Application of the essential work of fracture (EWF) concept for polymers, related blends and composites: A review. *Prog Polym Sci* **35**, 1257-1287 (2010).

40.   S. Hashemi, Work of fracture of high impact polystyrene (HIPS) film under plane stress conditions. *J Mater Sci* **38**, 3055-3062 (2003).

41.   M. L. Maspoch, D. Ferrer, A. Gordillo, O. O. Santana, A. B. Martinez, Effect of the specimen dimensions and the test speed on the fracture toughness of iPP by the essential work of fracture (EWF) method. *J Appl Polym Sci* **73**, 177-187 (1999).

42.   S. Hashemi, Work of fracture of PBT/PC blend: Effect of specimen size, geometry, and rate of testing. *Polym Eng Sci* **37**, 912-921 (1997).

43.   Y. W. Mai, B. Cotterell, R. Horlyck, G. Vigna, The Essential Work of Plane-Stress Ductile Fracture of Linear Polyethylenes. *Polym Eng Sci* **27**, 804-809 (1987).

44.   B. H. Choi, M. Demirors, R. M. Patel, A. W. deGroot, K. W. Anderson, V. Juarez, Evaluation of the tear properties of polyethylene blown films using the essential work of fracture concept. *Polymer* **51**, 2732-2739 (2010).

45.   S. Hashemi, Temperature and deformation rate dependence of the work of fracture in polycarbonate (PC) film. *J Mater Sci* **35**, 5851-5856 (2000).

46.   E. C. Y. Ching, W. K. Y. Poon, R. K. Y. Li, Y. W. Mai, Effect of strain rate on the fracture toughness of some ductile polymers using the essential work of fracture (EWF) approach. *Polym Eng Sci* **40**, 2558-2568 (2000).

47.   M. L. Maspoch, V. Henault, D. Ferrer-Balas, J. I. Velasco, O. O. Santana, Essential work of fracture on PET films: influence of the thickness and the orientation. *Polym Test* **19**, 559-568 (2000).

48.   E. C. Y. Ching, R. K. Y. Li, Y. W. Mai, Effects of gauge length and strain rate on fracture toughness of polyethylene terephthalate glycol (PETG) film using the Essential Work of Fracture analysis. *Polym Eng Sci* **40**, 310-319 (2000).

49. J. Karger-Kocsis, T. Czigany, E. J. Moskala, Deformation rate dependence of the essential and non-essential work of fracture parameters in an amorphous copolyester. *Polymer* **39**, 3939-3944 (1998).

50. A. Arkhireyeva, S. Hashemi, M. O'Brien, Factors affecting work of fracture of uPVC film. *J Mater Sci* **34**, 5961-5974 (1999).

51. J. Karger-Kocsis, T. Czigany, Strain rate dependence of the work of fracture response of an amorphous poly(ethylene-naphthalate) (PEN) film. *Polym Eng Sci* **40**, 1809-1815 (2000).

52. S. Hashemi, Determination of the fracture toughness of polybutylene terephthalate (PBT) film by the essential work method: Effect of specimen size and geometry. *Polym Eng Sci* **40**, 798-808 (2000).

53. S. Hashemi, Fracture toughness evaluation of ductile polymeric films. *J Mater Sci* **32**, 1563-1573 (1997).

54. X. M. Zhang, S. Elkoun, A. Ajji, M. A. Huneault, Oriented structure and anisotropy properties of polymer blown films: HDPE, LLDPE and LDPE. *Polymer* **45**, 217-229 (2004).

55. J. J. Lu, H. J. Sue, Morphology and mechanical properties of blown films of a low-density polyethylene/linear low-density polyethylene blend. *J Polym Sci Pol Phys* **40**, 507-518 (2002).

56. A. K. Babel, G. A. Campbell, A Model Linking Process Variables to the Strength of Blown Films Produced from Ldpe and Lldpe. *Tappi J* **78**, 199-204 (1995).

57. E. W. Kuijk, P. P. Tas, P. Neuteboom, A rheological model for the prediction of polyethylene blown film properties. *J Reinf Plast Comp* **18**, 508-517 (1999).

58. C. F. Lee, H. J. Sue, D. M. Fiscus, Refined fixture design for effective essential work of fracture toughness characterization of m-LLDPE thin films. *Polym Test* **32**, 256-264 (2013).

59. Y. Ide, Z. Ophir, Orientation Development in Thermotropic Liquid-Crystal Polymers. *Polym Eng Sci* **23**, 261-265 (1983).

60. U. Yilmazer, Effects of the Processing Conditions and Blending with Linear Low-Density Polyethylene on the Properties of Low-Density Polyethylene Films. *J Appl Polym Sci* **42**, 2379-2384 (1991).

61. M. Rennert, M. Nase, R. Lach, K. Reincke, S. Arndt, R. Androsch, W. Grellmann, Influence of low-density polyethylene blown film thickness on the

mechanical properties and fracture toughness. *J Plast Film Sheet* **29**, 327-346 (2013).

62.   J. S. S. Wong, D. Ferrer-Balas, R. K. Y. Li, Y. W. Mai, M. L. Maspoch, H. J. Sue, On tearing of ductile polymer films using the essential work of fracture (EWF) method. *Acta Mater* **51**, 4929-4938 (2003).

63.   Y. V. Kissin, Elmendorf Tear Test of Polyethylene Films: Mechanical Interpretation and Model. *Macromol Mater Eng* **296**, 729-743 (2011).

64.   L. T. Kale, T. A. Plumley, R. M. Patel, O. D. Redwine, P. Jain, Structure-property relationships of ethylene/1-octene and ethylene/1-butene copolymers made using INSITE* technology. *J Plast Film Sheet* **12**, 27-40 (1996).

65.   A. Dasari, S. J. Duncan, R. D. K. Misra, Atomic force microscopy of scratch damage in polypropylene. *Mater Sci Tech-Lond* **18**, 1227-1234 (2002).

66.   A. Dasari, R. D. K. Misra, On the strain rate sensitivity of high density polyethylene and polypropylenes. *Mat Sci Eng a-Struct* **358**, 356-371 (2003).

67.   T. Hameed, I. A. Hussein, Rheological study of the influence of M-w and comonomer type on the miscibility of m-LLDPE and LDPE blends. *Polymer* **43**, 6911-6929 (2002).

68.   R. Alamo, R. Domszy, L. Mandelkern, Thermodynamic and Structural-Properties of Copolymers of Ethylene. *J Phys Chem-Us* **88**, 6587-6595 (1984).

69.   Y. L. Huang, N. Brown, Dependence of Slow Crack-Growth in Polyethylene on Butyl Branch Density - Morphology and Theory. *J Polym Sci Pol Phys* **29**, 129-137 (1991).

70.   K. B. Broberg, Crack-Growth Criteria and Non-Linear Fracture Mechanics. *J Mech Phys Solids* **19**, 407-418 (1971).

71.   M. L. Maspoch, J. Gamez-Perez, A. Gordillo, M. Sanchez-Soto, J. I. Velasco, Characterisation of injected EPBC plaques using the essential work of fracture (EWF) method. *Polymer* **43**, 4177-4183 (2002).

72.   A. Arkhireyeva, S. Hashemi, Effect of temperature on work of fracture parameters in poly(ether-ether ketone) (PEEK) film. *Eng Fract Mech* **71**, 789-804 (2004).

73.   J. S. Wu, Y. W. Mai, The essential fracture work concept for toughness measurement of ductile polymers. *Polym Eng Sci* **36**, 2275-2288 (1996).

74. T. Pardoen, Y. Marchal, F. Delannay, Essential work of fracture compared to fracture mechanics - towards a thickness independent plane stress toughness. *Eng Fract Mech* **69**, 617-631 (2002).

75. A. Arkhireyeva, S. Hashemi, Fracture behaviour of polyethylene naphthalate (PEN). *Polymer* **43**, 289-300 (2002).

76. K. Saminathan, P. Selvakumar, N. Bhatnagar, Fracture studies of polypropylene/nanoclay composite. Part 1: Effect of loading rates on essential work of fracture. *Polym Test* **27**, 296-307 (2008).

77. E. Q. Clutton, ESIS TC4 experience with the essential work of fracture method. *European Structural Integrity Society* **27**, 187-199 (2000).

78. E. Q. Clutton, Essential work of fracture. *Fracture Mechanics testing methods for polymers, adhesives and composites* **28**, 177-195 (2001).

79. J. KargerKocsis, T. Czigany, E. J. Moskala, Thickness dependence of work of fracture parameters of an amorphous copolyester. *Polymer* **38**, 4587-4593 (1997).

80. J. Karger-Kocsis, D. Ferrer-Balas, On the plane-strain essential work of fracture of polymer sheets. *Polym Bull* **46**, 507-512 (2001).

81. D. E. Mouzakis, J. Karger-Kocsis, E. J. Moskala, Interrelation between energy partitioned work of fracture parameters and the crack tip opening displacement in amorphous polyester films. *J Mater Sci Lett* **19**, 1615-1619 (2000).

82. Y. W. Mai, B. Cotterell, On the Essential Work of Ductile Fracture in Polymers. *Int J Fracture* **32**, 105-125 (1986).

83. A. B. Martinez, J. Gamez-Perez, M. Sanchez-Soto, J. I. Velasco, O. O. Santana, M. L. Maspoch, The Essential Work of Fracture (EWF) method - Analyzing the Post-Yielding Fracture Mechanics of polymers. *Eng Fail Anal* **16**, 2604-2617 (2009).

84. J. Karger-Kocsis, E. Moskala, Relationships between molecular and plane-stress essential work of fracture parameters in amorphous copolyesters. *Polym Bull* **39**, 503-510 (1997).

85. M. L. Maspoch, J. Gamez-Perez, J. Karger-Kocsis, Effects of thickness, deformation rate and energy partitioning on the work of fracture parameters of uPVC films. *Polym Bull* **50**, 279-286 (2003).

86.   D. Ferrer-Balas, M. L. Maspoch, A. B. Martinez, O. O. Santana, On the essential work of fracture method: Energy partitioning of the fracture process in iPP films. *Polym Bull* **42**, 101-108 (1999).

87.   H. J. Kwon, P. Y. B. Jar, New energy partitioning approach to the measurement of plane-strain fracture toughness of high-density polyethylene based on the concept of essential work of fracture. *Eng Fract Mech* **74**, 2471-2480 (2007).

88.   P. Y. B. Jar, R. Adianto, S. Muhammad, A mechanistic approach for determining plane-stress fracture toughness of polyethylene. *Eng Fract Mech* **77**, 2881-2895 (2010).

89.   P. Y. B. Jar, W. Cao, A deformation-mechanism-based energy partitioning approach for measurement of plane-stress fracture toughness of low-density polyethylene. *Eng Fract Mech* **96**, 179-191 (2012).

90.   H. J. Sue, A. F. Yee, Deformation-Behavior of a Polycarbonate Plate with a Circular Hole - Finite-Elements Model and Experimental-Observations. *Polymer* **29**, 1619-1624 (1988).